Na^+ channels enhance low contrast signalling in the superior-coding direction-selective circuit

by

Amanda J. McLaughlin
B.Sc., Dalhousie University, 2012

A Dissertation Submitted in Partial Fulfillment
of the Requirements for the Degree of

DOCTOR OF PHILOSOPHY

in the Department of Biology (Neuroscience)

Supervisory Committee

Na^+ channels enhance low contrast signalling in the superior-coding direction-selective circuit

by

Amanda J. McLaughlin
B.Sc., Dalhousie University, 2012

Supervisory Committee

Dr. John Taylor (Department of Biology)
Supervisor

Dr. Raad Nashmi (Department of Biology)
Departmental Member

Dr. Craig Brown (Division of Medical Sciences)
Outside Member

Abstract

Light entering the eye is transformed by the retina into electrical signals. Extensive processing takes place in the retina before these signals are transmitted to the brain. Beginning in the outer retina, light-evoked electrical signals are distributed into parallel pathways specialized for different visual tasks, such as the detection of dark vs. bright ambient light, the onset or offset of light, and the direction of stimulus motion. Pathway diversity is a consequence of cell type diversity, differential cell connectivity, synapse organization, receptor expression, or any combination thereof. Cell connectivity itself can be accomplished through excitatory or inhibitory chemical synapses, or electrical coupling via gap junctions. Gap junctions are further specialized based on the expression of different connexin subunit isoforms. In aggregate, this diversity gives rise to ganglion cells with highly specialized functions, including ON and/or OFF responses, contrast-tuning and direction-selectivity (DS).

The directionally-selective circuit, a circuit specialized for the encoding of stimulus motion, makes use of many of these circuit specializations. Bipolar cells, in response to glutamate release from cone photoreceptors, provide highly-sensitive glutamatergic input to amacrine cells and DS ganglion cells (DSGCs) in this circuit, while amacrine cells provide cholinergic and directionally-tuned GABAergic input to DSGCs. One population of DSGCs also transmit signals laterally to one another via gap junctions. Thus numerous specializations in bipolar cells, amacrine cells and ganglion cells endow DSGCs with their unique encoding abilities.

In Chapters 2 and 3 of this dissertation I focus on synchronized firing between gap junction-coupled DSGCs. sDSGCs exhibit fine-scale correlations, with action

potentials in an sDSGC more likely within ~2ms of action potential firing in a coupled neighbour. I first characterize electrical coupling of DSGCs through the identification of the molecular composition of DSGC gap junctions (Chapter 2). Physiological and immunohistochemical methods allowed me to demonstrate an important role for connexin 36 subunits in DSGC electrical coupling. Next (Chapter 3) I investigate the sub-cellular mechanisms underlying neuronal correlations between electrically coupled DSGCs. Using paired recordings, I show that chemical input (from bipolar cells and amacrine cells), electrical input (from gap junctions), and Na^+ channel activity in DSGC dendrites underlie the generation of correlated spiking activity. While a common feature of electrically coupled networks, the mechanisms underlying correlations were previously unclear.

In Chapter 4 I focus on the mechanisms within the DS circuit that endow these neurons with impressive sensitivity to stimulus contrast. Using physiological and pharmacological methods I first assess the relative contrast sensitivity of ganglion cells and starburst amacrine cells (SACs) in the DS circuit. The sensitivity of DSGC and SAC excitatory currents to antagonists of Na^+ channels suggests an important role for these channels in amplifying low contrast responses and other weak inputs to the circuit. This role is later attributed to the differential expression of voltage-gated Na^+ channels in specific bipolar cell populations.

In aggregate, this dissertation describes several novel circuit mechanisms within the well-studied DS circuit. I also provide specific roles for such specializations in visual coding.

Publications

Original Research:

1. Yao, X., Cafaro, J., McLaughlin, AJ., Postma, FR., Paul, DL., Awatramani, G., Field, GD. Gap junctions contribute to differential light adaptation across direction selective retinal ganglion cells. *[in preparation]*
2. Sethuramanujam, S., McLaughlin, AJ., DeRosenroll, G., Hoggarth, A., Schwab, D.J. & Awatramani, GA. (2016). A central role for mixed acetylcholine/GABA transmission in direction coding in the retina. *Neuron.* 90(6):1243-1256.
3. Hoggarth, A., McLaughlin, AJ., Ronellenfitch, K., Trenholm, S., Vasandani, R., Sethuramanujam, S., Schwab, D., Briggman, KL., Awatramani, GB. (2015). Specific wiring of distinct amacrine cells in the directionally selective retinal circuit permits independent coding of direction and size. *Neuron.* 86(1):276-91
4. McLaughlin, A.J.*, Trenholm S.*, Schwab, D.J., Turner, M.H., Smith, R.G., Rieke, F., Awatramani, G.B. (2014). Nonlinear dendritic integration of electrical and chemical synaptic inputs mediates fine-scale neural correlations. *Nature Neuroscience*. 17(12):1759-66 (*****co-first authors).
5. Trenholm S., McLaughlin, AJ., Schwab, D., Awatramani, GB. (2013). Dynamic tuning of electrical and chemical synaptic transmission in a network of motion coding retinal neurons. *The Journal of Neuroscience*. 33(37):14927-38

Conference Presentations:

1. McLaughlin, AJ. Connexin 36 gap junctions are important for electrical coupling of Hb9 DSGCs. Oral presentation. Symposium conducted at the Biology Graduate Symposium. 2016: November 7-8; Victoria, BC.
2. Hoggarth A, Sethuramanujam, S., Jain, V., McLaughlin, AJ & Awatramani, GB. Control of excitation-inhibition balance in the directionally selective circuit in mouse retina by nicotinic acetylcholine receptors. Poster presented at: Society for Neuroscience 2015. 2015: October 17-21; Chicago, Illinois, US
3. McLaughlin, AJ. Addition and multiplication by multiple excitatory inputs to direction-selective ganglion cells. Oral presentation. Symposium conducted at the Biology Graduate Symposium. 2015: November 9-10; Victoria, BC.
4. McLaughlin, AJ. & Awatramani, G.B. Synaptic mechanisms underlying contrast coding in the directionally-selective circuit in the mouse retina. Poster presented at: Canadian Association for Neuroscience Satellite Symposium. 2015: May 24; Vancouver, BC.
5. McLaughlin, AJ. Non-linear integration of electrical and chemical synapses mediates fine-scale neural correlations. Oral presentation in *Information Encoding in the Retina*. Symposium conducted at: FASEB Retinal Neurobiology and Visual Processing conference. 2014: June 22-27; Saxtons River, VT.
6. Hoggarth, A, Ronellenfitch, K, Trenholm, S, McLaughlin, AJ, Vasandani, R, Schwab, D, Briggman, K, Awatramani, GB. Direction coding in the presence of ambient light dependent changes in global inhibition. Poster session presented at: FASEB Retinal Neurobiology and Visual Processing conference. 2014: June 22-27; Saxtons River, VT.

7. McLaughlin, AJ**.** Fine-scale neural correlations in electrically coupled ganglion cells. Oral presentation. Symposium conducted at the Biology Graduate Symposium. 2014: November 13-14; Victoria, BC
8. McLaughlin, AJ, Trenholm, S, Schwab, D & Awatramani, GB. Electrical and chemical synapses drive fine-scale correlations in the retina. Poster session presented at SfN 2013: 43rd annual meeting for Neuroscience. 2013: November 9-13; San Diego, CA.
9. Hoggarth, A, Trenholm, S, McLaughlin, AJ, Awatramani, GB. Multiple layers of inhibition are differentially modified by light. Poster presented at SfN 2013. 43rd annual meeting for Neuroscience. 2013: November 9-13; San Diego, CA.
10. McLaughlin, AJ. Characterization of a protein-protein interaction between NOS1AP and mammalian zyxin homologs. Oral presentation. Dalhousie University Biochemistry & Molecular Biology Honours Student Seminar. 2012: March 21; Halifax, NS.

Table of Contents

List of Abbreviations

18βGA – 18 beta-glycyrrhetinic acid
ACh – acetylcholine
AMPA – α-amino-3-hydroxy-5-methyl-4-isoxazolepropionic acid
AMPAR – α-amino-3-hydroxy-5-methyl-4-isoxazolepropionic acid receptor
AP-5 – (2R)-amino-5-phosphonovaleric acid
BC – bipolar cell
C_{50} – half-maximal contrast
Ca_v – voltage-gated calcium channel
CBC – cone bipolar cell
CC – current-clamp
CCG – cross-correlogram
ChAT – choline acetyltransferase
CI – correlation index
CNS – central nervous system
CRF – contrast response function
CX – connexin
CX36/CX45 – connexin 36/connexin 45
CX36KO/$CX36^{-/-}$ – connexin 36 knock-out
DA – dopamine
DS – directionally-selective
DSGC – directionally-selective ganglion cell
DSi – directionally-selective index
EPSC – excitatory post-synaptic current
FACx – FSTL4creER::Ai9fl::CX36fl
FSTL4 – follistatin Like 4
GC – ganglion cell
GFP – green fluorescent protein
Gj – junctional conductance
Hb9 – homeobox gene 9
Hex – hexamethonium
HSBC – high-sensitivity bipolar cell
Ij – transjunctional current
IPSC – inhibitory post-synaptic current
K_v – voltage-gated potassium channel
LSBC – low-sensitivity bipolar cell
mGluR6 – metabotropic glutamate receptor 6
nAChR – nicotinic acetylcholine receptor
Na_v – voltage-gated sodium channel
NBQX - 2,3-dihydroxy-6-nitro-7-sulfamoyl-benzo[f]quinoxaline-2,3-dione
NMDA – N-methyl-D-aspartate
NMDAR – N-methyl-D-aspartate receptor
NR – Naka-Rushton equation
ONα – ON alpha ganglion cell
PSP – post-synaptic potential

PR – photoreceptor
Ptx – Picrotoxin
RBC – rod bipolar cell
RF – receptive field
ROI – region of interest
SAC – starburst amacrine cell
sDSGC – superior-coding DSGC
SR95531 – 6-Imino-3-(4-methoxyphenyl)-1(6H)-pyridazinebutanoic acid hydrobromide
TPMPA – 1,2,5,6-Tetrahydropyridin-4-yl)methylphosphinic acid
TRP – transient receptor potential
TTX – tetrodotoxin
VC – voltage-clamp
V_j – transjunctional voltage
WAC – wide-field amacrine cell
WT – wildtype
YFP – yellow fluorescent protein

List of Figures

Acknowledgments

This work was funded by an Alexander Graham Bell scholarship to Amanda McLaughlin as well as research grants to Dr. Gautam Awatramani from the Canadian Institute for Health Research, the National Science and Engineering Research Council, and the Foundation Fighting Blindness.

I have so many people to thank for making this pursuit possible. I am truly humbled by the kindness, generosity and love I have been shown by friends, family and mentors alike over these six years. These words will do no justice to my appreciation for the numerous individuals who have made this degree a possibility.

First and foremost, as an uninvited settler to these lands, I wish to honour and recognize the Songhees, Esquimalt and WSÁNEĆ peoples. It was upon their lands this research was performed and this dissertation was written.

To my friends, and chosen family, in particular my partner Alex Hoggarth, my incredible friends Patrick Reeson, Lena Chen, Kara Ronellenfitch, Ben Murphy-Baum, Maeve Cox, Finn St.Dennis, Trent Folan and the women of my book club. You have all provided me with shoulders to cry on and inspirational pep talks, at times almost daily. Patrick, Lena and Alex you've read and edited my work and been my cheerleaders for every presentation. Lena and Kara, you've put a roof over my head time and time again. Every single one of you has pushed me out of my comfort zone. You've challenged my beliefs, my opinions and my intellectual and physical limits. I am infinitely better off having met you. Thank you. I love and appreciate you.

To my family: Mom, Dad, Kyle and Leanne (+Timmy, Horton, Nala). Thank you for your constant support and advice. I know we've all had moments where we wished I'd chosen to do something different, but you've nonetheless frequently listened to me

whine, cry and panic and never once questions my decisions. Thank you for supporting this starving student many years longer than you thought you'd have to. I love you.

To my academic mentors: John Taylor, Steve Perlman, Craig Brown, Raad Nashmi, Marsha Runtz, and Annalee Lepp; my lab mates Stu, Alex, Santhosh, Varsha, Laura (and so many others!); and my external examiners Peter Lukasiewicz and Malcolm Slaughter. Your contributions to my work have made me grow as a scientist and I and my work are better because of your thoughtful insights. Marsha, Steve and especially John, thank you for going the extra mile to make my degree a reality. Thank you for believing in me, my abilities, and my experiences. John, Steve, and Annalee your respective passion for your work and for the pursuit of knowledge more generally, is palpable and contagious. You've treated me more like a colleague than a clueless graduate student, and have taught me that my opinions have merit. It's people like you that remind me why I came to grad school, and inspire me to stay in academia.

Finally to my greater campus community. To Kenya, Maks, Lane and Emma; you have boldly demanded better for our community, often at great personal expense. I admire your courage, your strength, and your tremendous empathy for others. I thank you enough for your friendship, your advocacy, and your general bad-assity. To Stacy, Brandy (+Sita), and the rest of my GSS community (Katrina, Susan, Elissa, sasha, Julie, Danny, Hilary, Nick, Marie, Cory […]), it has been a privilege to work with you. I am eternally grateful for the skills, experiences and friendships I've gained within this organization. Not only did you give me a home on campus, you gave me a purpose. Your trust in me gave me the strength and courage to do some of the most meaningful work of my life. I appreciate you, your commitment and your passion, and I will miss you greatly.

Dedication

To my family and chosen family,

I dedicate this dissertation to you. Without you I would have neither the means, nor the strength or the stamina to make it this far.

I love and appreciate you,

Amanda

1 Introduction

1.1. An introduction to the retina

1.1.1 The retina encodes the visual world

Seeing begins when the cornea and lens project light onto the retina at the back of the eye (Figure 1). In the eyes of vertebrates, the retina is a multi-layered network of neural tissue. It serves as the interface between the light reflected from the physical world and the central nervous system, transmitting action potentials to the brain via the optic nerve. This information is however not blindly transferred in a pixel-by-pixel fashion to the brain. Instead, complex computations about stimulus contrast, motion, and size, to name a few examples, are encoded within the retina itself, and this integrated signal comprises the retinal output.

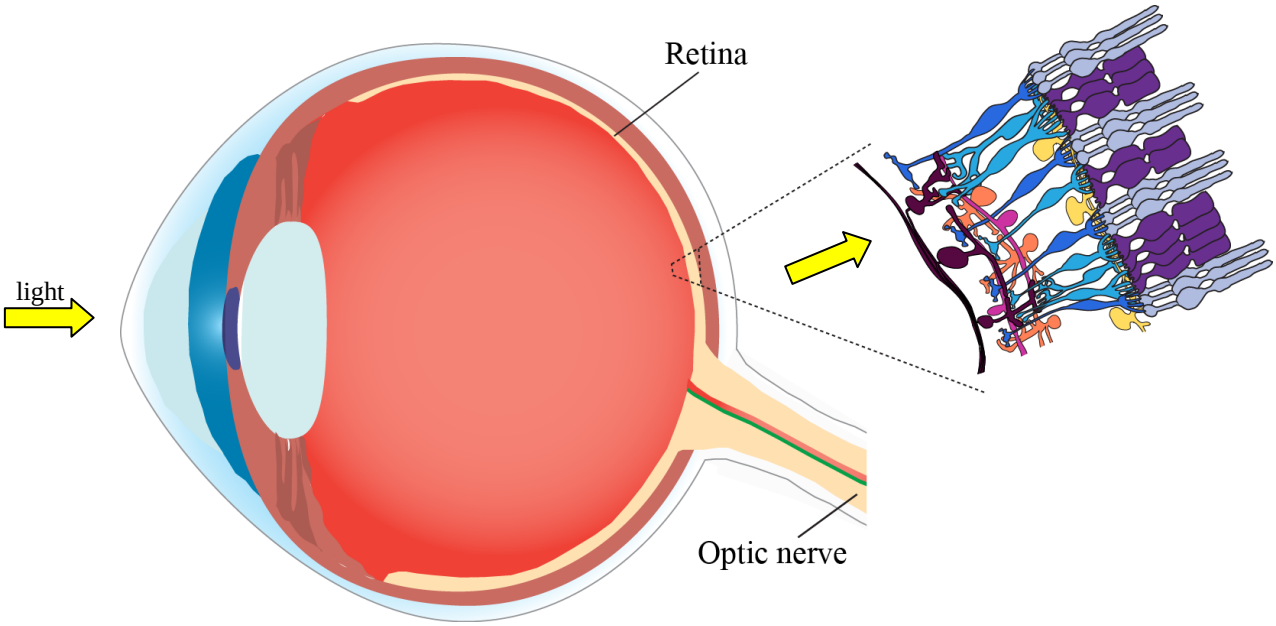

Figure 1. The retina
The retina is a thin neural tissue at the back of the eye. Rod and cone photoreceptors (grey and purple) are located distally and are the sensory neurons of the visual system. Ganglion cells (burgundy) are located proximally in the eye. Ganglion cell axons form the optic nerve, the output of the retina.

1.1.2. The retina as an accessible part of the central nervous system

The study of retinal anatomy, connectivity and signal integration serves not only to further our understanding of the visual system, but neuronal circuits in general. Vertebrate brains are extraordinarily complex, containing between 10^{10} and 10^{12} neurons each forming 10^{3} to 10^{4} synaptic connections. While some researchers have utilized computational models, or large scale anatomical and physiological studies in attempts to tackle this complexity top-down, an alternative is to rely on a bottom-up approach to circuit analysis, focussing on simpler nervous systems (such as those found in invertebrates) or simpler regions within the nervous system, such as the retina. The retina has proven to be especially useful for experimentation and analysis, for several reasons. First, despite being a part of the central nervous system, and being derived from the same progenitor cells that give rise to the brain, the retina is separated from the rest of the CNS. This segregation allows for simple tissue dissection and, of particular importance for early physiological experiments, easy access to the optic nerve for the recording of action potential firing (Granit, 1933; Hartline, 1937). Second, the retina can be exposed to light, in a manner that mimics normal function (Hartline, 1937). Finally, the ordered anatomical organization of the retina facilitates anatomical and physiological experimentation. Neuronal cell bodies make up three clearly defined layers in the retina (nuclear layers), separated by two bands of neuronal processes (axons and dendrites), or plexiform layers (**Figure 2**). Each nuclear layer contains few cell classes, distinct from layer to layer, facilitating cell classification while synaptic contacts, which are constrained primarily to the two plexiform layers, provide an ideal substrate for network reconstruction. Thus, the retina makes feasible the detailed study of neuronal circuits, the

analysis of which will inform our understanding of neuronal circuits and mechanisms elsewhere in the vertebrate brain.

1.1.3. Cellular structure of the retina

The retina is composed of five major cell classes (each composed of several subclasses or types), distinguishable on the basis of the location and morphology of their cell bodies (within nuclear layers), axons and dendritic arbors (within plexiform layers) (for reviews see Masland, 2001, 2012a). Photoreceptors, the predominant light-sensitive cells in the eye, are the only neuronal class with cell bodies in the outer nuclear layer (**Figure 2**). Their axon terminals form the outer plexiform layer, where they contact bipolar cells and horizontal cells, the cell bodies of which are found in the inner nuclear layer. While bipolar cells span the inner nuclear layer to form synapses with ganglion cell and amacrine cell dendrites in the inner plexiform layer, horizontal cell dendrites and axons are restricted to the outer plexiform layer.

Amacrine cells are the most diverse retinal cell class (Masland, 2012b). Amacrine cells have dendrites in the inner plexiform layer, forming synapses with bipolar cells, ganglion cells, and other amacrine cells, but with few exceptions exhibit no visible axons. Amacrine cell somata are largely found in the inner nuclear layer however some are also found in the third neuronal layer, termed the ganglion cell layer. Here the cell bodies of ganglion cells are found, while ganglion cell axons form the optic nerve which exits the retina (**Figure 2**).

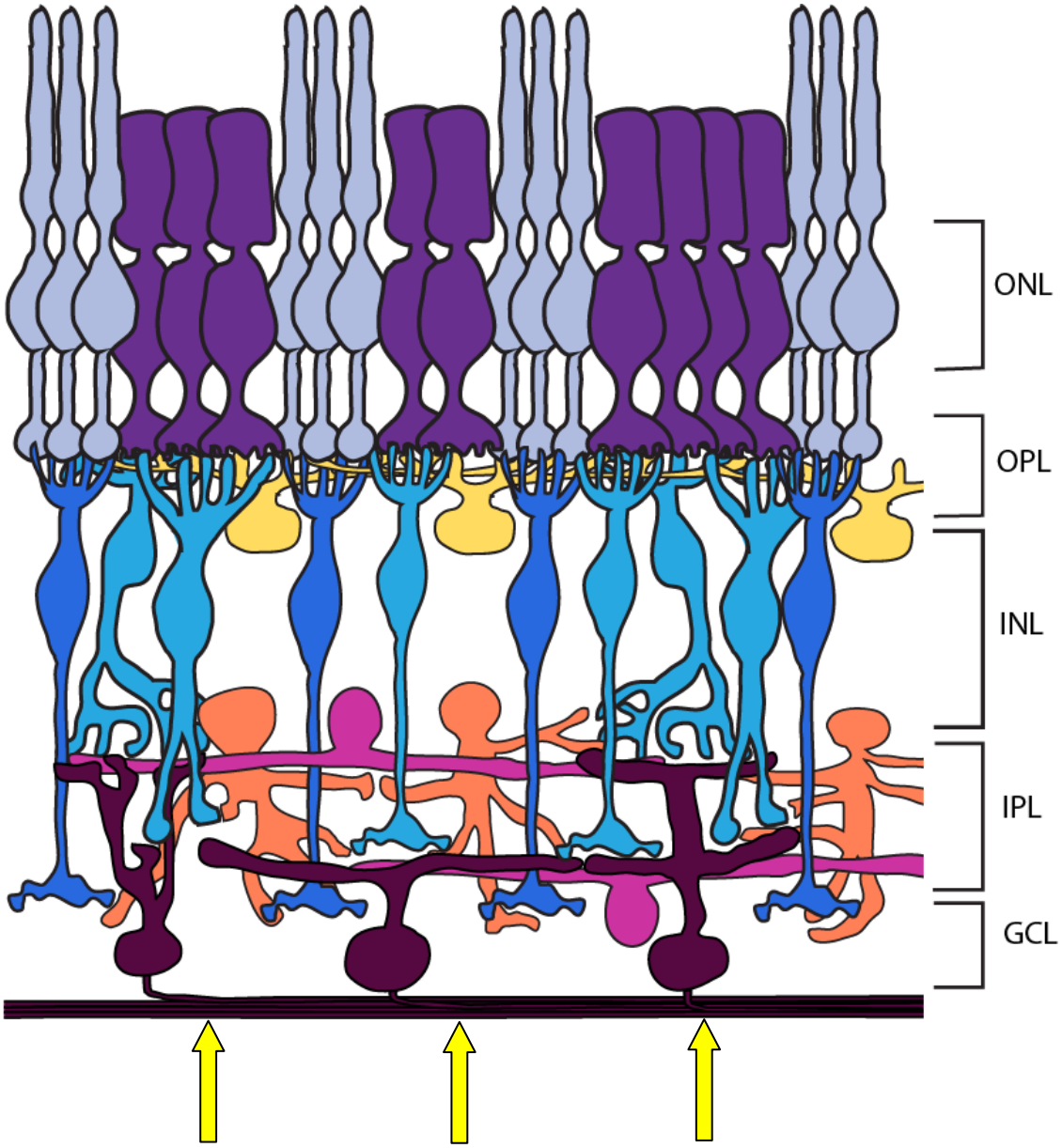

Figure 2. The retina is a layered structure
Retinal cell bodies are located in one of three nuclear layers, the outer nuclear layer (ONL), the inner nuclear layer (INL) or the ganglion cell layer (GCL). Photoreceptors (rods and cones; grey and purple) contact horizontal cells (yellow) and bipolar cells (blue) in the outer plexiform layer (OPL), while bipolar cells contact amacrine cells (orange and pink) and ganglion cells (burgundy) in the inner plexiform layer.
Rod and cone photoreceptors contact rod (dark blue) and cone (light blue) bipolar cells respectively. Bipolar cell subpopulations can be identified based on their stratification within the IPL. Ganglion cells sample from one or multiple populations of bipolar cells, extending dendrites into one or multiple IPL sublaminae.
In the eye, light (arrows) first reaches the ganglion cell layer. It then crosses the retina, before reaching the photosensitive rods and cones in the outer nuclear layer.

Counterintuitively, the outer nuclear layer is located behind the ganglion cell layer (**Figure 1**). As a result, light enters the eye and passes through the ganglion, amacrine and bipolar cells prior to being captured by the outer segments of photoreceptors. Photons are absorbed by visual pigments in the outer segments of the photoreceptors. These pigments, comprised of membrane-bound opsin proteins and a chromophore, initiate the phototransduction cascade and are responsible for transforming light into a graded chemical signal, specifically, the graded release of the neurotransmitter glutamate (see Yau & Hardie, 2009 for review). As may be evident based on the anatomical organization of the retina, signals are transmitted from photoreceptors to ganglion cells via glutamatergic bipolar cells. Horizontal cells and amacrine cells, while present in the inner nuclear layer, are primarily inhibitory and perform critical roles in the modulation of excitatory signalling within the outer nuclear layer and inner nuclear layer respectfully.

1.1.4. Tools for studying retinal circuits

Several methods have been utilized for the study of retinal circuit function over the past several decades, and remain of critical importance. Below I describe the attributes of key components of retinal circuit analysis: the retinal preparation, electrophysiological recording configurations and the use of transgenic mouse models, all of which are utilized in this thesis.

1.1.4.1. Ex-vivo whole-mount retinal preparations

The most commonly used preparation for the study of retinal circuits, and in particular the study of ganglion cell physiology, is the whole-mount retinal preparation. In this protocol the retina is kept largely intact, following its dissection from the eye, which includes the removal of the vitreous humor and the severing of the optic nerve. As

with most physiological preparations, the perfusion of well-oxygenated artificial media allows the retina to remain alive for several hours following dissection. Compared to slice preparations frequently used for the study of other brain areas, the retinal whole mount avoids severing dendrites and axons within the preparation, allowing greater confidence that physiological recordings represent *in vivo* neural activity. The light-sensitive nature of the retinal whole-mount also allows light, projected directly onto the photoreceptors, to serve as physiological stimulation in lieu of electrical stimulation. Because of the layered nature of the retina, sharp electrode recordings (narrow electrodes inserted directly into the intracellular space of neurons) have been made from retinal whole mounts with the cell type inferred from retinal depth. Retinas are mounted 'upside down' for electrophysiological recordings, with photoreceptors laid downwards and ganglion cells on top. Light therefore enters the preparation from the opposite direction compared to in intact eyes (**Figure 3**). This allows physiological recordings to be easily made directly from ganglion cell axons, or from ganglion cell somata within the ganglion cell layer (**Figure 3**).

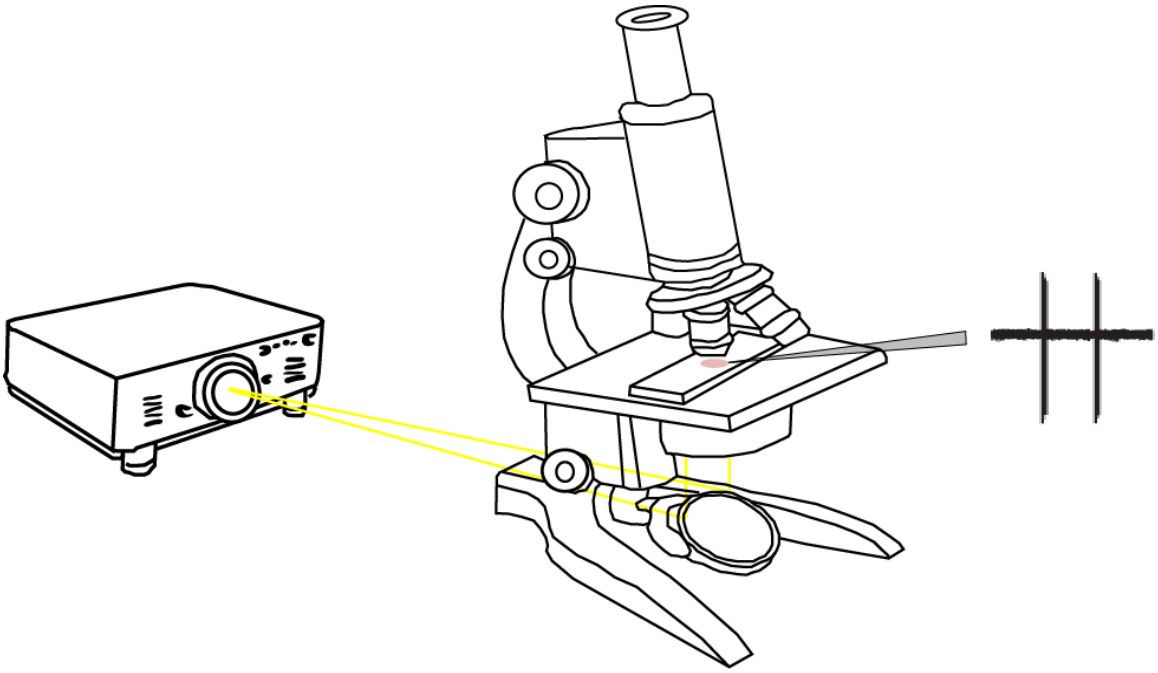

Figure 3. Experimental setup
Dissected whole-mount retinas (pink) are mounted in custom recording chambers and perfused with oxygenated Ringers solution (not shown). Retinal neurons and recording electrodes are visualized using a light-microscope. Light stimuli are presented using a projector, and focussed on retinal photoreceptors through the microscope sub-stage condenser.

1.1.4.2. Electrophysiological techniques allow for circuit analysis

Recording of spike trains from the optic nerve has been used to study retinal output since the early 20th century (Granit, 1933; Hartline, 1937). Similarly, sharp electrode recordings from multiple cell types were performed throughout the 20th century in order to understand how different classes of retinal neurons respond to light stimuli (Werblin & Dowling, 1969). An important early finding of these experiments was the observation that ganglion cells exhibited classical action potentials, while most other retinal neurons exhibited graded potentials (Werblin & Dowling, 1969).

The advent of whole-cell recordings has provided further insights into the stimulus responses and wiring of retinal neurons. In this configuration, the electrode is

placed on the cell membrane, and suction is applied such that the electrode becomes continuous with the cytoplasm of the neuron. The lower resistance of the larger electrode tip in whole-cell configurations provides better electrical access to the neuron. In this thesis I have used both current-clamp and voltage-clamp whole-cell configurations. Current-clamp recordings allow for the recording of membrane voltage, similar to the sharp electrode recordings, with the benefit of greater signal sensitivity. Voltage-clamp recordings on the other hand provide direct control over the membrane voltage, enabling current-voltage relationships to be drawn. These measurements provide useful insights into neuronal membrane dynamics and pre-synaptic inputs. Taking advantage of channel reversal potentials, voltage-clamp recordings have improved our understanding of the wiring of individual retinal circuits, because they allow for the isolation of excitatory and inhibitory inputs.

I performed extensive physiological recordings, in both current- and voltage-clamp configurations in order to understand a particular circuit in the mouse retina, and the mechanisms by which signals are integrated across retinal populations, or within single retinal neurons.

1.1.4.3. Transgenic mouse lines as anatomical and functional tools

Early work in visual neuroscience relied on electrophysiological recordings from a wide host of model organisms, ranging from teleost fish, to amphibians, to rabbits and cats. However, current studies focus primarily on mice, given the breadth of genetic tools available in mice compared to other species. Expression of fluorescent markers, driven by cell-specific transcription factors, has allowed both for identification and targeting of distinct subpopulations of retinal neurons and subsequently facilitated identification of

such neurons for anatomical or physiological experiments. In addition to expressing exogenous proteins, the expression of endogenous proteins can be reduced or eliminated in transgenic mice. These genetic knock-outs have been used to assess the physiological relevance of numerous genes, proteins, and even cell types through anatomical or physiological comparisons between knock-out mouse retinas and wild-type controls. These tools have been further refined through the development of site-specific recombinase technology, allowing expression or deletion to be limited to specific neuronal populations, and inducible recombinase systems, allowing for precise control over the timing of recombination.

In this work, I target specific retinal populations for electrophysiological recordings by utilizing target-specific mouse lines expressing fluorescent proteins within specific cell populations (Chapter 2 and 4). I also utilized knock-out mice to assess the role of a single protein (which forms gap junction connections between cells) in the electrical coupling of neighbouring ganglion cells (Chapter 3).

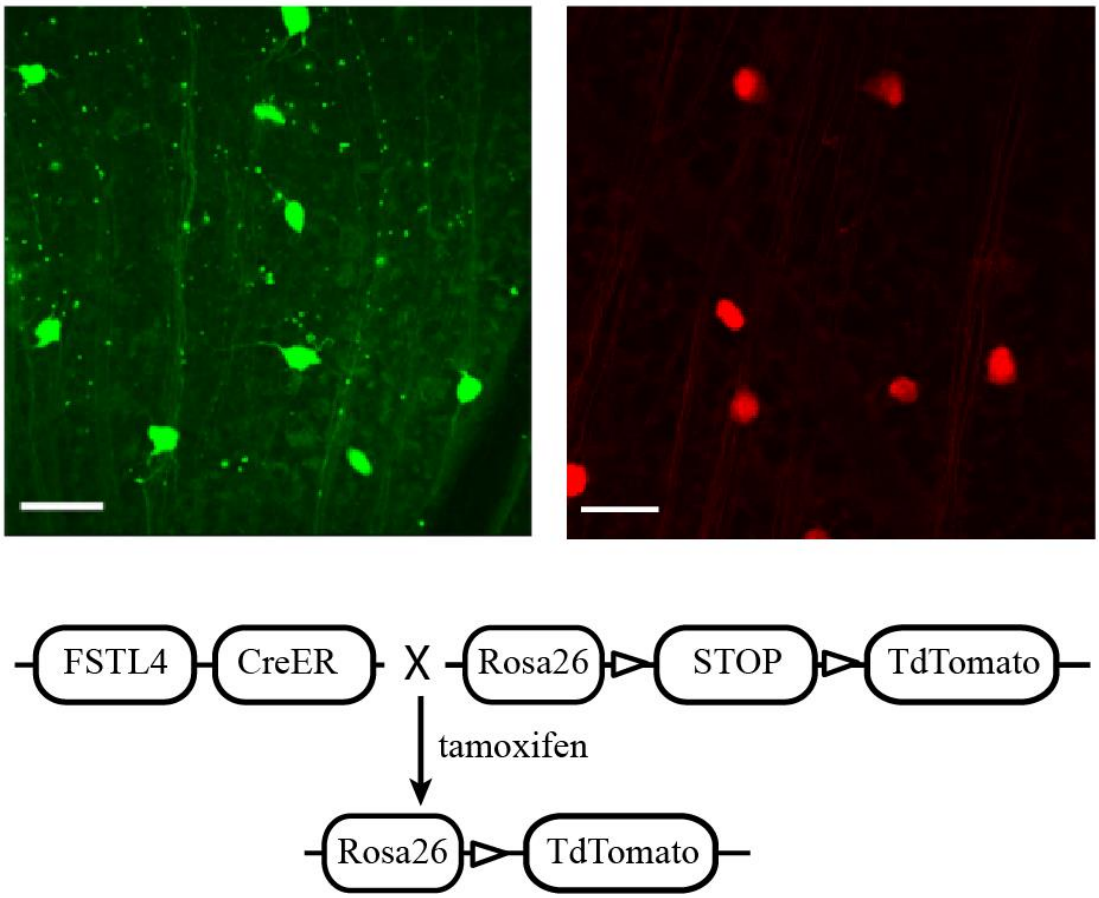

Figure 4. Two transgenic mouse lines label superior-coding DSGCs.
Transgenic mouse lines can be used to visualize subpopulations of retinal neurons. Two-photon imaging of retinal whole-mounts reveals green fluorescent protein (GFP)- or tdTomato-labelled somata.
Chapters two to four investigate signal integration in a population of directionally-selective ganglion cells (DSGCs) which are constitutively labelled in the Hb9::GFP (left) mouse line and conditionally labelled in the FSTL4creER::Ai9flox (right). FSTL4creER mice conditionally express the Cre protein under control of the FSTL4 transcription factor only following the injection of tamoxifen. Cre expression excises the STOP codon, allowing for expression of the fluorescent reporter in Cre expressing neurons.

1.2. Retinal organization establishes circuit function

1.2.1. Discrete neural circuits for different visual tasks

Complex encoding of light stimuli takes place in the retina, prior to information transmission to the brain. This is made possible through numerous parallel retinal pathways, each encoding different features of the visual input. Since the earliest recordings of ganglion cell responses, evidence of such differential encoding have been apparent at the level of retinal output. In the mudpuppy retina (*Necturus maculosus*) Thibos & Werblin (1978) and Werblin & Dowling (1969) demonstrated that some ganglion cells responded to light onset (ON-ganglion cells), while others responded to light offset (OFF-ganglion cells). These responses differed further in exhibiting either transient or sustained response kinetics (Thibos & Werblin, 1978; Werblin & Dowling, 1969). Experiments in ganglion cells of the rabbit retina showed more complex response properties, such as the encoding of stimulus motion, with some ganglion cells responding strongly to visual stimuli moving in one direction, but not others (directionally-selective ganglion cells; Barlow & Hill, 1963). Efforts over the past several decades have expanded upon these studies, leading to the identification of at least 30 types of ganglion cells in the mouse retina, each presumed to be involved in unique tasks (Sanes & Masland, 2015). This suggests at least 30 parallel pathways exist within the retina, even more if we consider the possibility of several outer retinal pathways converging onto single populations of ganglion cells.

Below I will outline several examples of parallel processing across retinal layers, and the mechanisms (molecular or anatomical) that allow the incoming signal to be separated into discrete components. First, I describe how the precise wiring of

photoreceptor types endows the retina with circuits specialized for dim and bright ambient light conditions (1.2.2.1). Then, I will explain how the presence of different glutamate receptors within cone bipolar cells leads to circuits specialized to respond to light onset or light offset (1.2.2.2). Finally, I provide an example of how specific wiring in the inner plexiform layer (specific wiring of inhibitory amacrine cells to ganglion cells) generates additional parallel pathways within the retina, creating ganglion cell circuits specialized to detect movement, indeed motion in particular directions. Importantly, these retinal functions – dim vs bright visual function, ON vs OFF discrimination, and selectivity to specific directions – converge in the directionally selective ganglion cells. These cells form the main area of study in this thesis.

1.2.2. Discrete circuits are established through differential connectivity and receptor expression

1.2.2.1. Dim and bright light circuits are established in the outer retina

The functional complexity of retinal circuits begins at the level of the photoreceptors themselves. Most vertebrate retinas have two types of photoreceptors, rods and cones. Rod photoreceptors are specialized for scotopic conditions (dim ambient light), displaying changes in their membrane potential in response to even single photon absorptions (Baylor *et al.*, 1979; Schneeweis & Schnapf, 1995). Cone photoreceptors are instead specialized for photopic conditions (bright ambient light). Rods and cones are also differentially wired to bipolar cells in the outer plexiform layer, contacting rod- and cone-specific bipolar cells respectively. Thus, photoreceptor diversity, both mechanistically and in their differential wiring to bipolar cell subpopulations, establishes parallel pathways in the outer retina, each suited to different ambient light conditions.

Interestingly, these pathways are not distinguishable in the retinal output, as rod and cone bipolar cells do not contact distinct ganglion cell populations. While cone bipolar cell wiring to ganglion cell circuits is highly specific, as will be described in the following section (1.2.2.2.), rod bipolar cells indirectly provide input to many ganglion cell populations, all of which are also connected to cone bipolar cells. In the inner retina, rod bipolar cells also contact specialized amacrine cells (reviewed in Bloomfield & Dacheux, 2001; Sharpe & Stockman, 1999), which in turn form contacts with several populations of cone bipolar cells (Deans *et al.*, 2002), functionally high-jacking cone pathways. Given that rod and cone pathways are utilized across different light conditions, they nonetheless represent functionally important parallel pathways in the retina.

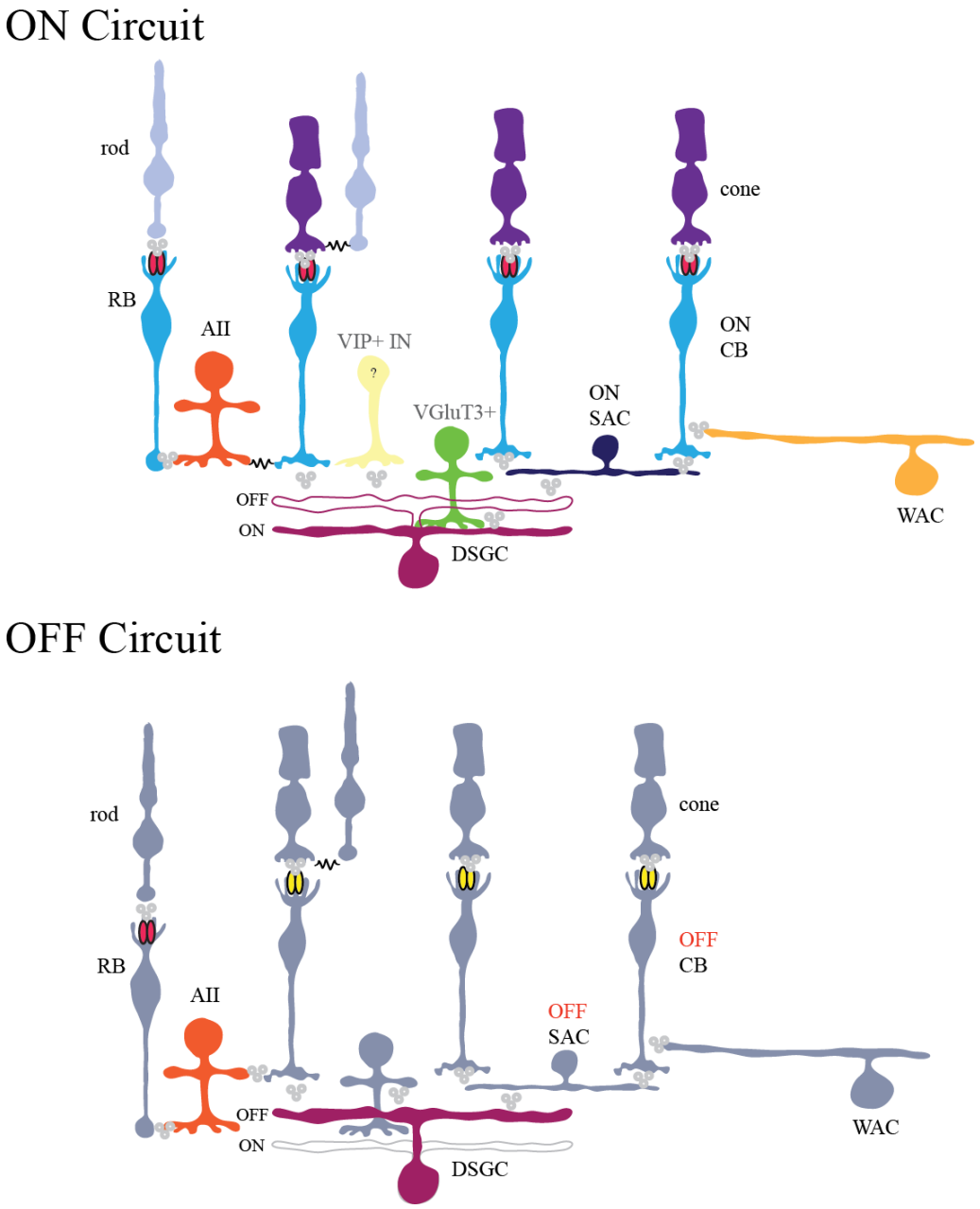

Figure 5. Rod- and cone-mediated ON-OFF direction-selective pathways in the mouse retina.
In bright ambient light conditions, ON and OFF signals are carried separately in the retina. Cones form synapses with ON or OFF type cone bipolar cells (CBCs) which in turn contact DSGC ON and OFF dendritic arbors respectively. ON cone bipolar cells express mGluR6, while OFF cone bipolar cells express AMPA-type glutamate receptors.
In dim ambient light conditions, both ON and OFF signals are carried by rod photoreceptors and rod bipolar cells. Signals are carried to ON cone bipolar cells via gap junctions or OFF cone bipolar cells via glycinergic chemical synapses.
Directionally selective ganglion cells also receive input from ON and OFF type starburst amacrine cells (SACs), which receive inhibitory input from other SACs and wide-field amacrine cells (WACs).
Recent work has also putatively identified VGluT3 amacrine cells and VIP interneurons within the DS circuit.

1.2.2.2. ON and OFF circuits are established in the outer plexiform layer

Stimulus encoding is further refined in the outer retina, with different cone bipolar cells responding to either light onset or light offset. The mechanisms driving these 'ON' and 'OFF' pathways puzzled scientists for several decades. In the 1960's physiological recordings established that photoreceptors depolarize (releasing glutamate) in the dark, and generate graded hyperpolarizations (which reduce glutamate release) in the light (Werblin & Dowling, 1969). The glutamate release from photoreceptors in the dark depolarizes OFF bipolar cells by opening glutamatergic cation channels whereas the light-induced decreases in glutamate depolarizes ON bipolar cells (Werblin & Dowling, 1969). Almost 30 years later it was shown that the ON-bipolar cells express a metabotropic glutamate receptor called mGluR6 (Masu *et al*., 1995). Glutamate release in darkness (in response to photoreceptor depolarization) activates mGluR6, which leads to the closing of TRP channels and the hyperpolarization of ON cone bipolar cells.

Further diversity in retinal circuits arises as a result of additional bipolar cell specializations. When the presence or absence of voltage-gated channels, anatomical stratification within the inner plexiform layer, and the expression of voltage-gated channels are considered, at least eight types of ON bipolar cells and six types of OFF bipolar cells can be identified in the mouse retina (Zeng & Sanes, 2017). These bipolar cell classes differ in their kinetics (Baden *et al.*, 2013; Ichinose *et al.*, 2014) and contrast sensitivities (Odermatt *et al.*, 2012; Poleg-Polsky & Diamond, 2016). Broadly, it is clear that differences in bipolar cell receptor expression, best exemplified by the expression of ionotropic or metabotropic glutamate receptors, establishes parallel complementary pathways within the inner nuclear layer of the retina.

Unlike retinal signalling across ambient light conditions (described in section 1.2.2.1), ON and OFF responses to light stimuli are passed to distinct ganglion cell populations. In some of the first ganglion cell recordings, it was noted that ganglion cells responded to either light onset, light offset, or responded transiently to both the onset and offset of light (ON-OFF ganglion cells; Werblin & Dowling, 1969). It is now clear that such responses are established based on the ganglion cell's specific sampling of cone bipolar cell populations: ON and OFF ganglion cells receive inputs from ON **or** OFF cone bipolar cells respectively, while ON-OFF ganglion cells sample from both ON **and** OFF types of cone bipolar cells.

1.2.2.3. Wiring in the inner plexiform layer further specializes circuit function

Given the diversity of cone bipolar cell and amacrine cell types, differential wiring of these neurons to ganglion cells could substantially increase the number of parallel pathways within the inner retina. Additionally, the complexity of bipolar cell and amacrine cell signalling, an example of which will be detailed below, can also endow ganglion cells with highly specialized response properties. Above I have briefly described how the wiring of ganglion cells to broad categories of bipolar cells (ON or OFF cone bipolar cells) endows ganglion cells with certain features of their light response, the ability to respond to light onset, light offset, or both. Here, I will focus instead on the wiring of amacrine cells to ganglion cells to demonstrate how these neurons endow retinal circuits with additional complexity.

While an accurate account of the number of amacrine cell types is complicated by our incomplete understanding of amacrine cells wiring specificity, studies in rabbit and cat have suggested at least 22, and upwards of 60 amacrine cell types exist in the

mammalian retina (Macneil *et al.*, 1999; Macneil & Masland, 1998; Vaney, 1990). Variation among amacrine cell types involves dendritic arbors, which range in length from tens of microns to several millimeters, and may extend processes in single or multiple sublamina of the inner plexiform layer (Macneil *et al*., 1999). Amacrine cells also differ in the neurotransmitters they release, releasing glycine, GABA, acetylcholine (ACh), dopamine (DA), or some combination of the above (for review see Vaney, 1990). In addition, amacrine cells have been shown to contact ganglion cells, bipolar cells and other amacrine cells (see Grimes, 2012; Zhang & McCall, 2012 for reviews). Amacrine cell signalling is therefore complex, with amacrine cell wiring able to establish feedforward (two excitatory synapses in series) or feedback (excitatory synapse from BCs to amacrine cells, which in turn inhibit BCs) networks within the inner plexiform layer.

1.2.2.3.1. Direction-selectivity is established in the inner plexiform layer

Starburst amacrine cells (SACs) are the best characterized amacrine cells in the mouse retina. This is a result of their abundance and their easy identification, due to their characteristic “star-like” morphology and unique expression of choline acetyltransferase (Famiglietti, 1983; Famiglietti, 1985; Masland & Mills, 1979). As is the case for most medium-field amacrine cells, synaptic inputs and neurotransmitter release mechanisms occur in close proximity within SAC dendrites (Famiglietti, 1991). SACs receive excitatory glutamatergic input from cone bipolar cells (Chen *et al.*, 2014) as well as inhibitory input from other SACs (Lee & Zhou, 2006; Munch & Werblin, 2006), and release both ACh and GABA (O’Malley & Masland, 1989; O’Malley *et al.*, 1992), though likely via distinct mechanisms (O’Malley *et al*., 1992). Interestingly however,

SAC dendrites are highly specialized. Starburst amacrine cell dendrites are highly directional. Landmark calcium imaging studies of SAC dendrites by Euler, Detweiler and Denk (2002) revealed strong calcium signals in individual SAC dendrites if the light stimulus moved in the direction of the cell soma to dendrites (i.e., centrifugally), but not when the stimulus moved from the dendrites toward the soma (centripetally). While the mechanisms for this direction selectivity are unclear (but see Vlasits *et al*., 2016), the implications for ganglion cell signalling have been extensively documented. The direction-selectivity of SACs provides four subpopulations of ganglion cells with the ability to respond preferentially to stimulus motion, with different subpopulations responding preferentially to one of the four cardinal directions (Briggman, Helmstaedter, & Denk, 2011; Yoshida *et al*., 2001; Barlow & Hill, 1963).

The relationship between SAC release of GABA and direction selectivity of ganglion cells remained incompletely understood until very recently. Early voltage-clamp experiments revealed a role for inhibition in establishing direction selectivity, by demonstrating that inhibition to DSGCs was asymmetric (Fried *et al.*, 2002; Yoshida *et al*., 2001). Work by Briggman and others (2011) revealed this asymmetry occurs as a result of the specific wiring of SACs to DSGCs, with dendrites in each SAC quadrant forming synapses with only one population of DSGCs. This wiring allows for GABAergic release from a population of SAC dendrites onto a given DGSC population only in response to stimulus motion along a given direction, that which maximally excites those SAC dendrites.

Thus the unique physiological properties and anatomical wiring of SACs, endows the retina not only with the ability to encode direction, but establishes several parallel

pathways within the inner plexiform layer, each specialized for motion along a given cardinal direction. This is only one example of how amacrine diversity and connectivity establishes parallel ganglion cell pathways, each specialized for unique visual features.

1.3. Signal integration is expanded through sub-cellular features

Above I described several examples of how specific wiring (i.e. interactions among a subset of retinal neurons) endows the retina with important specializations. I will now focus on two sub-cellular mechanisms, voltage-gated sodium channels and gap junctions, both widespread in the retina, which also contribute to the specificity of retinal circuits. I will provide an overview of the diversity and distribution of sodium channels and gap junctions, which will be discussed more thoroughly in the chapters that follow. I will subsequently provide examples of the role these features play in retinal encoding.

1.3.1 Voltage-gated Na^+ channels in the retina

Voltage-gated sodium channels (Na^+ channels) are transmembrane proteins that conduct sodium ions (Na^+) through the plasma membrane when activated by membrane depolarization. Na+ channels are a common feature of excitable cells, as they are required for the membrane depolarization associated with action potential generation. However, while early physiological recordings revealed action potentials in retinal ganglion cells, action potentials were largely absent from other cell classes (Werblin & Dowling, 1969). As such, Na^+ channels have been considered largely absent in retinal neurons, with the exception of ganglion cells.

Na^+ channel expression has however since been demonstrated, to varying degrees, in nearly all major classes of retinal neurons. The distribution (across and within cell

types) and functions of these channels will be described below. Nine voltage-gated Na^+ channel isoforms are known in mammals (Goldin *et al*., 2000), all members of the same voltage-gated Na^+ channel gene subfamily (Nav1). These isoforms are ordered from Nav1.1 to Nav1.9 (Catterall *et al.*, 2005). The functional properties of these Na^+ channels are similar when compared to the diversity other voltage-gated superfamilies (Kv, Cav) however, of importance for physiological experiments, these channels differ in their sensitivity to tetrodotoxin (TTX). Nav1.1, Nav1.2, Nav1.3, Nav1.4, Nav1.6 and Nav1.7 are sensitive to TTX (EC_{50}=1 nM-12nM), while Nav 1.5, Nav1.8 and Nav1.9 are TTX-resistant (EC_{50}=16-60mM; Catterall *et al*., 2005).

1.3.1.1. Na^+ channels in the outer retina

Human photoreceptors (rod and cones) require Na^+ channel activity, in addition to graded potentials, to fire action potentials that selectively amplify OFF responses (Kawai *et al.*, 2001). However while spiking has been demonstrated in the photoreceptors of primates and lizards (Bader *et al.*, 1982; Schneeweis & Schnapf, 1995; Yagi & Macleish, 1994), spiking has not been observed in rodent photoreceptors, with the exception of a brief role for photoreceptor Na^+ channels in retinal development (Cote *et al*., 2005). Anatomically, some evidence of Nav1.6 (Cote *et al*., 2005) and Nav1.9 (O'Brien *et al*., 2008) immunoreactivity has been demonstrated in mice, however this reactivity is much weaker than for other cell classes, and no evidence for Na^+ channels in photoreceptors was evident when retinas were labelled with non-isoform specific antibodies (Cote *et al*., 2005; Mojumder *et al.*, 2007). Further work will therefore be needed to conclusively determine the extent of Na^+ channel activity in rodent photoreceptors.

Stronger evidence exists for the presence of Na^+ channels in subtypes of bipolar cells. In goldfish, reverse transcriptase-PCR revealed four isoforms of Na^+ channels in bipolar cells, corresponding most closely to mammalian Nav1.1, Nav1.2, Nav1.3 and Nav1.6. In primates, at least one isoform, Nav1.1, is found in bipolar cells, and a role for such Na^+ channels has been demonstrated in augmenting excitatory inputs to specific ganglion cell pathways (Puthussery *et al.*, 2013). While the specific identity of Na^+ channels in rodent bipolar cells has been poorly studied, Na^+ channel currents have been detected in isolated bipolar cells (Pan & Hu, 2000) and several roles for such channels have been proposed. First, response kinetics of bipolar cells subpopulations have been shown to differ vastly, with several populations of bipolar cells exhibiting "spike-like" events. Differential expression of Na^+ channels across bipolar cell subpopulations has been proposed to account for such differences (Baden *et al.*, 2011; Baden *et al.*, 2013). Second, in ground squirrel (*Ictidomys tridecemlineatus*), one subpopulation of bipolar cells exhibits a TTX-sensitive current, and has been shown to play an important role in enhancing response amplitude and reliability for rapid changes in luminance (Saszik & DeVries, 2012). Both of these roles will be explored in greater detail in Chapter 4.

1.3.1.2. Na^+ channels in the inner retina

In amacrine cells, a large body of work has emerged surrounding the expression and functional importance of Na^+ channels. While the prevalence of Na^+ channels across amacrine cell populations is not yet clear, largely owing to the difficulties of identifying amacrine cell subtypes, several important and well-studied amacrine cell populations appear to utilize Na^+ channels. AII amacrine cells, which couple the rod pathway to cone bipolar cells, possess clusters of Na^+ channels on processes similar to an axon initial

segment (Wu *et al.*, 2011). Here Na^+ channels, specifically Nav1.1 (Kaneko & Watanabe, 2007), generate spike-like events (Boos *et al.*, 1993; Wu *et al.*, 2011), important for amplifying responses during dim light conditions (Tian *et al.*, 2010). Wide-field amacrine cells responsible for the inhibitory surround of several ganglion cell populations (Cook *et al.*, 1998; Flores-Herr *et al.*, 2001; Taylor, 1999) also exhibit Na^+ channel dependent spiking (Farrow *et al.*, 2013; Hoggarth *et al.*, 2015; Taylor, 1999). This may be necessary for neurotransmitter release given the long (2-3mm) dendritic arbors of these neurons (Bloomfield, 1996). Finally, starburst amacrine cells (SACs), of critical importance in the encoding of stimulus motion, also have Na^+ channels (Cohen, 2001; Kaneda *et al.*, 2007). SAC Na^+ channels play an important in establishing the SACs' centrifugal direction preferences (Oesch & Taylor, 2010), as discussed above (1.2.2.3.1). These channels however, unlike those found in wide-field and AII amacrine cells, appear to be TTX-insensitive (Mojumder *et al.*, 2007; Oesch & Taylor, 2010).

Na^+ channels are also common in ganglion cells, with six Na^+ channel isoforms found across ganglion cell types (Boiko *et al.*, 2001; Fjell *et al.*, 1997; O'Brien *et al.*, 2008; Van Wart *et al.*, 2007). While the presence of Na^+ channels in ganglion cells, which fire classical action potentials, is not surprising, an important finding is the evidence of Na^+ channels in dendrites of retinal ganglion cells. These Na^+ channels are able to initiate dendritic spikes (Oesch *et al.*, 2005; Sivyer & Williams, 2013; Velte & Masland, 1999), which can reliably generate somatic action potentials (Oesch *et al.*, 2005; Trenholm *et al.*, 2014). Functionally, these dendritic spikes have been shown to play important roles in direction tuning of directionally-selective ganglion cells (Oesch *et*

al., 2005; Sivyer & Williams, 2013). Further roles for Na^+ channels in the dendrites of DSGCs will be explored in Chapter 3.

Given the complex, and circuit specific functions of Na^+ channels, particularly in the inner retina, it is clear that retinal pathways, such as those that encode motion, are further refined by such sub cellular features.

1.3.2. Electrical coupling in the retina is extensive

Gap junctions, which are pore-like structures within and between the membranes of adjacent neurons, form the physical basis of electrical synapses (described further in 1.3.2.1). As such, I use the terms 'electrical synapse' and 'gap junction coupling' interchangeably in this dissertation. The vast majority of electrical synapses, the only ones we will discuss here, are membrane-to-membrane trans-cellular channels called gap junctions.

1.3.2.1. Structure and biophysical properties of gap junctions

Gap junctions are composed of two hemichannels called connexons, one located in each apposing membrane (**Figure 7**). Connexons form a channel that connects the cytoplasm of neighbouring cells, allowing the passage of cations, anions, second messengers and metabolites up to 1 kDa (for review see Sernagor *et al.*, 2001). This allows for the direct and rapid passage of electrical current between coupled neurons (compared to indirect and slower signal transmission via chemical synapses).

Six transmembrane protein subunits called connexins comprise each connexon. So far, 20 connexin isoforms have been identified in mice, and 21 in humans (Söhl *et al.*, 2000), the names of which are assigned based on their approximate molecular weight in kilodaltons. Connexons are typically composed six identical connexin subunits

(homomeric), however evidence exists for connexons composed of multiple connexin subunits (heteromeric). Similarly, gap junctions can be formed of two identical connexons (homotypic) or connexons of different subunit makeups (heterotypic). For simplicity we will focus here primarily on homomeric homotypic gap junctions.

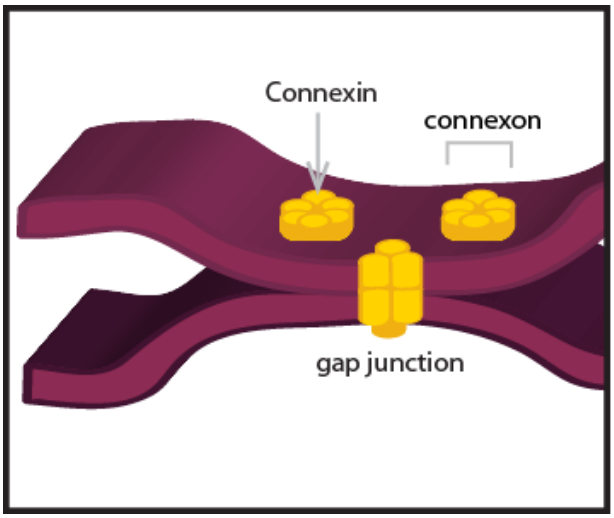

Figure 6. Gap junction structure.
Gap junctions are formed from two connexon hemi-channels, one in each apposing membrane. Each connexon is formed from six identical (homotypic) or non-identical (heterotypic) connexin protein subunits.

All gap junctions exhibit low-pass filter characteristics, preferentially transmitting low-frequency information (slow depolarizing or hyperpolarizing currents) while high-frequency information (including action potentials) is attenuated. This is a result of the resistance of the gap junction as well as the capacitance and resistance of the postsynaptic membrane. Here, the term “post-synaptic” membrane is a matter of perspective as electrical synapses are bilateral. In this dissertation I use the term post-synaptic, or post-junctional, to mean the cell which is receiving the electrical input. The pre-junctional neuron is often the neuron which first fires an action potential.

More specific physiological properties of gap junctions vary significantly across connexin isoforms. Single-channel (unitary) conductances of gap junctions for example, span a large range. Connexin 36 (CX36) (Teubner *et al.*, 2000) and CX45 (Moreno *et al.*, 1995) display only moderate conductances (10-15 pS) while the unitary conductance of CX50 is several fold larger (220 pS) (Manthey *et al.*, 1999). Connexin isoforms are also differentially sensitive to membrane voltage and transjunctional voltage, or the voltage difference between coupled neurons. Sensitivity to membrane voltage presents much like the voltage dependence of voltage-gated ion channels, with some connexin isoforms requiring post-synaptic depolarization to elicit significant conductance (Verselis *et al.*, 1991). Sensitivity to transjunctional voltage is independent of the absolute voltage of either coupled neuron. Curiously, most vertebrate gap junctions are sensitive to transjunctional voltage, exhibiting maximal conductance when $V_j = 0$ (Vj is the voltage difference between both cells) and declining as V_j increases in either direction. Among the connexin isoforms, CX36 channels are the least sensitive to transjunctional voltage, with conductance decreasing by less than half for even very large deviations ($V_j \pm 100$ mV) (Srinivas *et al*., 1999; Teubner *et al*., 2000). Some gap junction subunits exhibit gap junction closure (homologous to the inactivation of voltage-gated ion channels). CX45 exhibit significant closure within several hundred milliseconds of membrane depolarization (Barrio *et al.*, 1997). CX36, however, does not exhibit significant closure even over several milliseconds. Finally, gap junction molecular identity influences their permeabilities, with some isoforms more permeable to cations, and other to anions (reviewed in Harris, 2001), a feature that translates to the differential permeability of various fluorescent dyes.

The molecular makeup of gap junctions therefore has significant implications for gap junction biophysics, which in turn influences the roles served by gap junctions across cell types. In Chapter 2 we will utilize such differences to aid in the identification of gap junctions between a population of electrically coupled directionally-selective ganglion cell. First however, in the following paragraphs, I will discuss gap junction distribution in the retina, their isoform specificity, as well as several functions served by gap junctions.

1.3.2.2. Organization of gap junctions in the retina

Electrical coupling has been demonstrated in all five major retinal cell classes (Vaney, 2002), making the retina highly coupled relative to other areas of the central nervous system. Gap junctions are also highly diverse, with over 15 connexin isoforms found in the retina (Bolte *et al*., 2016). In the outer retina, gap junctions couple rods, cones and horizontal cells (**Figure 8**).

Gap junctions between horizontal cells were the first to be identified in the retina, prior even to the use of the term "gap junction" (Yamada & Ishikawa, 1965). This coupling is mediated by CX50- (Hombach *et al.*, 2004) or CX57-containing gap junctions (Shelley *et al*., 2006) and is so extensive that horizontal cell receptive fields can be up to 25 times larger than their individual dendritic arbours (Bloomfield *et al.*, 1995). Significant evidence exists to support the idea that these large receptive fields are responsible for establishing the inhibitory surround of some bipolar cell types (for review see Thoreson & Mangel, 2012). Such lateral signal transfer would seem problematic for rods and cones (or any excitatory retinal neurons), as it would reduce the acuity of the visual signal. Indeed coupling between cones does reduce visual acuity, however it provides the benefit of significantly increasing the signal-to-noise ratio of cone signalling

(by up to 80%; Devries *et al.*, 2002). Given that blurring of visual image already occurs on a larger scale simply due to the optics of the eye, the benefit of gap junctions in the reduction of noise far outweigh the consequences of a loss in acuity (Devries *et al.*, 2002). Similarly, coupling between neighbouring rod photoreceptors, while spreading information laterally across the retina, allows for the pooling of information during conditions with minimal light, which otherwise may not drive measureable signals in rod pathways.

Interestingly, rod pathways rely heavily on gap junction coupling for signal transmission at many levels in addition to rod-rod "binning" of weak hyperpolarizing signals (see Bloomfield & Völgyi, 2009 for review). As rod bipolar cells do not directly contact ganglion cells, rod pathways must utilize gap junctions between AII amacrine cells and ON cone bipolar cells, as well as gap junctions between rod and cone photoreceptors (**Figure 7**) to repurpose the cone circuit in order to transmit information to the inner retina. The subunit composition of connexons in rods is not known (Bolte *et al*., 2016) however cone connexons are composed of CX36. AII amacrine cells also utilize CX36, forming homotypic or heterotypic gap junctions (contacting CX45-containing subunits) with cone bipolar cells (Deans *et al.*, 2002; Feigenspan *et al.*, 2001).

In the inner retina, gap junctions couple neighbouring amacrine cells, neighbouring ganglion cells, amacrine cells and ganglion cells, as well as amacrine cells and bipolar cells (as described above for the AII amacrine cell). Gap junctions between amacrine cells have been described in several vertebrate populations, including salamander (MacLeish & Townes-Anderson, 1988), rat (Chun *et al.*, 1993) and rabbit (Bloomfield & Volgyi, 2007; Li *et al.*, 2002; Wright & Vaney, 2004; Xin & Bloomfield,

1997). Extensive coupling has also been shown between mouse amacrine cells and ganglion cells (Völgyi *et al.*, 2009), with 14 or 22 ganglion cell types exhibiting coupling to amacrine cells. The purpose of such coupling is however poorly understood, in part due to the great functional and anatomical diversity of amacrine cell populations. Further complicating the story, three connexin isoforms have been identified thus far in amacrine cell subpopulations: CX45 (Dedek *et al.*, 2009), CX36 (Kihara *et al*., 2009) and CX43 (Janssen-Bienhold *et al.*, 1998). One well-studied exception however, is the homologous coupling of AII amacrine cells. Gap junctions formed of CX36 subunits (Feigenspan *et al.*, 2001) allow for spatial averaging (Vardi & Smith, 1996) across AIIs, a feature important for increasing the signal-to-noise ratio of the rod pathway (Bloomfield & Völgyi, 2004; Smith & Vardi, 1995; Vardi & Smith, 1996; Volgyi, 2004).

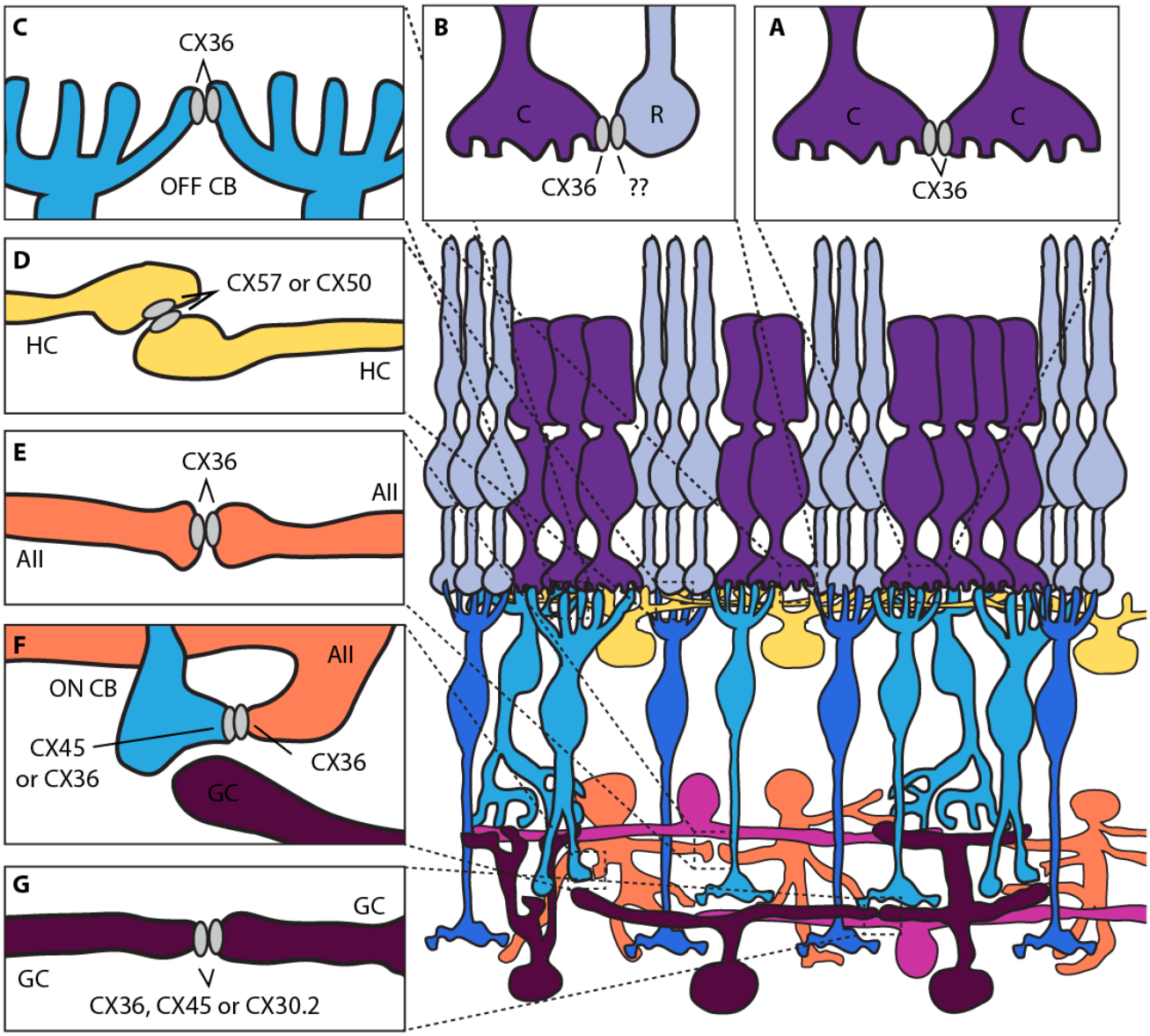

Figure 7. Gap junctions in the mouse retina.
Gap junctions in the mouse retina have been observed between rods, cones (a), rod and cones (b), OFF cone bipolar cells (CBs; c), horizontal cells (HCs; d), AII amacrine cells (AIIs; e), AIIs and ON CBs (f), ganglion cells (GCs; g), and ganglion cells and amacrine cells.
Gap junctions in photoreceptors are comprised of CX36 in cones, and an unknown connexin in rods. CX36 is also critically important for the coupling homologous coupling of OFF cone bipolar cells (c) and AII amacrine cells (e). AII CX36-containing gap junctions also couple AII amacrine cells to ON cone bipolar cells. This coupling may be homotypic or heterotypic, with ON CB gap junctions composed of either CX36 or CX45. Horizontal cell dendrites are extensively coupled by CX57 containing gap junctions, though some evidence exists for CX50 expression in some horizontal cell populations. Ganglion cell coupling, to other ganglion cells or amacrine cells, varies greatly across ganglion cell populations. Coupling can be heterologous or homologous, homotypic or heterotypic, and thus far ganglion cell gap junctions have been shown to contain CX36, CX45 and CX30.2.

1.3.2.3. Established roles for gap junction coupling in directionally-selective ganglion cells

Gap junctions have been studied in the superior-coding directionally-selective ganglion cells (sDSGCs), an electrically coupled population of ganglion cells, which respond preferentially to stimulus motion in the superior (i.e. upwards in the visual field) direction. The first evidence for gap junction coupling in superior-coding DSGCs was the labelling of neighbouring sDSGCs following the injection of a gap-junction permeable tracer into a single sDSGC. These experiments were performed in a mouse model in which sDSGCs are labelled with green fluorescent protein (GFP; Hb9GFP mouse line), allowing for the confirmation that sDSGCs were coupled only to other sDSGCs, and not to other ganglion or amacrine cell populations (Trenholm *et al.*, 2013a; Trenholm *et al.*, 2013b). The presence of gap junctions between ganglion cells was previously hypothesized to compromise visual acuity, however gap junctions between superior-coding DSGCs exhibit only moderate conductances (~1 nS; Trenholm *et al.*, 2013). This is consistent with the observation that the connexin subunits found in ganglion cells include CX45 and/or CX36 subunits (Degen *et al*., 2004; Güldenagel *et al*., 2000), which as mentioned display only moderate conductances. The molecular composition of sDSGC gap junctions will be the focus of Chapter 2.

Measurements of the receptive field of coupled DGSCs, based on ganglion cell spiking activity, also confirmed that gap junctions did not significantly expand the receptive field further than the spatial extent of sDSGC dendrites (Trenholm *et al*., 2013a). However, whole-cell patch clamp recordings revealed gap junctions endowed sDGSCs with expanded subthreshold fields, which become important in the context of moving stimuli (Trenholm, *et al*., 2013). At high stimulus speeds, such subthreshold

receptive fields endow sDSGCs with the ability to respond to moving stimuli much sooner than in the absence of gap junction coupling, providing an accurate representation of stimulus spatial location, a feature called lag normalization (Trenholm *et al*., 2013b).

An additional role previously attributed to gap junction coupling, is spike synchrony between the spike trains of neighbouring ganglion cells. In Chapter 3, I investigate the presence of correlated activity between sDSGCs, and explore the mechanisms by which small gap junction conductances can significantly influence spike timing.

In assessing the influence of gap junctions on coupled DSGCs alone, it is clear that gap junctions endow retinal circuits with enhanced complexity, further specializing retinal circuits.

1.4. Signal integration within the DS circuit

In the sections above I have provided numerous examples of how individual cell types can be specialized, establishing parallel pathways within the retina. Section 1.2.2.1. discussed how rods and cones are sensitive to different light intensities. Cone bipolar cells, as described in section 1.2.2.2., respond to either light onset or offset based on their specific expression of glutamate receptors. I also described, in section 1.3, how retinal cell subclasses can be further specialized based on their differential expression of gap junctions and voltage-gated channels. What I have not discussed thus far, is the complexity that arises when several of these specializations exist within individual retinal circuits. Specifically, how several pre-synaptic inputs, each specialized to different features of the visual scene, are integrated within post-synaptic neurons. Below, I will consider the superior-coding direction selective ganglion cell circuit. I will describe the

multiple specialized inputs that converge on these neurons, and discuss what I have learned about how these diverse signals are integrated. I will also describe how these distinct inputs are differentially recruited under different stimulus conditions, and the consequences of such differences on ganglion cell signalling.

1.4.1. Chemical and electrical inputs to DSGCs

Directionally-selective ganglion cells receive glutamatergic, cholinergic and GABAergic chemical input, via distinct chemical synapses, in addition to receiving electrical input via gap junctions. As previously discussed (see section 1.2.2.3.1), inhibitory GABAergic input is provided by starburst amacrine cells (SACs), and plays a critical role in establishing DGSC directional preferences. Starburst amacrine cells, however, are also cholinergic (Vaney & Young, 1988; O'Malley & Masland, 1989; Brecha *et al.*, 1988; Massey & Neal, 1979; Massey & Neal, 1983), releasing acetylcholine onto DSGCs. Acetylcholine and GABA are packaged into distinct neurotransmitter vesicles within SAC release sites, and may exhibit distinct release mechanisms (O'Malley *et al*., 1992). Whether this translates to directional or non-directional release of acetylcholine however remains controversial (Brombas *et al.*, 2017; Grzywacz *et al.*, 1998; Lee *et al.*, 2010; Pei *et al*., 2015). Glutamatergic input to DGSCs is provided by bipolar cells of at least two subtypes (type 5 and type 7) (Helmstaedter *et al*., 2013). As will be discussed further in Chapter 4, differential receptor and channel expression can impart bipolar cell subpopulations with unique response kinetics. Glutamatergic signalling at the bipolar cell-DSGC synapse is further complicated by the expression of two glutamate receptors in DSGC dendrites, NMDA- and AMPA-type receptors (Sethuramanujam *et al*., 2016). These receptors differ in their gating properties,

with NMDA receptors requiring not only the binding of glutamate but also post-synaptic depolarization for channel opening. In addition to these chemical inputs, as described in section 1.3.2.3, superior-coding DSGCs also receive electrical input from other superior-coding DGSCs (Trenholm *et al.*, 2013; Trenholm *et al.*, 2013).

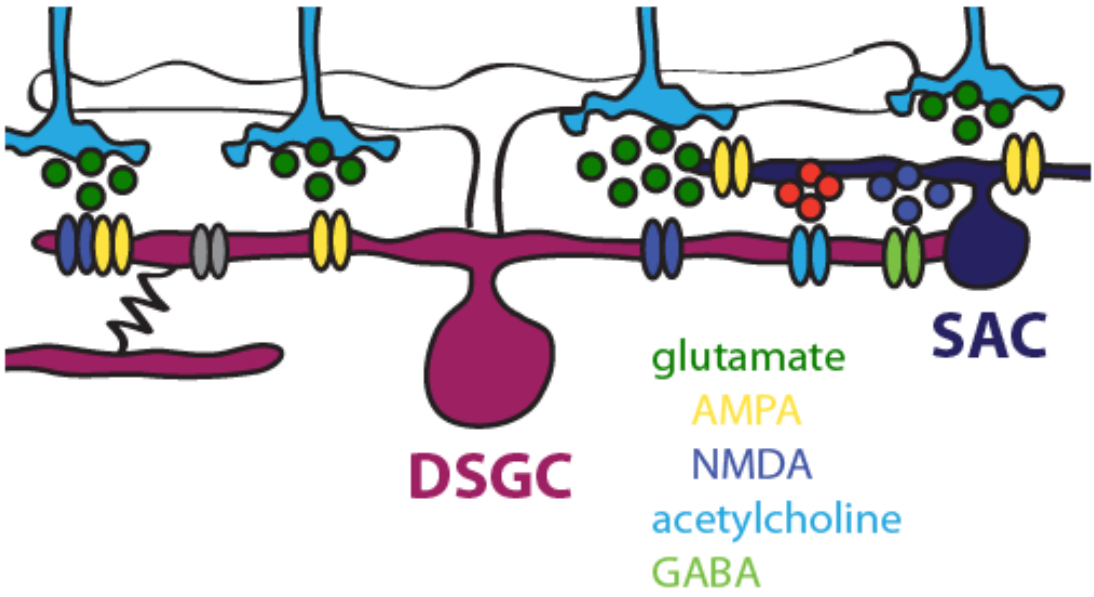

Figure 8. Chemical and electrical inputs to the directionally-selective circuit. Directionally-selective ganglion cells (DSGCs) receive glutamatergic input from ON and OFF cone bipolar cells (only the ON inputs are shown for simplicity). Glutamate binds to post-synaptic NMDA or AMPA receptors on DSGC dendrites. DSGCs also receive cholinergic and GABAergic input from starburst amacrine cells (SACs), which contact post-synaptic nicotinic acetylcholine receptors and ionotropic $GABA_A$ receptors respectively. SACs are excited pre-synaptically by glutamate release from bipolar cells onto post-synaptic AMPA receptors. Of the four populations of DSGCs, only sDSGCs are gap junction coupled to one another. These neurons, therefore, receive electrical input in addition to the excitatory and inhibitory chemical input.

1.4.2. Inputs are differentially recruited based on stimulus properties

DSGC inputs are differentially recruited based on the stimulus conditions, with all inputs to DGSCs exhibiting some degree of stimulus tuning. While spatial frequency, temporal frequency, and ambient light levels all have important consequences for

neuronal activation and transmitter release, I will focus only on a two visual features: stimulus direction of motion and stimulus contrast. Stimulus tuning of individual neurons within the DS circuit not only affects the absolute strength of the various inputs to sDSGCs, but also the relative strength of these inputs to each other.

GABA: The strong release of GABA from starburst amacrine cell dendrites in response to stimulus motion along the DSGC null direction, and weak release of GABA for stimulus motion along the preferred direction, is perhaps the most obvious example of stimulus specificity within the DS circuit (Taylor *et al.*, He *et al.*, 2000; Yoshida *et al*., 2001). Static stimuli drive GABA release intermediate to preferred- and null-direction motion (McLaughlin *et al.*, unpublished data). GABAergic input to DSGCs can therefore be modulated using stimulus motion and the direction of such motion.

Acetylcholine: Significant controversy exists over whether cholinergic input to DSGCs is directional (Brombas *et al.*, 2017; Grzywacz *et al.*, 1998; Lee *et al.*, 2010; Pei *et al*., 2015). Work from our group however suggests sDSGCs receive cholinergic input in response to both preferred and null directions of motion.

Acetylcholine and GABA: Our most recent work also suggested that cholinergic and GABAergic inputs to DSGCs are significantly more sensitive to contrast than glutamatergic inputs (Sethuramanujam *et al*., 2016). Both acetylcholine and GABAergic inputs produced measurable currents in DSGCs at contrasts which elicited no glutamatergic currents. Acetylcholine therefore provides the most important excitatory drive to DSGCs near contrast threshold, and these stimulus conditions can be used to preferentially recruit cholinergic inputs, often otherwise occluded by the large

glutamatergic currents generated at higher contrasts (Fried *et al.*, 2005; Lee *et al*., 2010; Park *et al.*, 2014).

Glutamate: Consistent with work in other retinal circuits (Beaudoin *et al.*, 2008; Burkhardt & Fahey, 1998; Odermatt *et al.*, 2012), glutamatergic inputs to sDSGCs also appear to differ in their sensitivity to stimulus contrast (Sethuramanujam *et al.*, 2016, 2017). Our recent work suggested sDSGCs receive input from both high- and low-sensitivity bipolar cells, whose threshold contrasts differed by over a log unit (Sethuramanujam *et al*., 2017). The relative sensitivities of these glutamatergic inputs will be explored in greater detail in Chapter 4, as well as the possibility that these bipolar cells contact different post-synaptic glutamate receptors (NMDA and AMPA respectively).

Gap junction inputs: Finally, electrical input to superior-coding DGSCs exhibit some degree of stimulus-tuning. Simplistically, depolarizing electrical input to DSGCs will be maximal when neighbouring coupled DSGCs are strongly stimulated, and will be minimal when neighbouring neurons are weakly stimulated. Therefore, large or moving spots could increase electrical inputs to DSGCs, while small static spots would be likely to result in minimal excitatory input. However, the effect of stimulus motion on gap junction currents is much more complex. Gap junction currents are passed equally between cells for preferred and null directions of motion, and gap junctions between DGSCs do not exhibit voltage-dependent conductances (Trenholm *et al*., 2013; see Chapter 2). When visual stimuli are moved across the retina, resulting in the stimulation of several DSGCs in sequence, gap junction input is more effectively transmitted from coupled DSGCs upstream than those downstream (Trenholm *et al.*, 2013). I previously

suggested these changes are the result of activity-dependent changes in the post-synaptic membrane that arise during spiking responses, such as the apparent increase in spike threshold (Benison *et al.*, 2001; Kim & Rieke, 2003; Wang *et al.*, 1998). Stimulus motion therefore affects the effectiveness of gap junction inputs, a feature I investigate further in Chapter 3.

1.5. Summary and research questions

1.5.1. Summary

The retina has been extensively studied by anatomists and physiologists alike, in large part because of its accessibility. Retinal preparations are easily dissected, the layered structure allows for easy identification of cell types, and the whole-mount retinal preparation allows for physiologically relevant stimulation as well as easy access for electrophysiological recordings. Transgenic mouse lines provide the additional advantage of easy identification of retinal subtypes. The retina is composed of five major cell types: photoreceptors, horizontal cells, bipolar cells, amacrine cells, and ganglion cells. Information is transmitted from photoreceptors, via glutamatergic synapses, to bipolar cells, which in turn form excitatory glutamatergic synapses onto ganglion cells (with the exception of rod bipolar cells; see **Figures 2 and 6**). Along the way, signals are shaped by inhibitory signalling from two interneuron populations (horizontal cells and amacrine cells, the latter of which are occasionally excitatory), as well as electrical signalling through gap junctions. Following signal integration, ganglion cells transmit all information about the visual scene to higher order visual centers, through the transmission of action potentials along the optic nerve.

Visual information is heavily processed prior to ganglion cell output. Beginning in the outer retina, visual information is distributed into parallel pathways, each specialized for different visual tasks. Above, I have described how differential expression of Na^+ ion channels across cell types or subtypes endows circuits with specific features. The wiring of the retina also relies heavily on electrical synapses, formed by gap junctions. Gap junctions, hexameric structures composed of transmembrane connexin protein subunits (**Figure 7**), exist within all layers of the retina (**Figure 8**), and impart retinal circuits with several important functions (Bloomfield & Völgyi, 2009). Connexin proteins, of which there are over 15 types in the retina (Bolte *et al*., 2016), differ significantly in their biophysical properties (Bennett & Verselis, 1992), providing further specificity to retinal circuits. Recent work has identified that a single subpopulation of DGSCs, those coding for superior motion, express gap junctions (Trenholm *et al.*, 2013) in addition to receiving the glutamatergic (via bipolar cells), cholinergic and GABAergic (both via SACs) inputs common to all DSGC populations (**Figure 9**). This complex wiring provides a unique opportunity to study the integration of multiple excitatory signals within a single cell population, and to assess how such inputs are differentially recruited in response to varying visual stimuli.

In this dissertation, I study multiple excitatory inputs to a single circuit, the superior-coding directionally-selective ganglion cell circuit, and how these inputs interact. I hypothesize that specializations within the DS circuit, either pre- or post-synaptically can impart DSGCs with additional computational features. Additionally, I predict that interactions between specialized inputs have important consequences for spiking output.

1.5.2. Introduction to research questions

This dissertation examines electrical and chemical input to superior-coding directionally-selective ganglion cells. In Chapter 2, I characterize electrical coupling of DSGCs through the identification of the molecular composition of DSGC gap junctions (**Figure 10**).

Using physiological and immunohistochemical methods in several transgenic mouse lines (differing in their connexin expression), I demonstrate an important role for CX36 in sDSGC coupling. Next (Chapter 3), I investigated interactions between electrical and chemical inputs in DSGC dendrites. Using a paired recording strategy, I show that coincident chemical and electrical input leads to the generation of correlated spike activity, a feature common of many electrically coupled networks, for whom the underlying mechanisms were previously unclear. In Chapter 4 of my dissertation, I focus on the excitatory chemical inputs to DSGCs. As our previous work demonstrates differences in the contrast sensitivities of glutamatergic inputs to DSGCs and SACs, I attempt here to characterize these differences, and investigate the underlying mechanisms. I provide evidence that specific bipolar cell subpopulations, those upstream of SACs, express Na^+ channels likely responsible for enhanced contrast sensitivity.

Altogether, this dissertation further characterises the well-studied directionally-selective circuit. I posit novel mechanisms and provide evidence for a specific role for each in visual coding.

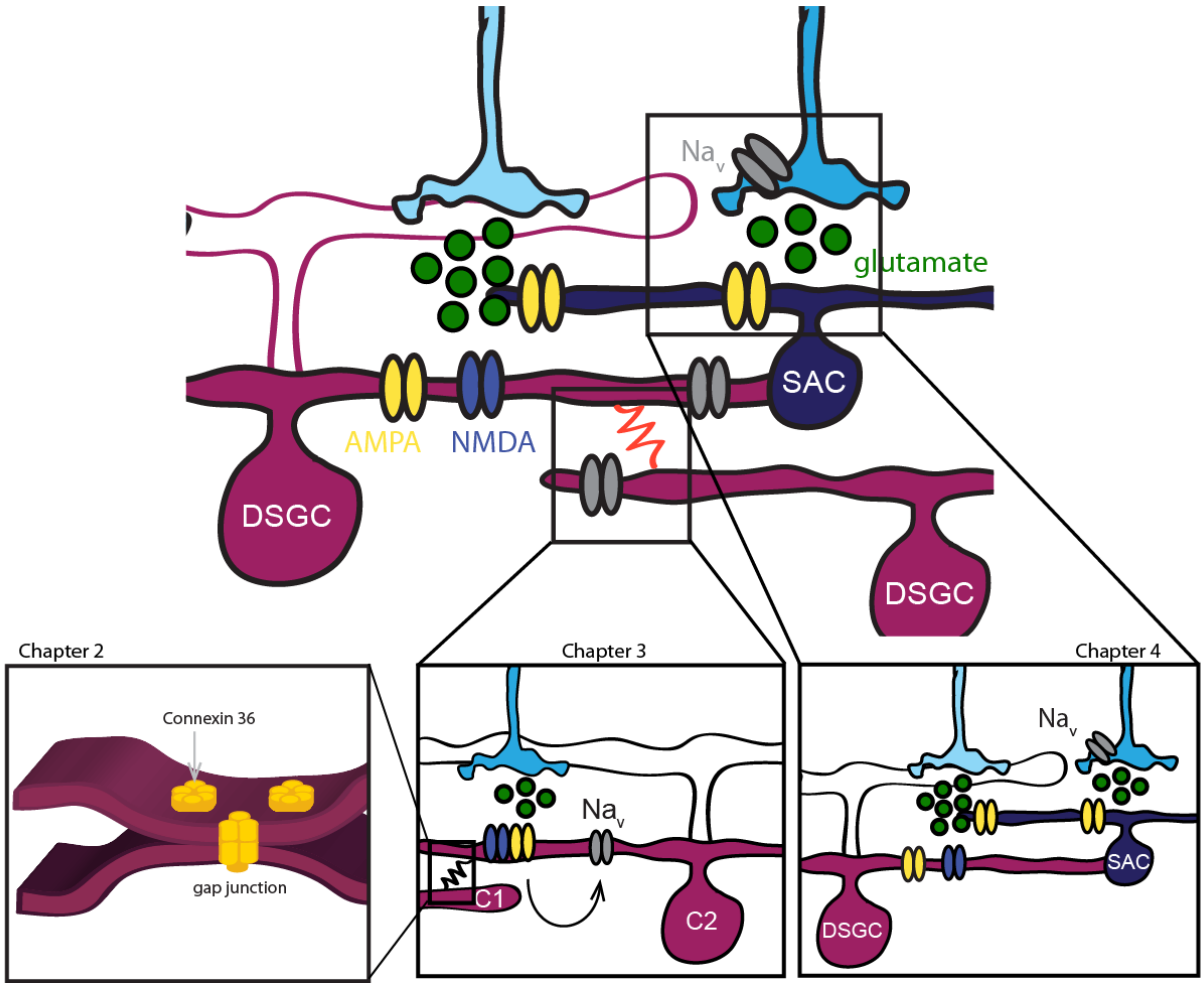

Figure 9. Dissertation outline.
This dissertation discusses signal integration in the directionally-selective (DS) circuit. Chapter 2 focusses on gap junction coupling of neighbouring DS ganglion cells (DSGCs). I characterize the subunit composition of these gap junctions. Chapter 3 focuses on the current flowing across gap junction between two DSGCs (cell 1 and cell 2; C1 and C2). I investigate how this electrical input is integrated with coincident chemical inputs from bipolar cells or starburst amacrine cells, and the purpose the integration of these coincident inputs serve. In Chapter 4 I focus exclusively on coincident chemical inputs to DSGCs. I investigate how inputs to DSGCs vary across stimulus conditions, and subsequently investigate selective voltage-gated Na+ channel expression as a mechanism by which stimulus sensitivities can be differentially established between DSGCs and starburst amacrine cells (SACs).

1.6. Bibliography

Baden, T., Berens, P., Bethge, M., & Euler, T. (2013). Spikes in mammalian bipolar cells support temporal layering of the inner retina. *Current Biology*, *23*(1), 48–52. http://doi.org/10.1016/j.cub.2012.11.006

Baden, T., Esposti, F., Nikolaev, A., & Lagnado, L. (2011). Spikes in retinal bipolar cells phase-lock to visual stimuli with millisecond precision. *Current Biology*, *21*(22), 1859–69. http://doi.org/10.1016/j.cub.2011.09.042

Bader, C., Bertrand, D., & Schwartz, E. (1982). Voltage-activated and calcium-activated currents studied in solitary rod inner segments from the salamander retina. *The Journal of Physiology*, *331*, 253–284.

Barlow, H. B., & Hill, R. M. (1963). Selective sensitivity to direction of movement in ganglion cells of the rabbit retina. *Science*, *139*(3553), 412–414.

Barrio, L. C., Capel, J., Jarillo, J. a, Castro, C., & Revilla, A. (1997). Species-specific voltage-gating properties of connexin-45 junctions expressed in Xenopus oocytes. *Biophysical Journal*, *73*(2), 757–69. http://doi.org/10.1016/S0006-3495(97)78108-6

Baylor, D. A., Lamb, T. D., & Yau, K. W. (1979). Responses of retinal rods to single photons. *The Journal of Physiology*, *288*, 613–634. http://doi.org/10.1113/jphysiol.1979.sp012716

Beaudoin, D. L., Manookin, M. B., & Demb, J. B. (2008). Distinct expressions of contrast gain control in parallel synaptic pathways converging on a retinal ganglion cell. *The Journal of Physiology*, *586*(Pt 22), 5487–502. http://doi.org/10.1113/jphysiol.2008.156224

Benison, G., Keizer, J., Chalupa, L. M., & Robinson, D. W. (2001). Modeling temporal behavior of postnatal cat retinal ganglion cells. *Journal of Theoretical Biology*, (210), 187–199. http://doi.org/10.1006/jtbi.2000.2289

Bennett, M. V., & Verselis, V. K. (1992). Biophysics of gap junctions. *Seminars in Cell Biology*, *3*(1), 29–47. http://doi.org/10.1016/S1043-4682(10)80006-6

Bloomfield, S. A. (1996). Effect of spike blockade on the receptive-field size of amacrine and ganglion cells in the rabbit retina. *Journal of Neurophysiology*, *75*(5), 1878–1893.

Bloomfield, S. A., & Dacheux, R. F. (2001). Rod vision: Pathways and processing in the mammalian retina. *Progress in Retinal and Eye Research*, *20*(3), 351–384. http://doi.org/10.1016/S1350-9462(00)00031-8

Bloomfield, S. A., & Volgyi, B. (2007). Response properties of a unique subtype of wide-field amacrine cell in the rabbit retina. *Visual Neuroscience*, *24*, 459–469.

Bloomfield, S. A., & Völgyi, B. (2004). Function and plasticity of homologous coupling between AII amacrine cells. *Vision Research*, *44*, 3297–3306. http://doi.org/10.1016/j.visres.2004.07.012

Bloomfield, S. A., Xin, D., & Persky, S. E. (1995). A comparison of receptive field and tracer coupling size of horizontal cells in the rabbit retina. *Visual Neuroscience*, *12*(5), 985–999. http://doi.org/10.1017/S0952523800009524

Bloomfield, S. a, & Völgyi, B. (2009). The diverse functional roles and regulation of neuronal gap junctions in the retina. *Nature Reviews Neuroscience*, *10*(7), 495–506. http://doi.org/10.1038/nrn2636

Boiko, T., Rasband, M. N., Levinson, S. R., Caldwell, J. H., Mandel, G., Trimmer, J. S., & Matthews, G. (2001). Compact myelin dictates the differential targeting of two sodium channel isoforms in the same axon. *Neuron*, *30*(1), 91–104. http://doi.org/10.1016/S0896-6273(01)00265-3

Bolte, P., Herrling, R., Dorgau, B., Schultz, K., Feigenspan, A., Weiler, R., Janssen-Bienhold, U. (2016). Expression and localization of connexins in the outer retina of the mouse. *Journal of Molecular Neuroscience*, *58*(2), 178–192. http://doi.org/10.1007/s12031-015-0654-y

Boos, R., Schneider, H., & Wassle, H. (1993). Voltage- and transmitter-gated currents of AII-amacrine cells in a slice preparation of the rat retina. *The Journal of Neuroscience*, *13*(7), 2874–2888.

Brecha, N., Johnson, D., Peichl, L., & Wassle, H. (1988). Cholinergic amacrine cells of the rabbit retina contain glutamate decarboxylase and gamma-aminobutyrate immunoreactivity. *Proceedings of the National Academy of Sciences*, *85*(16), 6187–6191. http://doi.org/10.1073/pnas.85.16.6187

Briggman, K. L., Helmstaedter, M., & Denk, W. (2011). Wiring specificity in the direction-selectivity circuit of the retina. *Nature*, *471*(7337), 183–8. http://doi.org/10.1038/nature09818

Brombas, A., Croft, S. K., & Williams, S. R. (2017). Dendro-dendritic cholinergic excitation controls dendritic spike initiation in retinal ganglion cells. *Nature Communications*, *8*(15683), 1–14. http://doi.org/10.1038/ncomms15683

Burkhardt, D. A., & Fahey, P. K. (1998). Contrast enhancement and distributed encoding by bipolar cells in the retina. *Journal of Neurophysiology*, *80*, 1070–1081.

Calderone, J. B., & Jacobs, G. H. (1995). Regional variations in the relative sensitivity to UV light in the mouse retina. *Visual Neuroscience*, *12*(3), 463–468.

Catterall, W. a, Goldin, A. L., & Waxman, S. G. (2005). Nomenclature and structure-function relationships of voltage-gated sodium channels. *Pharmacological Reviews*, *57*(4), 397–409. http://doi.org/10.1124/pr.57.4.4.and

Chen, M., Lee, S., Park, S. J. H., Looger, L. L., & Zhou, Z. J. (2014). Receptive field properties of bipolar cell axon terminals in direction-selective sublaminas of the mouse retina. *Journal of Neurophysiology*, *112*(8), 1950–62. http://doi.org/10.1152/jn.00283.2014

Chun, M., Han, S., Chung, J., & Wassle, H. (1993). Electron microscopic analysis of the rod pathway of the rat retina, *The Journal of Comparative Neurology*, *432*, 421–432.

Cohen, E. D. (2001). Voltage-gated calcium and sodium currents of starburst amacrine cells in the rabbit retina. *Visual Neuroscience*, *18*, 799–809.

Cook, P. B., Lukasiewicz, P. D., & McReynolds, J. S. (1998). Action potentials are required for the lateral transmission of glycinergic transient inhibition in the amphibian retina. *The Journal of Neuroscience*, *18*(6), 2301–2308. Retrieved from http://www.jneurosci.org/content/18/6/2301.full.pdf

Cote, P. D., De Repentigny, Y., Coupland, S. G., Schwab, Y., Roux, M. J., Levinson, S. R., & Kothary, R. (2005). Physiological maturation of photoreceptors depends on the voltage-gated sodium channel NaV1.6 (Scn8a). *The Journal of Neuroscience*, *25*(20), 5046–5050. http://doi.org/10.1523/JNEUROSCI.4692-04.2005

Deans, M. R., Volgyi, B., Goodenough, D. A., Bloomfield, S. A., & Paul, D. L. (2002). Connexin36 is essential for transmission of rod-mediated visual signals in the

mammalian retina. *Neuron*, *36*, 703–712.
Dedek, K., Breuninger, T., De Sevilla Muller, L. P., Maxeiner, S., Schultz, K., Janssen-Bienhold, U., Weiler, R. (2009). A novel type of interplexiform amacrine cell in the mouse retina. *European Journal of Neuroscience*, *30*(2), 217–228. http://doi.org/10.1111/j.1460-9568.2009.06808.x
Degen, J., Meier, C., Van Der Giessen, R. S., Söhl, G., Petrasch-Parwez, E., Urschel, S., Willecke, K. (2004). Expression pattern of lacZ reporter gene representing connexin36 in transgenic mice. *Journal of Comparative Neurology*, *473*(4), 511–525. http://doi.org/10.1002/cne.20085
Demb, J. B. (2007). Cellular mechanisms for direction selectivity in the retina. *Neuron*, *55*(2), 179–186. http://doi.org/10.1016/j.neuron.2007.07.001
Devries, S. H., Qi, X., Smith, R., Makous, W., & Sterling, P. (2002). Electrical coupling between mammalian cones. *Current Biology*, *12*, 1900–1907.
Enroth-cugell, C., & Robson, J. G. (1966). The contrast sensitivity of retinal ganglion cells of the cat. *Journal of Physiology*, *187*(1966), 517–552. http://doi.org/10.1113/jphysiol.1966.sp008107
Euler, T., Detwiler, P. B., & Denk, W. (2002). Directionally selective calcium signals in dendrites of starburst amacrine cells. *Nature*, *418*, 845–852.
Famiglietti, E. V. (1985). Starburst amacrine cells: morphological constancy and systematic variation in the anisotropic field of rabbit retinal neurons. *The Journal of Neuroscience*, *5*(2), 562–577.
Famiglietti, E. V. (1991). Synaptic organization of starburst amacrine cells in rabbit retina: Analysis of serial thin sections by electron microscopy and graphic reconstruction. *The Journal of Comparative Neurology*, *309*(1), 40–70. http://doi.org/10.1002/cne.903090105
Famiglietti, E. V. (1983). "Starburst" amacrine cells and cholinergic neurons: mirror-symmetric on and off amacrine cells of rabbit retina. *Brain Research*, *261*(1), 138–144. http://doi.org/10.1016/0006-8993(83)91293-3
Farrow, K., Teixeira, M., Szikra, T., Viney, T. J., Balint, K., Yonehara, K., & Roska, B. (2013). Ambient illumination toggles a neuronal circuit switch in the retina and visual perception at cone threshold. *Neuron*, *78*(2), 325–38. http://doi.org/10.1016/j.neuron.2013.02.014
Feigenspan, A., Teubner, B., Willecke, K., & Weiler, R. (2001). Expression of neuronal connexin36 in AII amacrine cells of the mammalian retina. *The Journal of Neuroscience*, *21*(1), 230–239. http://doi.org/21/1/230
Fjell, J., Dib-Hajj, S., Fried, K., Black, J. A., & Waxman, S. G. (1997). Differential expression of sodium channel genes in retinal ganglion cells. *Molecular Brain Research*, *50*(1–2), 197–204. http://doi.org/10.1016/S0169-328X(97)00187-3
Flores-Herr, N., Protti, D. A., & Wassle, H. (2001). Synaptic currents generating the inhibitory surround of ganglion cells in the mammalian retina. *The Journal of Neuroscience*, *21*(13), 4852–4863. http://doi.org/21/13/4852
Fried, S. I., Munch, T. A., & Werblin, F. S. (2002). Mechanisms and circuitry underlying directional selectivity in the retina. *Nature*, *420*, 411–414.
Fried, S. I., Münch, T.A, & Werblin, F. S. (2005). Directional selectivity is formed at multiple levels by laterally offset inhibition in the rabbit retina. *Neuron*, *46*(1), 117–27. http://doi.org/10.1016/j.neuron.2005.02.007

Goldin, A. L., Barchi, R. L., Caldwell, J. H., Hofmann, F., Howe, J. R., Hunter, J. C., Catterall, W. A. (2000). Nomenclature of voltage-gated sodium channels. *Neuron*, *28*(2), 365–368.

Granit, R. (1933). The components of the retinal action potential in mammals and their relation to the discharge in the optic nerve. *The Journal of Physiology*, *77*(3), 207–239. http://doi.org/10.1113/jphysiol.1933.sp002964

Grimes, W. N. (2012). Amacrine cell-mediated input to bipolar cells: Variations on a common mechanistic theme. *Visual Neuroscience*, *29*(1), 41–49. http://doi.org/10.1017/S0952523811000241

Grzywacz, N. M., Amthor, F. R., & Merwine, D. K. (1997). Necessity of acetylcholine for retinal directionally selective responses to drifting gratings in rabbit. *The Journal of Physiology*, *512*(2), 575–581.

Grzywacz, N. M., Amthor, F. R., & Merwine, D. K. (1998). Necessity of acetylcholine for retinal directionally selective responses to drifting gratings in rabbit, *The Journal of Physiology*, 575–581.

Güldenagel, M., Söhl, G., Plum, A., Traub, O., Teubner, B., Weiler, R., & Willecke, K. (2000). Expression patterns of connexin genes in mouse retina. *The Journal of Comparative Neurology*, *425*(2), 193–201.

Harris, A. L. (2001). Emerging issues of connexin channels: biophysics fills the gap. *Quarterly Reviews of Biophysics*, *34*(3), 2001.

Hartline, H. K. (1937). The response of single optic nerve fibers of the vertebrate eye to illumination of the retina. *American Journal of Physiology*, *121*(2), 400–415.

Haverkamp, S. (2005). The primordial, blue-cone color system of the mouse retina. *Journal of Neuroscience*, *25*(22), 5438–5445. http://doi.org/10.1523/JNEUROSCI.1117-05.2005

Helmstaedter, M., Briggman, K. L., Turaga, S. C., Jain, V., Seung, H. S., & Denk, W. (2013). Connectomic reconstruction of the inner plexiform layer in the mouse retina. *Nature*, *500*(7461), 168–74. http://doi.org/10.1038/nature12346

Hoggarth, A., McLaughlin, A. J., Ronellenfitch, K., Trenholm, S., Vasandani, R., Sethuramanujam, S., Awatramani, G. B. (2015). Specific wiring of distinct amacrine cells in the directionally selective retinal circuit permits independent coding of direction and size. *Neuron*, *86*(1), 276–291. http://doi.org/10.1016/j.neuron.2015.02.035

Hombach, S., Janssen-Bienhold, U., Sohl, G., Schubert, T., Bussow, H., Ott, T., … Willecke, K. (2004). Functional expression of connexin57 in horizontal cells of the mouse retina. *European Journal of Neuroscience*, *19*, 2633–2640. http://doi.org/10.1111/j.1460-9568.2004.03360.x

Ichinose, T., Fyk-Kolodziej, B., & Cohn, J. (2014). Roles of ON cone bipolar cell subtypes in temporal coding in the mouse retina. *The Journal of Neuroscience*, *34*(26), 8761–71. http://doi.org/10.1523/JNEUROSCI.3965-13.2014

Janssen-Bienhold, U., Dermietzel, R., & Weiler, R. (1998). Distribution of connexin43 immunoreactivity in the retinas of different vertebrates. *Journal of Comparative Neurology*, *396*, 310–321.

Jeon, C., Strettoi, E., & Masland, R. H. (1998). The major cell populations of the mouse retina. *The Journal of Neuroscience*, *18*(21), 8936–8946.

Kaneda, M., Ito, K., Morishima, Y., Shigematsu, Y., & Shimoda, Y. (2007).

Characterization of voltage-gated ionic channels in cholinergic amacrine cells in mouse retina. *Journal of Neurophysiology*, *97*, 4225–4234. http://doi.org/10.1152/jn.01022.2006.

Kaneko, Y., & Watanabe, S. I. (2007). Expression of Nav1.1 in rat retinal AII amacrine cells. *Neuroscience Letters*, *424*(2), 83–88. http://doi.org/10.1016/j.neulet.2007.07.023

Kawai, F., Horiguchi, M., Suzuki, H., & Miyachi, E. (2001). Na+ action potentials in human photoreceptors. *Neuron*, (30), 451–458.

Kihara, A. H., Paschon, V., Cardoso, C. M., Higa, G. S. V., Castro, L. M., Hamassaki, D. E., & Britto, L. R. G. (2009). Connexin36, an essential element in the Rod pathway, is highly expressed in the essentially rodless retina of *Gallus gallus*. *Journal of Comparative Neurology*, *512*(5), 651–663. http://doi.org/10.1002/cne.21920

Kim, K. J., & Rieke, F. (2003). Slow Na+ inactivation and variance adaptation in salamander retinal ganglion cells. *The Journal of Neuroscience*, *23*(4), 1506–1516. http://doi.org/23/4/1506

Lee, S., Kim, K., & Zhou, Z. J. (2010). Role of ACh-GABA cotransmission in detecting image motion and motion direction. *Neuron*, *68*(6), 1159–72. http://doi.org/10.1016/j.neuron.2010.11.031

Lee, S., & Zhou, Z. J. (2006). The synaptic mechanism of direction selectivity in distal processes of starburst amacrine cells. *Neuron*, *51*(6), 787–99. http://doi.org/10.1016/j.neuron.2006.08.007

Li, W., Zhang, J., & Massey, S. C. (2002). Coupling pattern of S1 and S2 amacrine cells in the rabbit retina. *Visual Neuroscience*, *19*(2), 119–131.

MacLeish, P., & Townes-Anderson, E. (1988). Growth and synapse formation among major classes of adult salamander retinal neurons in vitro. *Neuron*, *1*, 751–760.

Macneil, M. A., Heussy, J. K., Dacheux, R. F., Raviola, E., & Masland, R. H. (1999). The shapes and numbers of amacrine cells: matching of photofilled with golgi-stained cells in the rabbit retina and comparison with other mammalian species. *Journal of Comparative Neurology*, *413*, 305–326.

Macneil, M. A., & Masland, R. H. (1998). Extreme diversity among amacrine cells: implications for function. *Neuron*, *20*, 971–982.

Manthey, D., Bukauskas, F., Lee, C. G., Kozak, C. A., & Willecke, K. (1999). Molecular cloning and functional expression of the mouse gap junction gene connexin-57 in human HeLa cells. *Journal of Biological Chemistry*, *274*(21), 14716–14723.

Masland, R. H. (2001). The fundamental plan of the retina. *Nature Neuroscience*, *4*(9), 877–886. http://doi.org/10.1038/nn0901-877

Masland, R. H. (2012a). The neuronal organization of the retina. *Neuron*, *76*(2), 266–280. http://doi.org/10.1016/j.neuron.2012.10.002

Masland, R. H. (2012b). The tasks of amacrine cells. *Visual Neuroscience*, *29*(1), 3–9. http://doi.org/10.1017/S0952523811000344

Masland, R. H., & Mills, J. W. (1979). Autoradiographic identification of acetylcholine in the rabbit retina. *Journal of Cell Biology*, *83*, 159–178.

Massey, S. C., & Redburn, D.A., (1983). The cholinergic amacrine cells of rabbit retina receive ON and OFF input: an alaysis of [3H]-ACh releast using 2-amino-4-phosphonobutyric acid (APB) and chloride free medium. *Vision Research*, *23*(12), 1615–1620.

Massey, S. C., & Neal, M. J. (1979). The light evoked release of acetylcholine from the rabbit retina in vivo and its inhibition by GABA-aminobutyic acid. *Journal of Neurochemistry*, *32*, 1327–1329.

Masu, M., Iwakabe, H., Tagawa, Y., Miyoshi, T., Yamashita, M., Fukuda, Y., Nakanishi, S. (1995). Specific deficit of the ON response in visual transmission by targeted disruption of the mGIuR6 gene. *Cell*, *80*(5), 757–765. http://doi.org/10.1016/0092-8674(95)90354-2

Mojumder, D. K., Frishman, L. J., Otteson, D. C., & Sherry, D. M. (2007). Voltage-gated sodium channel alpha-subunits Na(v)1.1, Na(v)1.2, and Na(v)1.6 in the distal mammalian retina. *Molecular Vision*, *13*, 2163–2182. http://doi.org/v13/a247

Moreno, A. P., Laing, J. G., Beyer, E. C., & Spray, D. C. (1995). Properties of gap junction channels formed of connexin-45 endogenously expressed in human hepatoma (Skhep1) cells. *American Journal of Physiology*, *268*(2), 356–365.

Munch, T. A., & Werblin, F. S. (2006). Synaptic interactions within a homogenous starburst cell network can lead to robust asymmetries in dendrites of starburst amacrine cells. *Journal of Neurophysiology*, *96*, 471–477. http://doi.org/10.1152/jn.00628.2005.

Nomura, A., Shigemoto, R., Nakamura, Y., Okamoto, N., Mizuno, N., & Nakanishi, S. (1994). Developmentally regulated postsynaptic localization of a metabotropic glutamate receptor in rat rod bipolar cells. *Cell*, *77*(3), 361–369. http://doi.org/10.1016/0092-8674(94)90151-1

O'Brien, B. J., Caldwell, J. H., Ehring, G. R., Bumsted O'Brien, K. M., Luo, S., & Levinson, S. R. (2008). Tetrodotoxin-resistant voltage-gated sodium channels Na(v)1.8 and Na(v)1.9 are expressed in the retina. *The Journal of Comparative Neurology*, *508*(6), 940–51. http://doi.org/10.1002/cne.21701

O'Malley, D. M., & Masland, R. H. (1989). Co-release of acetylcholine and gamma-aminobutyric acid by a retinal neuron. *Proceedings of the National Academy of Sciences*, *86*(9), 3414–3418. http://doi.org/10.1073/pnas.86.9.3414

O'Malley, D. M., Sandell, H., & Masland, R. H. (1992). Co-release of acetylcholine and GABA by the starburst amacrine. *The Journal of Neuroscience*, *12*(4), 1394–1408.

Odermatt, B., Nikolaev, A., & Lagnado, L. (2012). Encoding of luminance and contrast by linear and nonlinear synapses in the retina. *Neuron*, *73*(4), 758–773. http://doi.org/10.1016/j.neuron.2011.12.023

Oesch, N., Euler, T., & Taylor, W. R. (2005). Direction-selective dendritic action potentials in rabbit retina. *Neuron*, *47*(5), 739–50. http://doi.org/10.1016/j.neuron.2005.06.036

Oesch, N. W., & Taylor, W. R. (2010). Tetrodotoxin-resistant sodium channels contribute to directional responses in starburst amacrine cells. *PloS One*, *5*(8), e12447. http://doi.org/10.1371/journal.pone.0012447

Pan, F., Paul, D. L., Bloomfield, S. a, & Völgyi, B. (2010). Connexin36 is required for gap junctional coupling of most ganglion cell subtypes in the mouse retina. *The Journal of Comparative Neurology*, *518*(6), 911–27. http://doi.org/10.1002/cne.22254

Pan, Z., & Hu, H. (2000). Voltage-dependent Na+ currents in mammalian retinal cone bipolar cells. *Journal of Neurophysiology*, *84*, 2564–2571.

Park, S. J. H., Kim, I.-J., Looger, L. L., Demb, J. B., & Borghuis, B. G. (2014).

Excitatory synaptic inputs to mouse on-off direction-selective retinal ganglion cells lack direction tuning. *The Journal of Neuroscience*, *34*(11), 3976–81. http://doi.org/10.1523/JNEUROSCI.5017-13.2014

Pei, Z., Chen, Q., Koren, D., Giammarinaro, B., Ledesma, H. A., & Wei, W. (2015). Conditional knock-out of vesicular GABA transporter gene from starburst amacrine cells reveals the contributions of multiple synaptic mechansims underlying direction selectivity in the retina. *The Journal of Neuroscience*, *35*(38), 13219–13232. http://doi.org/10.1523/JNEUROSCI.0933-15.2015

Poleg-Polsky, A., & Diamond, J. S. (2016). Retinal circuitry balances contrast tuning of excitation and inhibition to enable reliable computation of direction selectivity. *The Journal of Neuroscience*, *36*(21), 5861–5876. http://doi.org/10.1523/JNEUROSCI.4013-15.2016

Puthussery, T., Venkataramani, S., Gayet-Primo, J., Smith, R. G., & Taylor, W. R. (2013). Nav1.1 channels in axon initial segments of bipolar cells augment input to magnocellular visual pathways in the primate retina. *The Journal of Neuroscience*, *33*(41), 16045–16059. http://doi.org/10.1523/JNEUROSCI.1249-13.2013

Sanes, J. R., & Masland, R. H. (2015). The types of retinal ganglion cells: current status and implications for neuronal classification. *Annual Review of Neuroscience*, *38*(1), 221–246. http://doi.org/10.1146/annurev-neuro-071714-034120

Saszik, S., & DeVries, S. H. (2012). A mammalian retinal bipolar cell uses both graded changes in membrane voltage and all-or-nothing Na+ spikes to encode light. *The Journal of Neuroscience*, *32*(1), 297–307. http://doi.org/10.1523/JNEUROSCI.2739-08.2012

Schneeweis, D. M., & Schnapf, J. L. (1995). Photovoltage of rods and cones in the macaque retina. *Science*, *268*(5213), 1053–1056.

Schubert, T., Degen, J., Willecke, K., Hormuzdi, S. G., Monyer, H., & Weiler, R. (2005). Connexin36 mediates gap junctional coupling of alpha-ganglion cells in mouse retina. *Journal of Comparative Neurology*, *485*(3), 191–201. http://doi.org/10.1002/cne.20510

Sernagor, E., Eglen, S. J., & Wong, R. O. (2001). Development of retinal ganglion cell structure and function. *Progress in Retinal and Eye Research*, *20*(2), 139–174.

Sethuramanujam, S., McLaughlin, A. J., deRosenroll, G., Hoggarth, A., Schwab, D. J., & Awatramani, G. B. (2016). A central role for mixed acetylcholine/GABA transmission in direction coding in the retina. *Neuron*, *90*(6), 1243–1256. http://doi.org/10.1016/j.neuron.2016.04.041

Sethuramanujam, S., Yao, X., Rosenroll, G., Briggman, K. L., Field, G., & Awatramani, G. B. (2017). "Silent" NMDA synapses enhance motion sensitivity in a mature retinal circuit, *Neuron*, 96, 1-13

Sharpe, L. T., & Stockman, A. (1999). Rod pathways: The importance of seeing nothing. *Trends in Neurosciences*, *22*(11), 497–504. http://doi.org/10.1016/S0166-2236(99)01458-7

Shelley, J., Dedek, K., Schubert, T., Feigenspan, A., Schultz, K., Hombach, S., … Weiler, R. (2006). Horizontal cell receptive fields are reduced in connexin57-deficient mice. *European Journal of Neuroscience*, *23*(12), 3176–3186. http://doi.org/10.1111/j.1460-9568.2006.04848.x

Sivyer, B., & Williams, S. R. (2013). Direction selectivity is computed by active

dendritic integration in retinal ganglion cells. *Nature Neuroscience*, 16(12), 1848-56. http://doi.org/10.1038/nn.3565

Smith, R. G., & Vardi, N. (1995). Simulation of the AII amacrine cell of the mammalian retina: Functional consequences of electrical coupling and regenerative membrane properties. *Visual Neuroscience*, *12*, 851–860.

Söhl, G., Güldenagel, M., Traub, O., & Willecke, K. (2000). Connexin expression in the retina. *Brain Research Reviews*, *32*(1), 138–145. http://doi.org/10.1016/S0165-0173(99)00074-0

Srinivas, M., Rozental, R., Kojima, T., Dermietzel, R., Mehler, M., Condorelli, D. F., … Spray, D. C. (1999). Functional properties of channels formed by the neuronal gap junction protein connexin36. *The Journal of Neuroscience*, *19*(22), 9848–55. Retrieved from http://www.ncbi.nlm.nih.gov/pubmed/10559394

Szel, A., Rohlich, P., & Van Veen, T. (1993). Short-wave sensitive cones in the rodent retinas. *Experimental Eye Research*, *57*, 503–505.

Taylor, W. R. (1999). TTX attenuates surround inhibition in rabbit retinal ganglion cells. *Visual Neuroscience*, *16*(2), 285–90. http://doi.org/10.1017/S0952523899162096

Taylor, W. R., He, S., Levick, W. R., & Vaney, D. I. (2000). Dendritic computation of direction selectivity by retinal ganglion cells. *Science*, *289*(September), 2347–2351.

Teubner, B., Degen, J., Dermietzel, R. & Willecke, K. (2000). Functional expression of CX36 gene coding for a neuron-specific gap junction protein. *The Journal of Membrane Biology*, *176*(3), 249–262.

Thibos, L. N., & Werblin, F. S. (1978). The response properties of the steady antagonistic surround in the mudpuppy retina. *The Journal of Physiology*, (278), 79–99.

Thoreson, W. B., & Mangel, S. C. (2012). Lateral interactions in the outer retina. *Progress in Retinal and Eye Research*, *31*(5), 407–441. http://doi.org/10.1016/j.preteyeres.2012.04.003

Tian, M., Jarsky, T., Murphy, G. J., Rieke, F., & Singer, J. H. (2010). Voltage-gated Na channels in AII amacrine cells accelerate scotopic light responses mediated by the rod bipolar cell pathway. *The Journal of Neuroscience*, *30*(13), 4650–9. http://doi.org/10.1523/JNEUROSCI.4212-09.2010

Trenholm, S., McLaughlin, A.J., Schwab, D.J., & Awatramani, G.B. (2013). Dynamic tuning of electrical and chemical synaptic transmission in a network of motion coding retinal neurons. *The Journal of Neuroscience*, *33*(37), 14927–38. http://doi.org/10.1523/JNEUROSCI.0808-13.2013

Trenholm, S., McLaughlin, A.J., Schwab, D.J., Turner, M.H., Smith, R.G., Rieke, F., & Awatramani, G.B. (2014). Nonlinear dendritic integration of electrical and chemical synaptic inputs drives fine-scale correlations. *Nature Neuroscience*, *17*, 1759-66. http://doi.org/10.1038/nn.3851

Trenholm, S., Schwab, D.J., Balasubramanian, V., & Awatramani, G.B. (2013). Lag normalization in an electrically coupled neural network. *Nature Neuroscience*, *16*, 154–56. http://doi.org/10.1038/nn.3308

Van Wart, A., Trimmer, J.S., & Matthews, G. (2007). Polarized distribution of ion channels within microdomains of the axon initial segment. *The Journal of Comparative Neurology*, *500*, 339–352. http://doi.org/10.1002/cne

Vaney, D.I. (1990). The mosaic of amacrine cells in the mammalian retina. *Progress in Retinal Research*, *9*, 49–100. http://doi.org/10.1016/0278-4327(90)90004-2

Vaney, D.I. (2002). Retinal neurons: cell types and coupled networks. *Progress in Brain Research*, *136*, 239–254.

Vaney, D.I., & Young, H.M. (1988). GABA-like immunoreactivitiy in cholinergic amacrine cells of the rabbit retina. *Brain Research*, *438*, 369–373.

Vardi, N., & Smith, R.G. (1996). The AII amacrine network: coupling can increase correlated activity. *Vision Research*, *36*(23), 3743–3757.

Velte, T.J., & Masland, R.H. (1999). Action potentials in the dendrites of retinal ganglion cells. *Journal of Neurophysiology*, *81*, 1412–1417.

Verselis, V.K., Bennett, M.V., & Bargiello, T.A. (1991). A voltage-dependent gap junction in *Drosophila melanogaster*. *Biophysical Journal*, *59*(1), 114–126. http://doi.org/10.1016/S0006-3495(91)82204-4

Vlasits, A.L., Morrie, R.D., Tran-Van-Minh, A., Bleckert, A., Gainer, C.F., DiGregorio, D.A., & Feller, M.B. (2016). A role for synaptic input distribution in a dendritic computation of motion direction in the retina. *Neuron*, *89*(6), 1317–1330. http://doi.org/10.1016/j.neuron.2016.02.020

Völgyi, B. (2004). Convergence and segregation of the multiple rod pathways in mammalian retina. *Journal of Neuroscience*, *24*(49), 11182–11192. http://doi.org/10.1523/JNEUROSCI.3096-04.2004

Völgyi, B., Chheda, S., & Bloomfield, S. (2009). Tracer coupling patterns of the ganglion cell subtypes in the mouse retina. *The Journal of Comparative Neurology*, *512*(5), 664–87. http://doi.org/10.1002/cne.21912

Wang, G.-Y., Robinson, D.W., & Chalupa, L.M. (1998). Calcium-activated potassium conductances in retinal ganglion cells of the ferret. *Journal of Neurophysiology*, *79*, 151–158.

Werblin, F S., & Dowling, J.E. (1969). Organization of the retina of the mudpuppy, Necturus maculosus. II. Intracellular recording. *Journal of Neurophysiology*, *32*, 339–355.

Wright, L.L., & Vaney, D.I. (2004). The type 1 polyaxonal amacrine cells of the rabbit retina: a tracer-coupling study. *Visual Neuroscience*, *21*(2), 145–155. http://doi.org/10.1017/S0952523804042063

Wu, C., Ivanova, E., Cui, J., Lu, Q., & Pan, Z.-H. (2011). Action potential generation at an axon initial segment-like process in the axonless retinal AII amacrine cell. *The Journal of Neuroscience*, *31*(41), 14654–9. http://doi.org/10.1523/JNEUROSCI.1861-11.2011

Xin, D., & Bloomfield, S.A. (1997). Tracer coupling pattern of amacrine and ganglion cells in the rabbit retina. *The Journal of Comparative Neurology*, *383*(4), 512–528. http://doi.org/10.1002/(SICI)1096-9861(19970714)383:4<512::AID-CNE8>3.0.CO;2-5

Yagi, T., & Macleish, P. (1994). Ionic conductances of monkey solitary cone inner segments. *Journal of Neurophysiology*, *71*(2), 656–665.

Yamada, E., & Ishikawa, T. (1965). The fine structure of the horizontal cells in some vertebrate retinae. *Cold Spring Harbor Symposium on Quantitative Biology*, *30*, 383–392.

Yau, K.W., & Hardie, R.C. (2009). Phototransduction motifs and variations. *Cell*, *139*(2), 246–264. http://doi.org/10.1016/j.cell.2009.09.029

Yonehara, K., Farrow, K., Ghanem, A., Hillier, D., Balint, K., Teixeira, M., Roska, B.

(2013). The first stage of cardinal direction selectivity is localized to the dendrites of retinal ganglion cells. *Neuron*, *79*(6), 1078–85. http://doi.org/10.1016/j.neuron.2013.08.005

Yoshida, K., Watanabe, D., Ishikane, H., Tachibana, M., Pastan, I., & Nakanishi, S. (2001). A key role of starburst amacrine cells in originating retinal directional selectivity and optokinetic eye movement. *Neuron*, *30*(3), 771–80.

Zeng, H., & Sanes, J.R. (2017). Neuronal cell-type classification: challenges, opportunities and the path forward. *Nature Reviews Neuroscience*, *18*(9), 530-546, http://doi.org/10.1038/nrn.2017.85

Zhang, C., & McCall, M.A. (2012). Receptor targets of amacrine cells. *Visual Neuroscience*, *29*(1), 11–29. http://doi.org/10.1017/S0952523812000028

2. CX36 is critical for electrical coupling of superior-coding directionally-selective ganglion cells

The work presented in this Chapter was done in collaboration with Dr. Stuart Trenholm, Dr. Jeremy Kay and Dr. Gautam Awatramani. Stuart collected data presented in Figure 10, while Jeremy produced Figure 12.Gautam designed experiments. This work is unpublished, however modified versions of Figures 11 and 14 are in submission (see page v, Original Research #1).

2.1. Abstract

Electrical coupling is extensive in the retina, with evidence for gap junctions in each of the five major cell types (photoreceptors, horizontal cells, bipolar cells, amacrine cells, and ganglion cells) (for review see Bloomfield & Völgyi, 2009). Gap junctions in the retina serve many roles, from the coupling of rod and cone pathways (Deans *et al.,* 2002), to the coupling of horizontal cells which is important for establishing inhibitory surrounds (see Thorson & Mangel, 2012 for review). Gap junctions also couple one of the four populations of DSGCs, those encoding superior direction (sDSGCs). This population of GCs is labelled with green fluorescent protein in the Hb9GFP transgenic mouse line. Roles for sDSGC gap junctions have already been identified. Gap junctions expand sDSGC subthreshold receptive fields, priming sDGSCs to respond rapidly to moving objects (Trenholm *et al.,* 2013a), allowing for sDSGCs to respond earlier to rapidly moving objects and a more accurate representation of stimulus location (lag normalization; Trenholm *et al.*, 2013b).

However, despite some understanding of the roles gap junctions serve within this specialized circuit, the molecular identity of gap junctions coupling sDSGCs is not known. Given that gap junction composition, based on the expression of different connexin (CX) protein subunits, establishes the unique biophysical properties of

electrical coupling (Bennett & Verselis, 1992; Saez *et al.*, 2003), linking the physiological roles of gap junction to connexin composition is critical to our understanding of electrical synapses. Here, I ascertain the molecular identity of the connexin subunits forming gap junctions between sDSGCs.

All gap junctions are composed of two hemi-channels, each comprised of six transmembrane proteins called connexins (CX) (**Figure 6**). At least two connexins, CX36 and CX45 (named based on their molecular weight) have been localized to the inner plexiform layer (Güldenagel *et al.*, 2000), the location of sDSGC dendritic arbors. I have uncovered data indicating that sDSGCs rely on CX36. First, I have shown that sDSGC gap junctional conductances are not voltage-dependent (**Figure 10D**), consistent with the expression of CX36 which does not exhibit significant voltage-sensitivity (Al-Ubaidi *et al.*, 2000). Then, I uncovered immunohistochemical evidence for the presence of CX36 in sDSGCs. The hypothesis that CX36 are functional in sDSGCs was strengthened by an experiment showing loss of tracer coupling between sDSGCs in mice deficient for CX36. Finally, I validated the results of the above experiments using electrophysiological methods. I show that direct (paired current-clamp recordings; **Figure 13**) and indirect (feedback spikelets in voltage-clamp) measurements of gap junction coupling are absent in CX36-deficient mice. My results suggest that lag normalization, (**Figure 14**) and fine-scale correlations, two gap-junction dependent phenomena, are equally impaired in CX36-deficient retinas.

Collectively, the experiments outlined in this chapter establish CX36 as critical for coupling of superior coding DSGC, through complementary anatomical and

physiological experiments. This work resolves a critical outstanding question regarding the connexins that make up gap junctions in this ganglion cell type.

2.2. Introduction

Visual information in the retina is carried and modified both by chemical and electrical synapses from photoreceptors in the outer retina, to ganglion cells in the inner retina. Gap junctions, which form electrical synapses, are expressed in all layers and all major cellular types in the retinas of chordates (Abascal & Zardoya, 2013). They have been show to play many independent roles in the major visual circuits of the retina, including coupling rod and cone pathways, establishing receptive field structures, synchronizing firing between neighbouring ganglion cells (Bloomfield & Völgyi, 2009), and maintaining retinal waves (spontaneous rhythmic bursting activity necessary for neuronal development; Wong, 1999).

Gap junctions are intercellular channels that link adjacent cells. They are composed of two hexameric hemichannels, or connexons, one in each opposing cell membrane. Each connexon encompasses six transmembrane protein subunits, or connexins. Over 20 distinct connexin genes have been identified in the mouse genome (Söhl & Willecke, 2003), including 15 which are expressed in the retina (Bolte *et al*., 2016), and at least three of which are expressed in the inner plexiform layer (*CX36, CX45* and *CX30.2*) (Degen *et al*., 2004; Güldenagel *et al*., 2000; Muller *et al*., 2010). Unique connexin structures impart gap junctions with different properties, including varying permeabilities, voltage-gating mechanisms, regulatory mechanisms, and other biophysical characteristics (see Bloomfield & Völgyi, 2009 for review).

Recently, attempts have been made to understand the functional diversity of gap junctions in the inner plexiform layer (Degen *et al*., 2004; Han & Massey, 2005; Hilgen *et al.*, 2011; Pan *et al.*, 2010; Schubert *et al.*, 2005; Söhl *et al.*, 2000; Teubner *et al.*, 2000; Völgyi *et al.*, 2009), the final site of synaptic processing before visual information is passed to the thalamus and the superior colliculus. Gap junctions between ganglion cells are largely thought to contain CX36, CX45 or a combination of the two (Dedek *et al.*, 2006; Li *et al.*, 2008; Pan *et al*., 2010; Schubert *et al.*, 2005). Given the unique and divergent biophysical properties of these two connexins, knowing which connexins occur where is of critical importance to our understanding of the circuit.

Recent work on directionally-selective ganglion cells (DSGCs) has demonstrated that one of the four subtypes of DSGCs (the superior coding $Hb9^{+}$ DSGCs Trenholm *et al.*, 2011; Trenholm *et al.*, 2013a) express gap junctions. This gap junction coupling is important for spatial expansion of subthreshold receptive fields (Trenholm, *et al*., 2013a), lag normalization (Trenholm *et al*., 2013b), and the generation of fine-scale correlations between adjacent sDSGCs (Trenholm *et al*., 2014). However, while these studies expanded the roles gap junctions perform within this circuit, the molecular composition has not been conclusively determined. As molecular composition determines the unique biophysical properties of the gap junction, identifying connexin subunit composition is important to understanding the structure and function of the electrical synapse. Previous reports of DSGC coupling have provided conflicting reports. Tracer coupling experiments by Pan *et al.*, (2010) and Schubert *et al. (*2005) demonstrated the importance of CX45 in two populations of bistratified ganglion cells, and suggested CX36 was not important for a similar population of ganglion cells (G17 ganglion cells; likely DSGCs;

see Pan *et al*., 2010). Both studies conflict with recent physiological experiments in sDSGCs which suggested the necessity of CX36 for functional coupling (Trenholm *et al.*, 2014).

Given the lack of clarity surrounding connexin makeup of DSGC gap junctions, this study aimed to determine the connexin identity mediating electrical coupling of DSGCs, and specifically test the involvement of CX36. Given the conflicting nature of previous reports, we used genetic, electrophysiological and histochemical approaches to determine specific connexin involvement. The results of this study may lead to the discovery of a gap junction "code" that could be applied to other circuits in the retina and in other areas of the central nervous system. The experiments outlined below pair anatomical and physiological experiments, using two complementary mouse models of CX36 deficiency. Additionally, we combine qualitative and quantitative approaches to tracer coupling experiments in an attempt to reconcile differences in previously published work. Our results show that electrical coupling between DSGCs is dominated by CX36-containing gap junctions as the junctional conductance and physiological correlates of gap junction activity were largely abolished in both models of CX36-deficiency. However, residual coupling in quantitative anatomical experiments suggests a possible role for non-CX36 coupling of DSGCs. Collectively, these results establish CX36 as the main source of sDSGC electrical coupling and gap-junction mediated computations. Furthermore, our experiments suggest a possible role for CX45 coupling that is independent of functional electrical coupling.

2.3. Methods

2.3.1. Animals

All procedures were performed in accordance with the Canadian Council on Animal Care and approved by the University of Victoria Animal Care Committee. Experiments were performed on 21-60 day old mice of both sexes that were maintained on a 12-hour light/dark cycle. Experiments were performed using multiple mouse lines, including Hb9::eGFP transgenic mice (Arber *et al*., 1999) and Hb9::eGFP;CX36$^{-/-}$ mice (CX36 provided by D. Paul, Harvard University). We generated FSTL4creER::Ai9fl::CX36fl by crossing FSTL4creER (Kim *et al.,* 2010, provided by J. Sanes, Harvard University), Ai9fl (Madisen *et al.*, 2012) and Cx36fl (Wellershaus *et al*., 2008) such that mice were homozygous for Cx36fl$^{+/+}$. Tamoxifen (Sigma) was injected intraperitoneally (50 µl of a 2 mg/mL solution in corn oil) into triple transgenic mice at postnatal day 0 (P0) to activate CreER and initiate flox-mediated expression of Ai9 and excision of CX36. Experiments on triple transgenic animals were performed 3-4 weeks following injections.

2.3.2. Whole-mount preparation

Prior to dissection, mice were dark-adapted for approximately 60 minutes before being anesthetized with isoflurane and decapitated. This was done to standardize light-evoked responses across animals. Retinas were dissected in Ringer's solution (110 mM NaCl, 2.5 mM KCl, 1 mM $CaCl_2$, 1.6 mM $MgCl_2$, 10 mM glucose and 22 mM $NaHCO_3$, bubbled with carbogen (95% O_2-5% CO_2)) and mounted on a 0.22 mm membrane filter (Millipore) with a precut window that allowed light to reach the retina. The preparation was viewed under IR illumination using a Spot RT3 CCD camera (Diagnostic

Instruments) attached to an upright Olympus BX51WIfluorescent microscope equipped with a 40X water-immersion objective (Olympus Canada). The retina was continuously perfused with Ringer's solution maintained at 35-37°C.

2.3.3. Physiological recordings

Spike recordings were made using the loose cell-attached patch-clamp technique using 5–10-MΩ electrodes filled with Ringer's solution. Voltage-clamp whole-cell recordings were made using 4–7MΩ electrodes containing a Cs^+-solution comprised of 112.5 mM CH_3CsO_3S, 1 mM $MgSO_4$, 10 mM EGTA, 10 mM HEPES, 4 mM ATP-Mg_2, 0.5 mM GTP-Na_3, 5 mM QX-314, 0.025 mM Alexa Fluor 594 (Invitrogen), and 7.75 mM Neurobiotin-Cl (Vector Laboratories). The pH was adjusted to 7.2–7.3 with CsOH. For current-clamp experiments electrodes were filled with a K^+-solution containing 115mM K^+-gluconate, 9.7 KCl, 1 $MgCl_2$, 0.5 $CaCl_2$, 1.5 mM EGTA, 10 mM HEPES, 4 mM ATP-Mg_2, 0.5 mM GTP-Na_3, 0.025 mM Alexa Fluor 594, and 7.75 mM Neurobiotin-Cl. The pH was adjusted to 7.2–7.3 with KOH. Signals were digitized at 10 kHz (PCI-6036E acquisition board, National Instruments) and acquired using custom software written in LabVIEW. GFP^+ and $tdTomato^+$ ganglion cells were targeted for recordings using two-photon laser scanning microscopy techniques, at wavelength long enough to avoid stimulation of photoreceptors (λ = 950 nm).

2.3.4. Light stimulus

Light stimuli were generated with a digital projector (refresh rate 75 Hz; Cpx1, Hitachi) and controlled with custom software incorporating Psychtoolbox. Light stimuli were projected from below the preparation and focused on the photoreceptor outer segments using the sub-stage condenser. The ambient background intensity, measured

with a calibrated spectrophotometer (USB2000, Ocean Optics), was set to approximately ~500 to 1000 R* per rod per s.

2.3.5. Tracer coupling and image analysis

Following 30-minute intracellular filling with Neurobiotin, retinas were fixed in 4% paraformaldehyde for 30 minutes and washed in 0.1X phosphate buffered saline (PBS), pH 7.4 for 15 minutes. Retinas were post-fixed overnight in a 30% sucrose, 0.1X PBS solution then washed in 1X PBS for 15 minutes. To visualize Neurobiotin, retinas were incubated in streptavidin-containing solutions (streptavidin-Cy3 or streptavidin-Alexa488 in 0.3% Triton in PBS). Following final washes in PBS, retinas were mounted in Fluoromount mounting medium (Sigma-Aldrich). Coverslips were sealed for prolonged storage and slides were stored in at 4°C and protected from light.

Images were collected using an Olympus confocal microscope with a 20X objective (NA 0.75). Fluorophores (Tdtomato and AlexaFluor- 488) were excited with 554 nm and 493 nm lasers, respectively, and a pixel dwell time of 8.0 s/pixel. Image stacks were collected in 2 µm Z-steps at a resolution of 0.828m/pixel. For quantification, 10 planar images were Z projected (maximum intensity) and Gaussian filtered. Using Image J software, fixed-diameter circular ROIs were superimposed over tdTomato^{+} or GFP^{+} somata and intensity values were recorded.

2.3.6. Data analysis

Paired recordings were performed from neighbouring sDSGCs. Junctional conductance was measured using a dual voltage-clamp technique (Spray *et al.*, 1981) containing Cs^{+}-solution. Both cells were initially held at a holding potential of -60 mV. To measure junctional conductance, a voltage-clamp step was applied to one cell (donor)

while the other member of the pair (acceptor) was held at −60 mV. The change in current required to hold the cell at −40 mV during the voltage-clamp step was equal to the current flowing through the gap junction. Junctional conductance was calculated as the current produced in the acceptor cell divided by the step voltage applied to the donor cell.

Quantification of coupled spikelets, driven by action potential firing in neighbouring coupled neurons, was automated using Clampfit (Molecular Devices), using template driven event detection, the template of which produced using wildtype controls.

Junctional voltage during current clamp experiments was used to calculate coupling coefficients (CC) for current-clamp experiments. Measurements of voltage in the donor (Vdon) and acceptor (Vacc) cells were made during hyperpolarizing pulses and the coupling coefficient measured as $CC=V_{acc}/V_{don}$.

Spike rates for lag normalization and cross-correlation experiments were estimated by low-pass convolution-filtering of spike trains (using a Gaussian kernel with a fixed width (25 ms). For lag normalization experiments, spike rate was plotted as a function of the stimulus edge in space. The zero point on the abscissa indicates when the stimulus edge was at the soma of the cell of interest. I also corrected for the expected spatial lag that occurs from fixed transmission delays during which the moving stimuli covers a certain distance (Trenholm *et al*., 2013).

Cross-correlograms were computed from spike trains measured in neighbouring DSGCs, evoked by bars moving in the DSGC preferred direction (Trenholm *et al*., 2014). Cross-correlograms were constructed on the basis of the relative time differences between spikes observed in neighbouring neurons C1 and C2 (that is, using the spike

train from C1 as the reference and spikes from C2 to make the histogram). Relative spike times were parsed into 0.5-ms bins and the correlograms were averaged over multiple trials.

2.4. Results

2.4.1. Gap junction conductances of sDSGCs are not voltage-dependent

Previous anatomical work in bistratified ganglion cells suggested DSGCs were coupled through CX45-containing gap junctions (Schubert *et al*., 2005). Our first indication that non-CX45 gap junction were involved in this electrical coupling came from the calculation of sDSGC junctional conductances (Gj). Junctional conductance was determined using paired voltage-clamp recordings made from neighbouring DSGCs in Hb9GFP retinas. Voltage pulses of short duration (200ms) were applied to one cell of the pair (C1; donor) and junctional currents (Ij) were measured in the unstepped cell (C2; acceptor; **Figure 10A**). The junctional current versus voltage (Vj) relationship was plotted, and Gj was measured as the slope of the straight line fitted to the I-V relationship (**Figure 10B**). Gj was independent of voltage across the range of voltages measured (**Figure 10B**), inconsistent with reports of CX45 coupling (Barrio *et al.*, 1997; Moreno *et al.*, 1995; Steiner & Ebihara, 1996), in which Gj varies across voltage . CX45 gap junctions have also been shown to exhibit rapid Gj decay over time (Barrio *et al.*, 1997). In order to test the time-dependence of DSGC coupling, voltage pulses of one second were applied to one cell of the pair (**Figure 10D**). Despite the large Vj values used (+/- 60mV), currents measured did not decline significantly over time (**Figure 10D**), further arguing against the contribution of CX45 to DSGC electrical coupling. While heterotypic gap junction coupling has been previously described in the retina (Dedek *et al*., 2006; Li

et al., 2008), the junctional conductance of DSGC pairs was similar and symmetrical for both directions of coupling, suggesting homotypic coupling (**Figure 10B**). Taken together these experiments argue against significant electrical coupling of DSGCs by CX45, indicating instead an important role for weakly voltage-dependent homotypic gap junctions in DSGCs.

2.4.2. Neurobiotin tracer loading is reduced in CX36-deficient DSGCs

If DSGC gap junctions are not comprised of CX45, CX36-containing gap junctions may be expressed, given their pronounced expression throughout the inner nuclear layer, and demonstrated roles in the electrical coupling of other ganglion cell types (Pan *et al*., 2010; Schubert *et al*., 2005b). While the effect of *CX36* knock-out on tracer coupling has been previously studied in bistratified ganglion cells (Pan *et al*., 2010), studies have exclusively relied on developmental knock-out lines, and made only qualitative assessments of GC coupling.

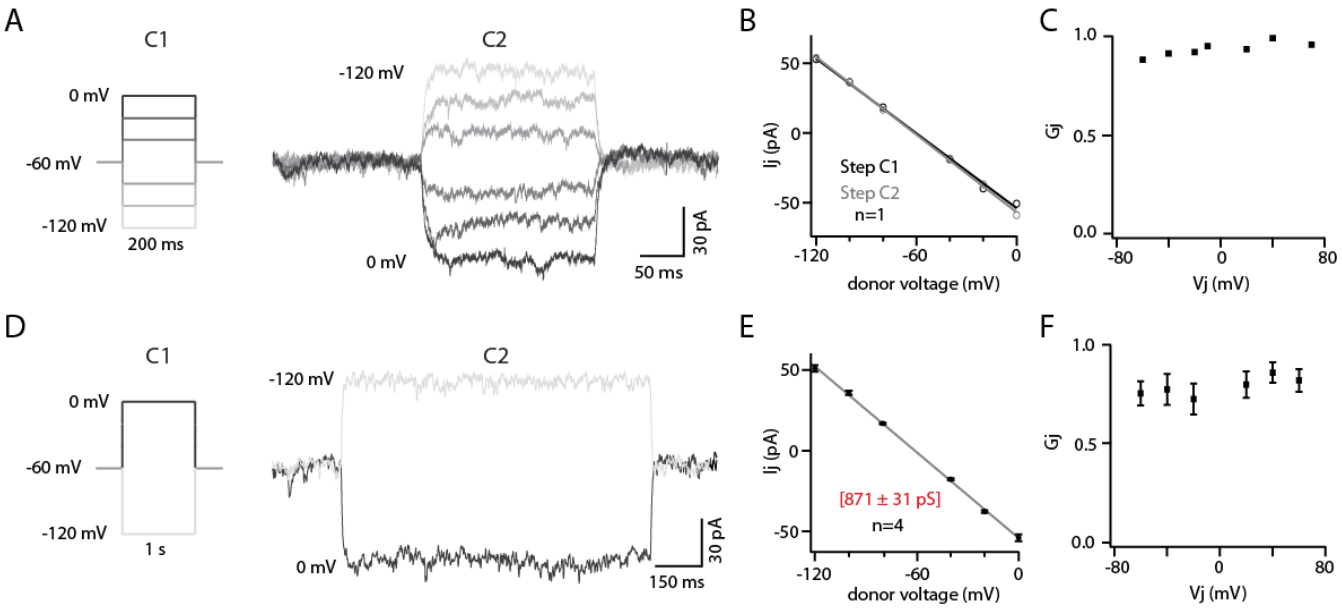

Figure 10. Gap junction conductances of Hb9 DSGCs are not voltage dependent
A Two neighbouring sDSGCs were patched in voltage-clamp configuration. One cell (donor; C1) was given increasing depolarizing or hyperpolarizing voltage pulses 200 ms in duration, while the neighbouring cell (acceptor, C2) was held at -60mV. Representative current traces are shown for C2 (right). Voltage-pulses in the donor cell produced visible response in the acceptor, observed as current injections required to hold the voltage of the acceptor at -60mV. **B** Current measured in C2 was plotted as a function of the voltage step applied to C1 (black). Transjunctional current was linear as a function of the voltage applied to C1 across a large range of voltage steps. When the reciprocal experiment was performed (C2 donor; C1 acceptor) similar results were observed (grey). Averaged current-voltage relationships are shown in **E**. **C** Junctional conductance plotted as a function stepped voltage in the donor cell. No voltage-dependence was observed in single cells (C) or in the averaged population (**F**; n=4). **D** 1-second voltage-pulses were applied to the donor cell. Representative traces are shown for the acceptor cell. No attenuation of the junctional current was visible over time.

To assess the importance of CX36 to DSGC coupling, we quantified tracer coupling across three transgenic mouse lines which differ in their expression of CX36. First, as functional controls (WT), we utilized Hb9GFP retinas in which electrically coupled DSGCs are labelled with GFP (Arber *et al*., 1999). Second, Hb9GFP mice were crossed with CX36 knock-out (CX36KO) lines (Hb9GFP::CX36-/-) (Deans, *et al.*, 2001), eliminating CX36 expression throughout the nervous system. Finally, in order to reduce compensation by other closely related gap junctions during development and to restrict

CX36 knock-out to DSGCs, minimizing off-target effects, we generated FSTL4creER::Ai9fl::CX36fl (FACx) mice by crossing FSLT4creER (Kim *et al*., 2010), Ai9fl (Madisen *et al*., 2012) and CX36fl (Wellershaus *et al*., 2008) until mice were homozygous for CX36fl. In this inducible cre-ER line, Cx36 was knocked-out specifically in FSTL4-positive cells (DSGCs) post-developmentally by tamoxifen injections.

Superiorly coding DSGCs (identified using GFP or TdTomato fluorescence) in all three mouse lines were filled with the gap junction permeable tracer neurobiotin during voltage-clamp experiments, and coupled cells were visualized using Cy3 or Alexa488 (**Figure 11A**, see Methods). The number of tracer-labelled cells and the fluorescent intensity of coupled cells relative to the single filled cell was quantified (**Figure 11C**). Consistent with previous studies (Pan *et al*., 2010), sDSGCs in Hb9GFP retinas (n=10, 6.0 ± 0.3 coupled cells) and *CX36* knock-out lines exhibited noticeable tracer transfer to neighbouring DSGCs. However, the number of neurobiotin positive coupled cells in CX36 deficient retinas was significantly lower than wildtype (CX36KO: 2.6 ± 0.4 coupled cells; FACx 4.0±0.5 coupled cells; and see **Figure 11C**). Thus, tracer coupling was significantly reduced, with CX36 full knock-outs exhibiting the least coupling. Importantly, when comparing the intensity of the soma of coupled cells relative to the filled cell, intensity ratios were lower in FACx mouse lines relative to functional controls. These experiments demonstrate that CX36-deficient DSGCs exhibit less frequent and weaker coupling.

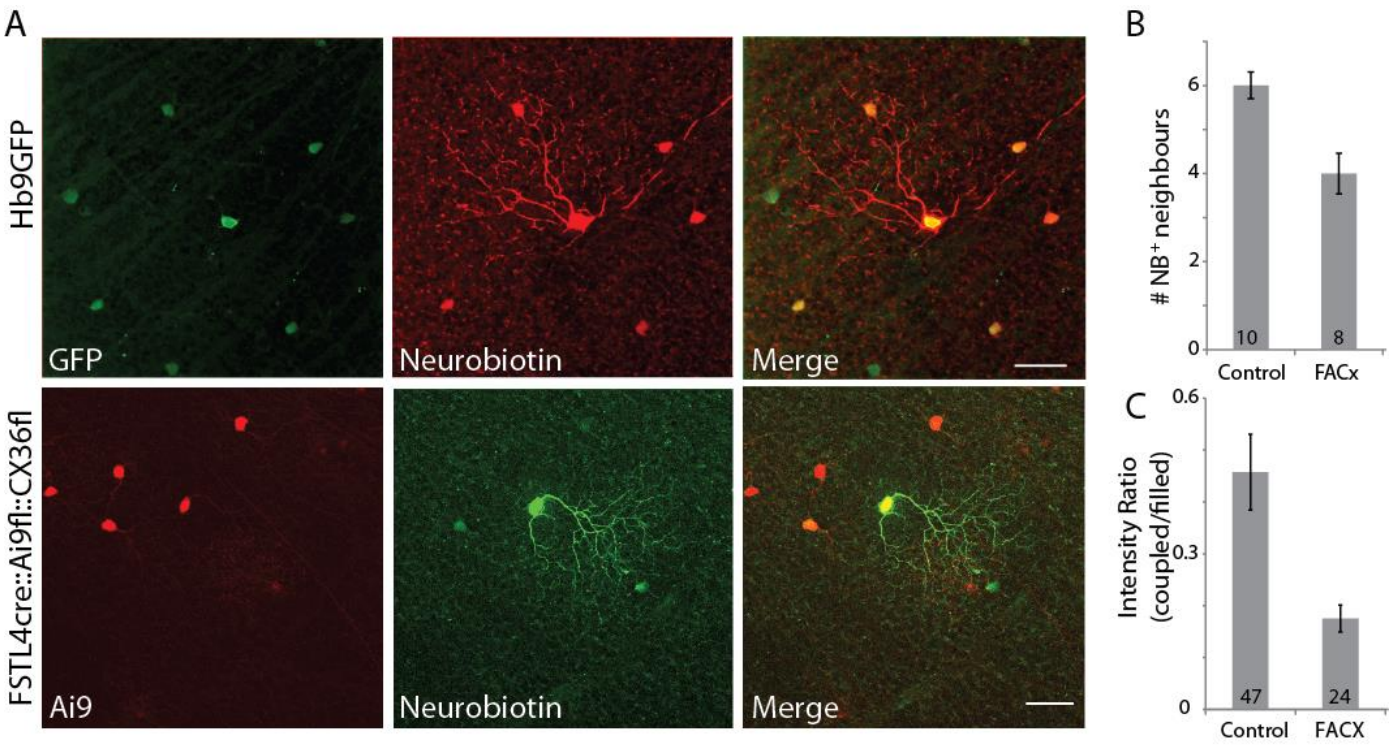

Figure 11. Neurobiotin tracer loading is reduced, but not lost in CX36-deficient retinas.
A Confocal images of whole-mount Hb9GFP (control; top) and FSTL4cre;Ai9fl;CX36fl (FACX; bottom) retinas. Single sDSGCs are filled with Neurobiotin conjugated to Cy3 (for control) or Alexa488 (FACx). Filled cells are labelled with arrows, and neighbouring cell somas are visible. Scale bars represent 20 µm. **B** Graph depicting the average number of tracer-filled neighbouring cells per single filled cell across mouse lines. **C** Average ratios of fluorescent intensities of tracer-filled neighbours over the fluorescent intensity of filled somata, across mouse lines. Tracer-filled DSGCs in FACx retinas exhibit significantly weaker tracer coupling than filled cells in control retinas.

To assess the effect of partial CX36 knockout, I took advantage of to the inducible nature of the FACx model (FSTL4creER;;$Ai9^{fl}$;;$CX36^{fl}$). In these mice expression of the Cre promoter, and thus knock-out of CX36 is incomplete. While all DSGCs filled in FACx retinas were $tdTomato^{+}$ (thus $CX36^{-/-}$), tracer coupling to neighbouring DSGCs could include $CX36^{+/+}$ ($tdTomato^{-}$) and $CX36^{-/-}$ ($tdTomato^{+}$) cells. We took advantage of this system to determine whether the absence of CX36 reduces the likelihood of tracer coupling, and whether this effect is graded based on neighbouring cell CX36 expression. Of all neighbouring DSGCs labelled with Neurobiotin in the FACx

mouse line, tracer coupling occurred more frequently to $CX36^{+/+}$ cells than $CX36^{-/-}$ cells (17 vs. 8 cells respectively for 7 filled DSGCs), indicating coupling was reduced when both neighbours lacked CX36. The converse was also true, if cells in the ROI lacked CX36 expression ($tdTomato^{+}$), tracer coupling was also likely to be absent (12 vs. 7 cells). This analysis demonstrated that loss of CX36 in single DSGC reduces the likelihood of tracer coupling, but this effect is compounded when CX36 knock-out affects both DSGCs in a pair.

Together tracer coupling experiments show that CX36-deficient retinas exhibit both less frequent and weaker coupling to neighbouring DSGCs, and suggests this effect may be graded depending on whether one or both DSGCs lack functional CX36. This first quantitative analysis of DSGC tracer coupling demonstrates an important and novel role for CX36 gap junctions in DSGC coupling.

2.4.3. Electrically coupled DSGCs express CX36

We next tested the expression of CX36 in DSGCs using immunohistochemistry. As antibody staining of connexin subtypes often lack specificity, we utilized heterozygous CX36-deficient mice ($Hb9GFP::CX36KO^{+/-}$) in which one CX36 allele has been substituted with the LacZ reporter, expressed under the control of the endogenous CX36 reporter (Deans *et al*., 2001). This expression system allows the visualization of CX36 through β-Galactosidase (β-Gal) immunoreactivity. DSGCs were stained for β-Gal, GFP (to enhance endogenous GFP expression in Hb9 DSGCs), in addition to Satb2, a marker for DSGCs. Across all four DSGC populations analyzed, ~35% of $Satb2^{+}$ cells also expressed β-Gal (data not shown), consistent with the fraction of electrically coupled DSGCs within the larger DSGC population. When GFP labelling was included, to

specifically identify superior coding DSGCs, 9 of 10 GFP and Satb2^{+} cells labelled were also positive for β-Gal puncta, indicating strong CX36 expression in the superior-coding DSGC population (**Figure 12**). Therefore, our histological data provides further support for the expression of CX36 by sDSGCs, and indicate this expression is ubiquitous in this population.

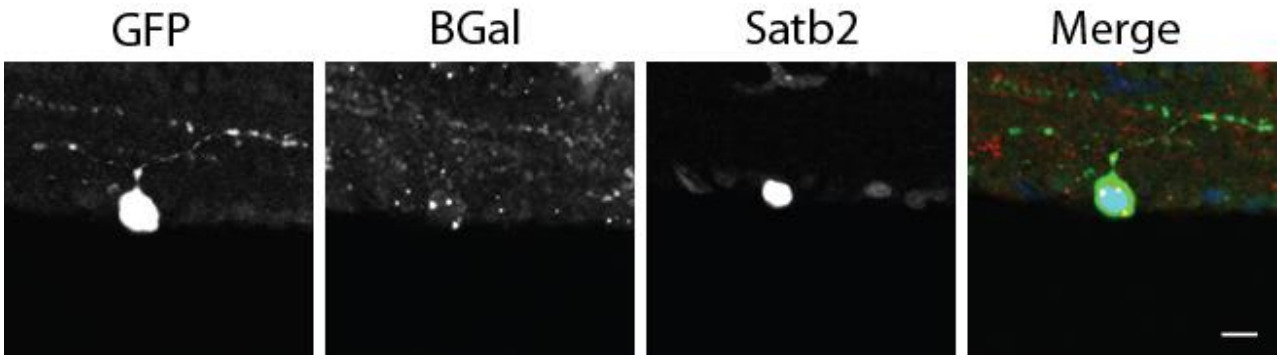

Figure 12. Hb9 DSGCs express CX36.
Confocal images of 20 µm sections of heterozygous CX36KO mice (Hb9GFP;CX36KO+/-), in which β-Gal expression is driven by the endogenous CX36 promoter. Retinas were immunolabelled for GFP (AlexaFluor 488; green), ß-galactosidase (ß-Gal; AlexaFluor 555; red), and Satb2 (AlexaFluor 350; blue) and imaged using confocal microscopy at 60X magnification. BGal puncta are visible in GFP^{+}/Sat2b^{+} somas (merge; far right), providing evidence for CX36 expression in GFP+ ganglion cells (sDSGCs). Scale bar represents 25 µm.

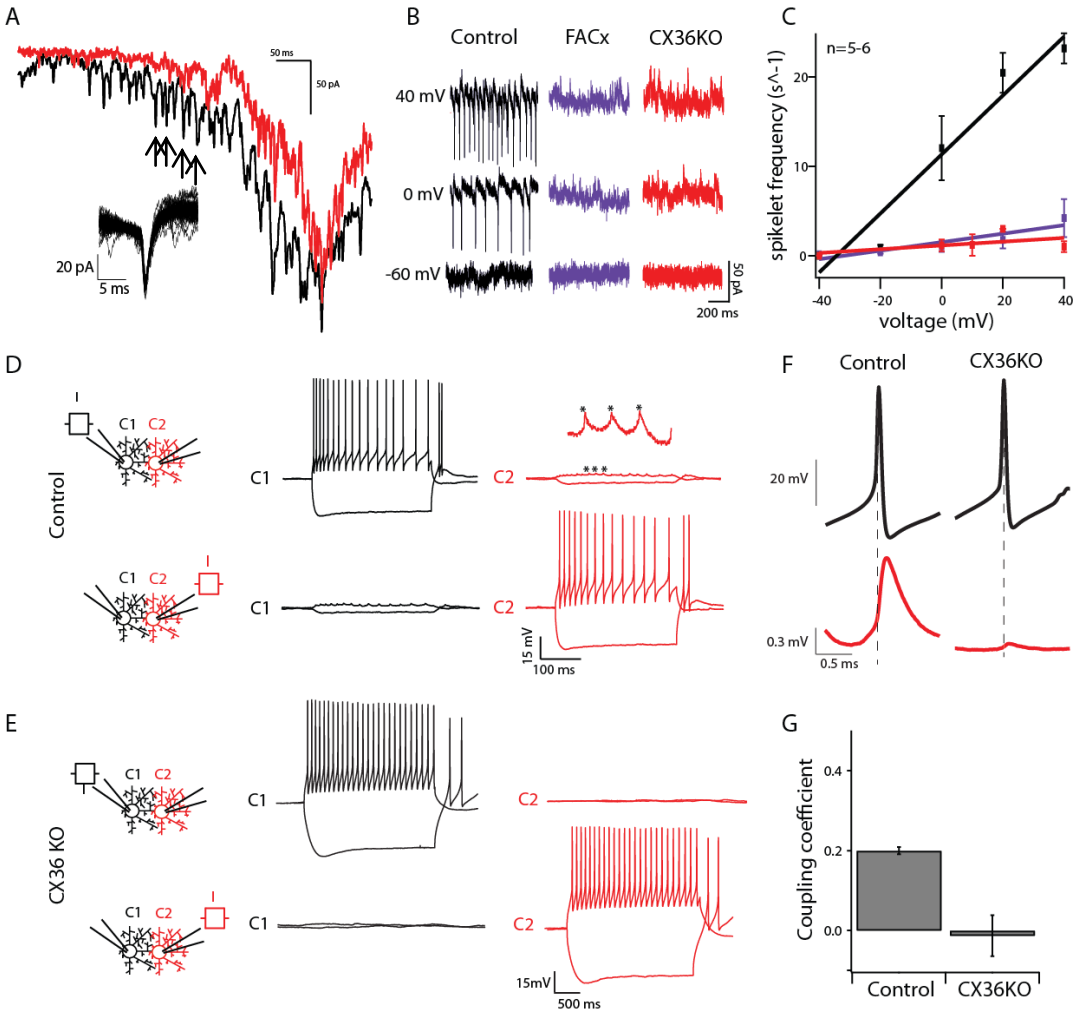

Figure 13. CX36 knock-out abolishes feedback spikelets.
A Representative trace from an sDSGC in voltage-clamp configuration (V_{hold}=-60mV) presented with moving bars of light in the DSGC's preferred direction. Moving bars first drive spiking in neighbouring sDSGCs, observed as small spikelets of negative current injections riding on DSGC light responses (black curve; see arrows). Average spikelet produced can be seen in the overlay. sDSGCs from CX36KO retinas do not exhibit spikelets in the rising phase. **B** Feedback spikelets can also be induced from the recording electrode. Representative current traces from voltage-clamped sDSGCs in control, FACx or CX36KO retinas, held at increasingly depolarized holding potentials (V_{hold}). Depolarized holding potentials drive action potentials in neighbouring cells, observed as small and fast inward currents. **C** Average frequency of reciprocal feedback spikelets is plotted as a function of V_{hold} for DSGCs in control (n=6), CX36KO (n=5) and FACx (n=6) retinas. Spikelet frequency increases with V_{hold} for wildtype retinas while DSGCs in CX36KO and FACx retinas exhibit few spikelets. **D-E** Gap-junction-mediated spikelets are also observable in current-clamp configuration. Paired current-clamp recordings were made from two neighbouring sDSGCs in control (**D**, top) and CX36 knockout (**E**, top) retinas. Representative traces are shown. Positive current injections drove spiking in the donor cell (C1), which also drove small fluctuations in voltage in the acceptor cell (C2) (top). Hyperpolarizing pulses in C1 also hyperpolarized C2. Similar voltage-deflections are also visible when current is injected in C2 and recorded from C1 (**D-E**, bottom). **F** Spike-triggered averages for all spikes driven in the donor cell. Control retinas drive ~1mV spikelets at the soma of the acceptor cell (left). Spikelets are reduced to ~0.1mV in CX36KO retinas (right). **G** Average coupling coefficients calculated from paired current-clamp experiments for control and CX36KO pairs in response to hyperpolarizing voltage steps. Coupling coefficient is reduced in CX36KO retinas.

2.4.4. Physiological evidence of gap junction coupling is reduced in CX36-deficient mice

While our immunohistochemical data suggests sDSGCs express CX36, physiological data is required to determine the precise roles and extent of CX36 electrical coupling. Stimulus-induced evidence for gap junction coupling can be observed in the rising phase of sDSGC EPSCs in response to moving stimuli. As neighbouring DSGCs fire action potentials, fast inward currents of ~40pA can be observed in DSGCs (Figure 13A, black, and inset; see also Trenholm *et al*., 2013). In CX36-deficient mice, moving stimuli produced EPSCs with far fewer spikelets in the initial phase of the response (**Figure 13A**) than wildtype retinas. Without paired recordings, individual events are not easily quantified for comparison between genotypes. We therefore assessed with paired recordings, across all three genotypes, DSGCs' capacity to drive reciprocal feedback spikelets when cells are voltage-clamped at depolarized potentials (+40 mV; **Figure 13B**). In these experiments, current flow through gap junctions triggers action potentials in coupled neighbours, which are in turn measured as fast inward spikelets, the frequency of which increases linearly with the holding potential (**Figure 13C**) (Trenholm *et al.*, 2013). CX36-deficient mice exhibit few-to-no feedback spikelets, regardless of the holding potential (**Figure 13C**). These indirect measurements of gap junction coupling, in both stimulus dependent- and independent-fashions, suggest gap junction coupling is largely absent following CX36 knock-down.

To directly measure the strength of residual DSGC coupling, dual current-clamp recordings were made from pairs of neighbouring sDSGCs. Current pulses were provided to one cell of the pair (C1; donor), and voltage-measurements were performed on the un-pulsed cell (C2; acceptor; **Figure 13D**, top). Reciprocal experiments were also performed to ensure current flow was symmetrical for both directions of coupling (**Figure 13D**, bottom).

While paired experiments were not possible in FACx retinas, due to the sparse labelling of the Ai9 promoter, paired experiments were performed for GFP^+ DSGCs in CX36KO mice. In control retinas, consistent with previous reports (Trenholm *et al*., 2013), hyperpolarizing current pulses produced hyperpolarizations of smaller amplitudes in the acceptor cell; while depolarizations sufficient to drive spiking in the donor cell drove a small depolarization in the acceptor cell, with small spikelets superimposed on the depolarized pulse (see inset). In CX36 knock-out mice however, large depolarizations and hyperpolarizations in donor cells produced no visible current in acceptor cells (**Figure 13D-E**). Strength of coupling was determined using a spike triggered average on spikes generated in the donor cell as well as coupling coefficients calculated from hyperpolarizing pulses (**Figure 13F-G**). Consistent with a diminished primary role for CX36 in coupling, knockout retinas had coupling coefficients near zero (**Figure 13G**). Spike-triggered averaging however, suggested residual coupling may exist following CX36 knockout. While not observable in individual traces, spike-triggered averaging of CX36KO retinas revealed small depolarizations (~0.1mV) in the acceptor cell in response to action potential firing in the donor cell (**Figure 13F**). This coupling was however weak compared to control data, which, as previously reported (Trenholm, *et al*., 2013)

produced ~1mV spikelets (**Figure 13F**). Taken together, these experiments suggest electrical coupling of DSGCs is largely dependent on CX36, however weak residual coupling may remain in developmental CX36 knockout retinas.

2.4.5. Phenomenological evidence for DSGC electrical coupling is lacking in CX36-deficient mice

Our experiments thus far have demonstrated that coupling of DSGCs is weak in the absence of CX36. However, given the large attenuation of gap junction signals in DSGC dendrites, our somatic recording experiments may underestimate the importance of CX36 in DSGC signalling (Trenholm *et al*., 2014). While direct dendritic recordings of gap junctional conductances are not possible in these animals, our previous work has shown that dendritic gap junction conductances are important in the generation of fine-scale correlations between pairs of neighbouring DSGCs (Trenholm *et al*., 2014). This behavioural correlate of gap junction activity is therefore an appropriate reflection of the strength of residual coupling in CX36-deficient mice.

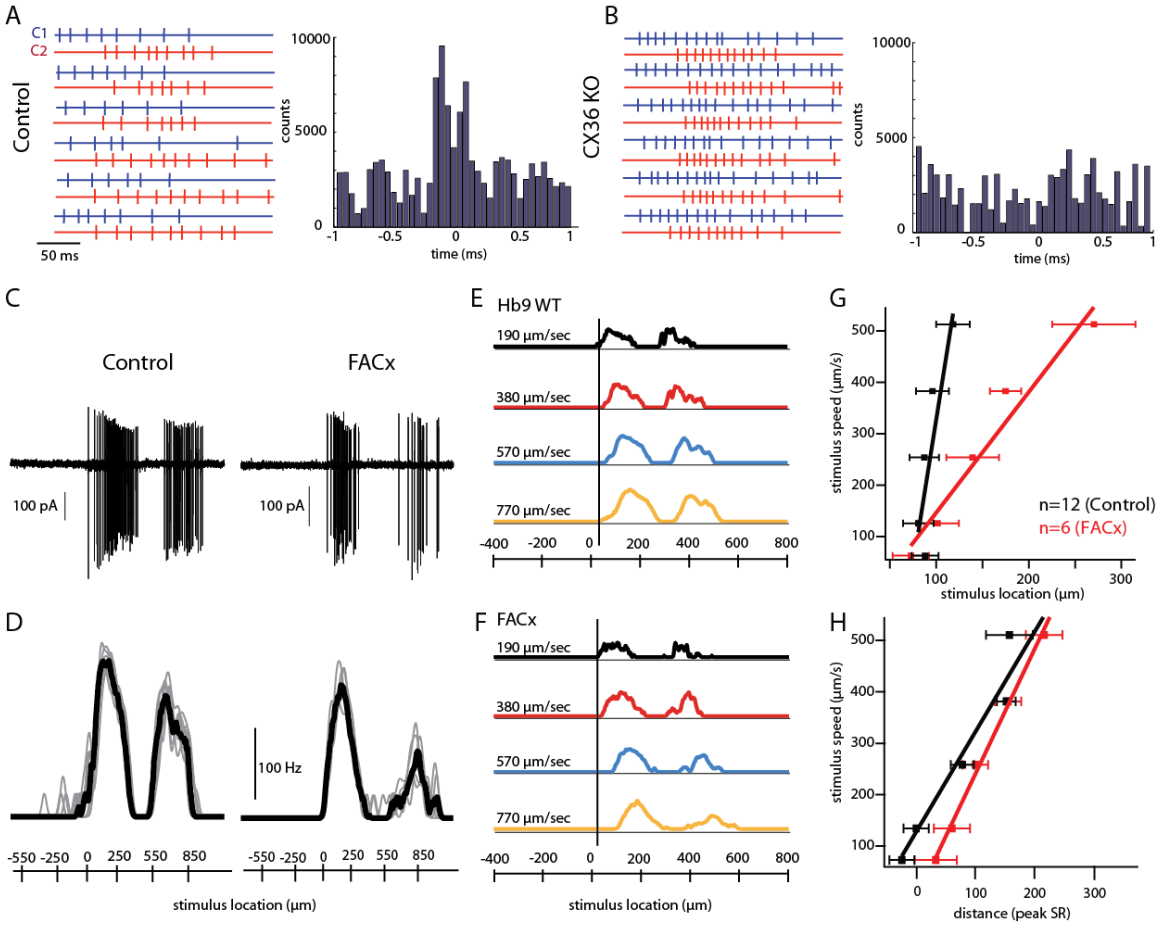

Figure 14. CX36 is required for gap junction-mediated phenomena.
A-B Representative spike trains recorded from neighbouring sDSGCs (C1 – blue, C2 – red) in control (**A**, left) and CX36KO (**B**, left) retinas recorded for moving spots in the preferred direction. Representative cross-correlograms produced from simultaneously recorded spike trains for controls (**A**, right) or CX36KO retinas (**B**, right). Spike trains from wildtype retinas exhibit fine-scale bimodal peaks (arrows), which are lost in CX36 KO retinas. **C** Spike trains recorded from control (left) and FACx retinas (right) in response to moving spots of light in the preferred direction. **D** Spike rates plotted across time and across spatial location of the presented stimulus, recorded from DSGCs in control (left) and FACx (right) retinas (grey – individual stimulus presentation, black-averaged across multiple presentations of the stimulus). **E** Spike rate as a function of stimulus spatial location for DSGC spike trains measured in control (E) and FACx (F) retinas. Coloured lines represent multiple stimulus velocities, with the black line representing the slowest stimulus velocity presented. Black lines indicate the timing of the first spike for the slowest stimulus speed presented. Stimulus location at which the first spike occurs is preserved across stimulus velocities in control retinas, while location of the first spike is shifted at high speeds in FACx retinas. **G** Average spatial location of the stimulus during firing of the first spike is plotted as a function of stimulus speed for sDSGCs in control (n=12) and FACx (n=6) retinas. DSGCs lacking CX36 perform significantly worse than those expressing CX36. **H** Average spatial location of the stimulus during peak spike firing plotted as a function stimulus speed. No significant differences in the location of the stimulus between DSGCs in control and CX36KO retinas.

To assess whether fine-scale correlations remained in CX36-deficient mice, pairs of stimulus-evoked spike trains were recorded using extracellular loose-patch techniques (**Figure 14A**, left). Consistent with previous reports (Trenholm *et al*., 2014), spike trains of neighbouring DSGCs produced bimodal peaks (**Figure 14A**, right), indicating an increased likelihood of action potential firing between one cell of a pair shortly after action potential firing in its coupled neighbour. Bimodal peaks occurred around ~2ms, a much shorter time scale than stimulus-driven correlations (~100ms), suggesting gap junction-mediated correlations. These fine-scale correlations were not apparent in CX36-deficient retinas (**Figure 14B**), indicating CX36 gap junctions are required for fine-scale correlations.

Gap junctions in sDSGCs also allow for lag normalization; that is, the ability to compensate for stimulus velocity and fire action potentials when the stimulus reaches a specific point in the receptive field (eliminating the lag associated with transmission of the signal from the photoreceptors to DSGCs; see Trenholm *et al*., 2013). Lag normalization was measured by recording spike trains from individual sDSGCs in response to stimuli of increasing velocities and plotting spike trains as a function of stimulus position (**Figure 14C-D**; stimulus position was approximated after subtracting to account for the delay of signal transmission, see section 2.3.6.). For wildtype retinas, across the range of stimulus velocities presented, the timing of the first spike consistently occurs when the stimulus reaches a given location (~0 µm, the edge of DSGC receptive field; **Figure 14E,G**). The ability to lag normalize was significantly impeded however in CX36-deficient mice (**Figure 14F-G**). While spike timing was unaffected at slower stimulus speeds, the timing of the first spike was significantly delayed relative to stimulus

position for higher stimulus velocities (**Figure 14F**). Consistent with previous reports (Trenholm, *et al.*, 2013), the stimulus location at which peak spike rate is met increased with spike rate, and did not depend on gap junction coupling, as evidenced by the insignificant differences between wildtype and CX36-deficient retinas (**Figure 14H**). Taken together, these experiments further demonstrate that CX36 is the primary gap junction underlying the gap junction-mediated behaviours in sDSGCs.

2.5. Discussion

These experiments make a strong case for the expression and functional importance of CX36 in DSGC coupling. First, gap junctions in sDSGCs are only weakly voltage-dependent, consistent with CX36 biophysical properties. Second, anatomical evidence suggests DSGCs express CX36 and that CX36-deficient DSGCs exhibit weaker tracer coupling Finally, direct physiological measurements indicate weaker coupling between neighbouring DSGCs in the absence of CX36, as well as reduced ability to lag normalize and drive fine-scale correlations, phenomena which are known to rely on gap junctions between in the circuit.

2.5.1. Complementary knock-out models to study CX36 expression

Our experiments utilized two different models of CX36-deficiency to assess the importance of CX36 to sDSGC coupling and signalling. Many studies of connexin subtypes have demonstrated that these closely related genes frequently compensate for each other following the loss of a single connexin (Iacobas *et al.*, 2007; Iacobas *et al.*, 2003; Spray & Iacobas, 2007). This likely occurs to mitigate the significant effects of gap junction loss during development (Belousov & Fontes, 2013). Compensation has also

been proposed in the retina between CX36 and CX45 specifically (Frank *et al*., 2010). In order to reduce possible substantial gap junction compensation during development, we utilized an inducible post-developmental knock-out model (FACx). While ideally suited to anatomical and single-cell physiological experiments, this mouse model requires low-dose tamoxifen to limit non-specific expression of the Cre promoter (Kay *et al*., 2011). Thus Cre expression, and therefore tdTomato expression and CX36 knock-out, are sparse, making the model less suitable to paired whole-cell recordings.

For such recordings, we reverted to the use of CX36KO mice previously described. Given the similarity of results between the two models in our single-cell recordings (**Figure 13**), we determined the use of either model was sufficient. However, both mouse lines were used where possible to further rule out limited expression or compensatory confounds. My findings are strengthened by the use of both models, superseding the caveats of each individual model to emphasize the presence of CX36 in DSGCs.

2.5.2. Reconciling tracer coupling with electrophysiological measurements

While tracer coupling has frequently been used as a measure of gap junction coupling, little evidence exists correlating the strength of coupling with tracer coupling. While tracer coupling is unlikely in cells which express no gap junctions, it is unclear how tracer coupling would differ in conditions where gap junction coupling has been reduced or modified. In the experiments performed, physiological data suggested gap junction coupling was lost entirely in CX36-deficient mice (**Figures 13-14**), conflicting with our tracer coupling experiments and those described by others (Pan *et al*., 2010). The discrepancy can be mitigated in some respects by our quantitative assessment of gap

junction tracer coupling (**Figure 10**). Our analysis revealed that while coupling is still observed in CX36-deficient animals, the strength and extent of coupling is significantly reduced (**Figure 10**). This emphasizes the need for quantitative assessments of tracer coupling, but also demonstrates the importance of pairing tracer coupling experiments with physiological approaches.

It is possible however, that our anatomical coupling data may more accurately reflect the extent of gap junction coupling, with somatic physiological measurements underestimating the strength of current through gap junctions in the distal dendrites (Trenholm *et al*., 2014). Small spikelets revealed by spike-triggered averaging (**Figure 13**) suggest residual coupling may exist in CX36KO animals. Residual coupling could be explained in several ways. As described above, given the developmental knock-out of CX36 in the CX36KO mouse line, compensation by other connexins is possible (Frank *et al.*, 2010; Iacobas *et al*., 2003). While such compensation is unlikely in the FACx mice, given the post-developmental nature of the knock-out and the short time frame over which experiments were performed, it is possible that sparse Cre labelling prevents full knock-out of CX36. Thus in both knock-out models residual, yet artificial, gap junction coupling may exist.

2.5.3. Possible roles for co-expression of CX36 and CX45

Our results have demonstrated an important role for CX36 in sDSGCs coupling, however we have not ruled out the presence of other gap junctions, such as CX45 (Schubert *et al.*, 2005). CX45 subunits may form distinct (homomeric) gap junctions in sDSGCs or may interact directly with CX36 to form heteromeric gap junctions.

Heteromeric gap junctions between sDSGCs may explain why the knock-out of either CX36 or CX45 subunits decreases tracer coupling (Chapter 4; Schubert *et al.*, 2005). Heteromeric gap junctions have been previously demonstrated in the retina, between AII amacrine cells and ON cone bipolar cells with AII amacrine cells expressing CX36 and cone bipolar cells expressing CX45 (Dedek *et al.*, 2006; Feigenspan *et al.*, 2001; Han & Massey, 2005). Subtype-specific expression of connexins has been measured physiologically in cardiac tissue, with the voltage-gating of heteromeric gap junctions appearing asymmetric for current injections in both directions (Palacios-Prado & Bukauskas 2009; Steiner & Ebihara 1995). Our results however revealed no such asymmetry (**Figure 10**). This does not necessarily rule out such an expression system; asymmetric conductances may be more difficult to measure in retinal tissue.

Alternatively, the symmetrical junctional current-voltage relationships could be evidence either for the presence of homomeric CX36 and CX45 gap junctions (discussed below), or for heteromeric gap junctions between sDSGCs which are symmetrical, with both CX36 and CX45 connexons of the heteromeric gap junction found on each side of the electrical synapse. The advantage to this symmetrical arrangement however, would require further study.

If sDSGC gap junctions are homomeric, CX45 expression may be minimal compared to the expression of CX36. This is expected given that biophysical characteristics of CX45 (Barrio *et al.*, 1997; Moreno *et al*., 1995; Steiner & Ebihara, 1996) are poorly represented in overall measurements of junctional conductance. Alternatively CX45 and CX36 may be important under different circumstances.

Connexins are known to be regulated by phosphorylation by protein kinases through activation by a number of second messengers, including cAMP, Ca^{2+}-calmodulin, cyclic GMP, and nitric oxide (see Bloomfield, & Volgyi, 2009 for review). Interestingly, CX36 and CX45 exhibit opposite regulation in many cases. While acidification increases the conductance of CX45 (Church & Baimbridge, 1991; Spray *et al.,* 1981), conductance through CX36-containing gap junctions decreases (Gonzalez-Nieto *et al*., 2008). Phosphorylation by protein kinase A decreases CX45 conductance (Van Veen *et al.,* 2000) while increasing CX36 conductance in some cases (Kothmann, *et al.,* 2009; Li *et al.*, 2009; but see Urschel *et al*., 2006).

It is therefore possible that expression levels of CX36 and CX45 are similar, but cellular physiology is dominated by one gap junction subtype, and the dominating subtype differs based on ambient light conditions exhibited by the retina. Future studies will be needed to assess if gap junction expression differs across conditions, and to determine how the biophysical differences of CX36 and CX45 make them optimally suited for distinct conditions.

CX45 may serve a different purpose altogether, as a channel for intercellular metabolic coupling. CX45 gap junctions exhibit strong voltage-gating (Barrio *et al*., 1997; Moreno *et al*., 1995; Steiner & Ebihara, 1996). Junctional conductance is highest in depolarized cells with low junctional voltage, while junctional conductance is suppressed at lower membrane potentials and when junctional voltage is high. DSGCs dendrites exhibit strong depolarizations during firing of dendritic spikes and as a result of back-propagating action potentials, both important aspects of DSGC electrical transmission (Trenholm *et al*., 2014). In addition, gap junctions have specifically been shown to be

important for leading edge stimuli during which neighbouring cells are relatively silent (Trenholm *et al*., 2013). These parameters suggest dendrites of DSGCs are optimally suited to gap junctions which do not exhibit strong voltage-gating, such as those containing CX36. Since CX45-comprising gap junctions play a minimal role in electrical coupling of sDSGCs, they may instead be important in metabolic coupling, as has previously been shown for CX45 in cell culture systems and cardiac tissue (Bedner *et al*., 2006; Kumai *et al*., 2000; Nishii *et al*., 2003). Permeability of second messengers may in fact be higher for CX45 than CX36 (Bedner *et al*., 2006) making them ideally suited to this role in DSGCs. Given the strong junctional conductance through CX45 channels at depolarized potentials, CX45 may be involved in intracellular metabolic coupling during periods of high activity, when neighbouring dendrites are simultaneously active, a period during which electrical transmission through gap junctions plays a minimal role in signalling (Trenholm *et al*., 2013). Further work will however be required to assess whether gap junctions in DSGCs participate in metabolic coupling of DSGCs and what purposes this coupling may serve.

2.5.4 Conclusions

Understanding the molecular composition of electrical synapses in ganglion cells informs not only our greater understanding of the retina and visual perception but also informs our understanding of other electrically coupled circuits in the central nervous system, which has lagged greatly behind our understanding of chemical synapses. As the precise connexin makeup of gap junctions determines the biophysical properties of electrical synapses, the determination of connexin expression in DSGCs is vital to our understanding of this complex circuit. Here I have demonstrated, using complementary

genetic, electrophysiological and histochemical approaches, that electrical coupling of sDSGCs relies strongly on CX36. In this instance, the minimal voltage-dependence of CX36 may be uniquely positioned to allow for gap junction-dependent phenomena previously described for this population.

2.6. Bibliography

Abascal, F., & Zardoya, R. (2013). Evolutionary analyses of gap junction protein families. *Biochimica et Biophysica Acta*, *1828*(1), 4–14. http://doi.org/10.1016/j.bbamem.2012.02.007

Arber, S., Han, B., Mendelsohn, M., Smith, M., Jessell, T. M., & Sockanathan, S. (1999). Requirement for the homeobox gene Hb9 in the consolidation of motor neuron identity. *Neuron*, *23*(4), 659–674. http://doi.org/10.1016/S0896-6273(01)80026-X

Barrio, L. C., Capel, J., Jarillo, J.A, Castro, C., & Revilla, A. (1997). Species-specific voltage-gating properties of connexin-45 junctions expressed in *Xenopus oocytes*. *Biophysical Journal*, *73*(2), 757–69. http://doi.org/10.1016/S0006-3495(97)78108-6

Bedner, P., Niessen, H., Odermatt, B., Kretz, M., Willecke, K., & Harz, H. (2006). Selective permeability of different connexin channels to the second messenger cyclic AMP. *Journal of Biological Chemistry*, *281*(10), 6673–6681. http://doi.org/10.1074/jbc.M511235200

Belousov, A. B., & Fontes, J. D. (2013). Neuronal gap junctions: Making and breaking connections during development and injury. *Trends in Neurosciences*, *36*(4), 227–236. http://doi.org/10.1016/j.tins.2012.11.001

Bloomfield, S.A, & Völgyi, B. (2009). The diverse functional roles and regulation of neuronal gap junctions in the retina. *Nature Reviews Neuroscience*, *10*(7), 495–506. http://doi.org/10.1038/nrn2636

Bolte, P., Herrling, R., Dorgau, B., Schultz, K., Feigenspan, A., Weiler, R., Janssen-Bienhold, U. (2016). Expression and localization of connexins in the outer retina of the mouse. *Journal of Molecular Neuroscience*, *58*(2), 178–192. http://doi.org/10.1007/s12031-015-0654-y

Church, J., & Baimbridge, K. G. (1991). Exposure to high-pH medium increases dye coupling between rat hippocampal vitro the incidence and extent of CA1 pyramidal neurons in vitro. *The Journal of Neuroscience*, *11*(10), 3289–3295.

Deans, M. R., Gibson, J. R., Sellitto, C., Connors, B. W., & Paul, D. L. (2001). Synchronous activity of inhibitory networks in neocortex requires electrical synapses containing connexin36. *Neuron*, *31*(3), 477–85.

Dedek, K., Schultz, K., Pieper, M., Dirks, P., Maxeiner, S., Willecke, K., Janssen-Bienhold, U. (2006). Localization of heterotypic gap junctions composed of connexin45 and connexin36 in the rod pathway of the mouse retina. *European Journal of Neuroscience*, *24*(6), 1675–1686. http://doi.org/10.1111/j.1460-9568.2006.05052.x

Degen, J., Meier, C., Van Der Giessen, R. S., Söhl, G., Petrasch-Parwez, E., Urschel, S., Willecke, K. (2004). Expression pattern of lacZ reporter gene representing connexin36 in transgenic mice. *Journal of Comparative Neurology*, *473*(4), 511–525. http://doi.org/10.1002/cne.20085

Frank, M., Eiberger, B., Janssen-Bienhold, U., de Sevilla Muller, L. P., Tjarks, A., Kim, J. S., Willecke, K. (2010). Neuronal connexin-36 can functionally replace connexin-45 in mouse retina but not in the developing heart. *Journal of Cell Science*, *123*(Pt 20), 3605–3615. http://doi.org/10.1242/jcs.068668

Gonzalez-Nieto, D., Gomez-Hernandez, J. M., Larrosa, B., Gutierrez, C., Munoz, M. D.,

Fasciani, I., Barrio, L. C. (2008). Regulation of neuronal connexin-36 channels by pH. *Proceedings of the National Academy of Sciences*, *105*(44), 17169–17174. http://doi.org/10.1073/pnas.0804189105

Güldenagel, M., Söhl, G., Plum, A., Traub, O., Teubner, B., Weiler, R., & Willecke, K. (2000). Expression patterns of connexin genes in mouse retina. *Journal of Comparative Neurology*, *425*(2), 193–201.

Han, Y., & Massey, S. C. (2005). Electrical synapses in retinal ON cone bipolar cells: subtype-specific expression of connexins. *Proceedings of the National Academy of Sciences*, *102*(37), 13313–13318. http://doi.org/10.1073/pnas.0505067102

Hilgen, G., von Maltzahn, J., Willecke, K., Weiler, R., & Dedek, K. (2011). Subcellular distribution of connexin45 in OFF bipolar cells of the mouse retina. *Journal of Comparative Neurology*, *519*(3), 433–50. http://doi.org/10.1002/cne.22526

Iacobas, D. A., Suadicani, S. O., Iacobas, S., Chrisman, C., Cohen, M. A., Spray, D. C., & Scemes, E. (2007). Gap junction and purinergic P2 receptor proteins as a functional unit: Insights from transcriptomics. *Journal of Membrane Biology*, *217*(1-3), 83–91. http://doi.org/10.1007/s00232-007-9039-7

Iacobas, D. A., Urban-Maldonado, M., Iacobas, S., Scemes, E., & Spray, D. C. (2003). Array analysis of gene expression in connexin-43 null astrocytes. *Physiological Genomics*, *15*(3), 177–90. http://doi.org/10.1152/physiolgenomics.00062.2003

Kay, J. N., De La Huerta, I., Kim, I.-J., Zhang, Y., Yamagata, M., Chu, M. W., Sanes, J. R. (2011). Retinal ganglion cells with distinct directional preferences differ in molecular identity, structure, and central projections. *Journal of Neuroscience*, *31*(21), 7753–7762. http://doi.org/10.1523/JNEUROSCI.0907-11.2011

Kim, I.-J., Zhang, Y., Meister, M., & Sanes, J. R. (2010). Laminar restriction of retinal ganglion cell dendrites and axons: subtype-specific developmental patterns revealed with transgenic markers. *The Journal of Neuroscience*, *30*(4), 1452–1462. http://doi.org/10.1523/JNEUROSCI.4779-09.2010

Kothmann, W. W., Massey, S. C., & O'Brien, J. (2009). Dopamine-stimulated dephosphorylation of connexin 36 mediates AII amacrine cell uncoupling. *The Journal of Neuroscience*, *29*(47), 14903–14911. http://doi.org/10.1523/JNEUROSCI.3436-09.2009

Kumai, M., Nishii, K., Nakamura, K., Takeda, N., Suzuki, M., & Shibata, Y. (2000). Loss of connexin45 causes a cushion defect in early cardiogenesis. *Development*, *127*(16), 3501–3512.

Li, H., Chuang, A. Z., & O'Brien, J. (2009). Photoreceptor coupling is controlled by connexin 35 phosphorylation in zebrafish retina. *The Journal of Neuroscience*, *29*(48), 15178–15186. http://doi.org/10.1523/JNEUROSCI.3517-09.2009

Li, X., Kamasawa, N., Ciolofan, C., Olson, C. O., Lu, S., Davidson, K. G. V, Nagy, J. I. (2008). Connexin45-containing neuronal gap junctions in rodent retina also contain connexin36 in both apposing hemiplaques, forming bihomotypic gap junctions, with scaffolding contributed by zonula occludens-1. *The Journal of Neuroscience*, *28*(39), 9769–89. http://doi.org/10.1523/JNEUROSCI.2137-08.2008

Madisen, L., Mao, T., Koch, H., Zhuo, J., Berenyi, A., Fujisawa, S., Zeng, H. (2012). A toolbox of Cre-dependent optogenetic transgenic mice for light-induced activation and silencing. *Nature Neuroscience*, *15*(5), 793–802. http://doi.org/10.1038/nn.3078

Moreno, A. P., Laing, J. G., Beyer, E. C., & Spray, D. C. (1995). Properties of gap

junction channels formed of connexin-45 endogenously expressed in human hepatoma (Skhep1) cells. *American Journal of Physiology*, *268*(2), 356–365.

Muller, L. P., Dedek, K., Janssen-Bienhold, U., Meyer, A., Kreuzberg, M. M., Lorenz, S., Weiler, R. (2010). Expression and modulation of connexin 30.2, a novel gap junction protein in the mouse retina. *Visual Neuroscience*, *27*(3-4), 91–101. http://doi.org/10.1017/S0952523810000131

Nishii, K., Kumai, M., Egashira, K., Miwa, T., Hashizume, K., Miyano, Y., & Shibata, Y. (2003). Mice lacking connexin45 conditionally in cardiac myocytes display embryonic lethality similar to that of germline knockout mice without endocardial cushion defect. *Cell Communication Adhesion*, *10*(4-6), 365–369. http://doi.org/10.1080/15419060390263173

Pan, F., Paul, D. L., Bloomfield, S.A, & Völgyi, B. (2010). Connexin36 is required for gap junctional coupling of most ganglion cell subtypes in the mouse retina. *The Journal of Comparative Neurology*, *518*(6), 911–27. http://doi.org/10.1002/cne.22254

Schubert, T., Degen, J., Willecke, K., Hormuzdi, S. G., Monyer, H., & Weiler, R. (2005). Connexin36 mediates gap junctional coupling of alpha-ganglion cells in mouse retina. *Journal of Comparative Neurology*, *485*(3), 191–201. http://doi.org/10.1002/cne.20510

Schubert, T., Maxeiner, S., Krüger, O., Willecke, K., & Weiler, R. (2005). Connexin45 mediates gap junctional coupling of bistratified ganglion cells in the mouse retina. *The Journal of Comparative Neurology*, *490*(1), 29–39. http://doi.org/10.1002/cne.20621

Söhl, G., Güldenagel, M., Traub, O., & Willecke, K. (2000). Connexin expression in the retina. *Brain Research Reviews*, *32*(1), 138–145. http://doi.org/10.1016/S0165-0173(99)00074-0

Söhl, G., & Willecke, K. (2003). An update on connexin genes and their nomenclature in mouse and man. *Cell Communication & Adhesion*, *10*(4-6), 173–180. http://doi.org/10.1080/15419060390262877

Spray, D. C., & Iacobas, D. A. (2007). Organizational principles of the connexin-related brain transcriptome. *Journal of Membrane Biology*, *218*(1-3), 39–47. http://doi.org/10.1007/s00232-007-9049-5

Spray, D.C., Harris, A., & Bennett, M. (1981). Gap junctional conductance is a simple and sensitive function of intracellular pH. *Science*, *211*(4483), 712–715. http://doi.org/10.1126/science.6779379

Steiner, E., & Ebihara, L. (1996). Functional characterization of canine connexin45. *The Journal of Membrane Biology*, *150*(2), 153–61.

Teubner, B., Degen, J., Dermietzel, R. & Willecke. (2000). Functional expression of CX36 gene coding for a neuron-specific gap junction protein. *Journal of Membrane Biology*, *176*(3), 249–262.

Trenholm, S., Johnson, K., Li, X., Smith, R. G., & Awatramani, G. B. (2011). Parallel mechanisms encode direction in the retina. *Neuron*, *71*(4), 683–694. http://doi.org/10.1016/j.neuron.2011.06.020

Trenholm, S., McLaughlin, A. J., Schwab, D. J., & Awatramani, G. B. (2013). Dynamic tuning of electrical and chemical synaptic transmission in a network of motion coding retinal neurons. *The Journal of Neuroscience*, *33*(37), 14927–38.

http://doi.org/10.1523/JNEUROSCI.0808-13.2013

Trenholm, S., McLaughlin, A. J., Schwab, D. J., Turner, M. H., Smith, R. G., Rieke, F., & Awatramani, G. B. (2014). Nonlinear dendritic integration of electrical and chemical synaptic inputs drives fine-scale correlations. *Nature Neuroscience*, *17*, 1759-66. http://doi.org/10.1038/nn.3851

Trenholm, S., Schwab, D. J., Balasubramanian, V., & Awatramani, G. B. (2013). Lag normalization in an electrically coupled neural network. *Nature Neuroscience*, *16*, 154–56. http://doi.org/10.1038/nn.3308

Urschel, S., Hoher, T., Schubert, T., Alev, C., Sohl, G., Worsdorfer, P., Willecke, K. (2006). Protein kinase A-mediated phosphorylation of connexin36 in mouse retina results in decreased gap junctional communication between AII amacrine cells. *Journal of Biological Chemistry*, *281*(44), 33163–33171. http://doi.org/10.1074/jbc.M606396200

Van Veen, T.A.B., Van Rijen, H. V. M., & Jongsma, H. J. (2000). Electrical conductance of mouse connexin45 gap junction channels is modulated by phosphorylation. *Cardiovascular Research*, *46*(3), 496–510. http://doi.org/10.1016/S0008-6363(00)00047-X

Völgyi, B., Chheda, S., & Bloomfield, S. a. (2009). Tracer coupling patterns of the ganglion cell subtypes in the mouse retina. *The Journal of Comparative Neurology*, *512*(5), 664–87. http://doi.org/10.1002/cne.21912

Wellershaus, K., Degen, J., Deuchars, J., Theis, M., Charollais, A., Caille, D., Willecke, K. (2008). A new conditional mouse mutant reveals specific expression and functions of connexin36 in neurons and pancreatic beta-cells. *Experimental Cell Research*, *314*(5), 997–1012. http://doi.org/10.1016/j.yexcr.2007.12.024

3. Non-linear dendritic integration of electrical and chemical synaptic inputs drives fine-scale correlations

The work presented below is largely published (Trenholm et al., 2014; and see page v, Original Research #4) in collaboration with Dr. Stuart Trenholm (ST), Dr. David Schwab, Dr. Maxwell Turner (MT), Dr. Robert Smith, Dr. Fred Rieke and Dr. Gautam Awatramani. ST collected data for Figures 16 and 24. MT produced Figure 18. ST and I collaborated in producing Figures 15, 17, and 21.

3.1. Abstract

One of the hallmarks of electrically coupled neuronal networks is neuronal synchronization. That is, the correlated firing of action potentials between neighbouring neurons (for reviews see Bennett & Zukin, 2004; Connors & Long, 2004). CX36-containing gap junctions, such as those found in superior-coding DSGCs (see Chapter 2), have been shown to drive neuronal synchronization in other regions of the central nervous system (Deans *et al.*, 2001; Long *et al.*, 2002; Long *et al.*, 2004). However whether sDSGCs exhibit synchronization has not been established. Further, the mechanism by which weak CX36-containing gap junctions drive correlated firing is unclear.

In Chapter 3, we demonstrate correlated firing between electrically coupled DSGCs. Given that gap junction input alone appear to be insufficient to drive correlated firing, we propose a model in which coincident chemical activity (from glutamatergic or cholinergic synapses) is also required. We propose that the summation of temporally and spatially coincident electrical and chemical inputs depolarizes DGSC dendrites sufficiently to activate dendritic Na^+ channels. These dendritic "spikes" then trigger correlated spiking at the DSGC soma.

This model is based on several important findings. First, injections of excitatory currents at DSGC somas, simulating weak gap junction input, were insufficient to significantly influence spike timing. Correlations between coupled sDSGCs nonetheless required gap junction input, as correlations were lost when gap junctions were inhibited pharmacologically. Thus gap junctions were required but not sufficient to elicit correlated spiking. Second, dendritic spikes were required for the generation of correlations, as application of the Na^+ channel inhibitor tetrodotoxin on DSGC dendrites abolished correlations. Also consistent with my model, when dendritic spikes were isolated in a single cell, correlations could be observed between pre-synaptic spikes and post-synaptic dendritic spikes. Finally, experiments that spatially separated electrical and chemical inputs to sDSGCs demonstrated a role for spatial coincidence in the generation of correlations.

Taken together these experiments showed that sDSGCs exhibit fine-scale correlations that depend on CX36-containing gap junctions. Importantly, this work also provides for the first time physiological evidence for a mechanism by which weak gap junction input can drive neuronal synchronization in electrically coupled networks.

3.2. Introduction

Retinal neurons make use of extensive electrical coupling, with all major cell classifications in the retina (photoreceptors, horizontal cells, bipolar cells, amacrine cells and ganglion cells) exhibiting some degree of gap junction coupling (Vaney, 2002). Formed by two hemichannels, each comprised of six connexin (CX) subunits, the molecular composition of gap junction shows a high degree of diversity across retinal cell types (Bolte *et al*., 2016; Dermietzel *et al*., 2000; Güldenagel *et al*., 2000). The connexin

family includes 20 genes in rodents (21 in humans), with at least 15 of these 20 genes expressed in the retina (Bolte *et al.*, 2016). Further, diversity of CX proteins is also found within retinal cell types. Most retinal cell types utilize one or two types of connexin subunits while gap junction formation in ganglion cells consists of at least three (Degen *et al*., 2004; Güldenagel *et al*., 2000; Muller *et al*., 2010). Gap junctions also differ in their coupling patterns (coupling similar or dissimilar cell populations; see Völgyi *et al.*, 2013), their biophysical properties (Nielsen *et al*., 2012) and the mechanisms by which their expression is regulated (Bloomfield & Völgyi, 2009). This diversity translates to a large number of functional roles for gap junctions in the retina, several of which have been studied in great detail (Bloomfield & Völgyi, 2009). One of these roles is neuronal synchronization: the firing of action potentials in near perfect synchrony by neighbouring coupled neurons. Synchronization is also the most commonly described functional role for electrical coupling elsewhere in the CNS (see Bennett & Zukin, 2004 for review). Correlated firing plays an important role in the widespread network oscillations (of the membrane potential) thought to underlie neuronal processing in the hippocampus (LeBeau *et al.*, 2003) as well as oscillations important for retinal circuit development (Blankenship *et al.*, 2011; Sernagor *et al.*, 2001; Syed *et al.*, 2004). Synchronization may also provide a mechanism for more effective transmission of information, increasing the bandwidth of the optic nerve through transmission of a separate simultaneous stream of information (synchrony) in addition to information contained in the spike rate code (Meister & Berry, 1999).

Correlated firing patterns can arise as a result of several circuit arrangements, but can be differentiated based on the time-scales over which they operate (Aertsen *et al.*,

1989; Brivanlou *et al*, 1998; Gerstein & Perkel, 1969). Neurons sharing excitatory input from another neuron, such as neighbouring ganglion cells receiving input from the same bipolar cell, would tend to fire over the same broad (~100 ms) period. On a much smaller time-scale, cells coupled by gap junctions are able to reciprocally excite each other and drive correlated firing over several milliseconds (fine-scale correlations; Mastronarde, 1989; Meister *et al.*, 1995). Despite a large body of work describing fine-scale correlations in the retina (Brivanlou *et al*., 1998; Devries, 1999; Mastronarde, 1983a-c; Meister *et al*., 1995) and elsewhere in the CNS (Galarreta & Hestrin, 1999; Gibson *et al.*, 1999; Landisman *et al*., 2002; Mann-Metzer & Yarom, 1999), the specific mechanisms by which weak gap junction inputs are able to influence spike timing remain poorly understood. This is a consequence of the distal dendritic locations and small unitary conductances that characterize most gap junction-mediated connections (Bennett & Zukin, 2004; Connors & Long, 2004).

Gap junction input within many retinal circuits appears to be relatively small when compared to chemical synaptic inputs generated in response to light stimulation. Action potential firing in retinal ganglion cells (~60mV in amplitude) generates only weak (~1mV) depolarizations at the somas of coupled neurons. This attenuation is largely the result of the high capacitance and resistance of the post-synaptic membrane (of the coupled neighbour) which attenuates and low-pass filters the current (Bennett & Zukin, 2004; Connors & Long, 2004; and see Trenholm *et al.*, 2013). Some studies have speculated that depolarizations of this amplitude could be sufficient to influence spike timing, provided the cell membrane is approaching spike threshold (Brivanlou *et al*., 1998; Trenholm *et al*., 2013). Others however have argued that dendritic mechanisms are

required to amplify such weak gap junction inputs (Migliore *et al.*, 2005; Turecek *et al.*, 2014). These hypotheses have not been tested experimentally however, owing to the difficulty of recording from paired coupled neurons or directly from dendrites where such mechanisms would be present. Studies of the mechanisms underlying nonlinear dendritic mechanisms thus far have therefore relied on computational models, current injections simulating dendritic activity, or glutamate uncaging techniques to generate localized depolarization (Landisman *et al.*, 2002; Migliore *et al.*, 2005; Vervaeke *et al.*, 2012).

Here, I make use of the light-sensitive and planar nature of the retina to study the biophysical mechanisms underlying fine-scale correlated spiking between retinal ganglion cells. Specifically, I measure correlated firing in a population of directionally-selective ganglion cells (DSGCs), which preferentially encode stimulus movement in the superior direction. sDSGCs are electrically coupled and labelled by a fluorescent reporter in the Hb9GFP transgenic mouse line (Trenholm *et al.*, 2013). I make paired recordings from neighbouring sDSGCs and measure light-evoked spike trains to compute fine-scale correlations. Using pharmacological and physiological approaches, I demonstrate that not only do fine-scale correlations in coupled sDSGCs rely on gap junctions, but that correlated firing relies on the activity of dendritic Na^+ channels. I demonstrate that coincident electrical (gap junction) and chemical inputs, but not electrical inputs alone, allow for the recruitment of dendritic Na^+ channels required for the generation of correlated action potentials.

3.3. Methods

3.3.1. Animals

Experiments were performed with adult transgenic mice, of both sexes, maintained on a 12-h light/dark cycle. Experiments were performed on retinal preparations from three transgenic mouse lines: Hb9::eGFP (RRID: MGI_109160), C57Bl/6 mice (wild type; RRID:IMSR_JAX:000664) or *Cx36*$^{-/-}$ mice (kindly provided by D. Paul, Harvard University). All procedures were either performed in accordance with the Canadian Council on Animal Care and approved by the University of Victoria's Animal Care Committee or were approved by the University of Washington's Animal Care Committee.

3.3.2. Whole-mount retinal preparation

Mice were dark-adapted for approximately 30–60 min to ensure similar gap junction coupling across retinal preparations. Mice were then anesthetized by inhalation of isofluorane or injected with a lethal dose of pentobarbital, via intra-peritoneal injection, and decapitated. Eyes were removed using forceps (severing the optic nerve), with a small incision made on the nasal side of the cornea to assist with later identification of retinal orientation. The retina was dissected under infrared light in Ringer's solution containing 110 mM NaCl, 2.5 mM KCl, 1 mM $CaCl_2$, 1.6 mM $MgCl_2$, 10 mM glucose and 22 mM $NaHCO_3$, bubbled with carbogen (95% O_2-5% CO_2). The isolated retina was then mounted on a 0.22-mm membrane filter (Millipore) with a pre-cut window through which light could reach the retina. The preparation was viewed with infrared light using a Spot RT3 CCD camera (Diagnostic Instruments) attached to an upright Olympus BX51WI fluorescent microscope outfitted with a 40× water-immersion

lens (Olympus Canada). The isolated retina was then perfused with heated Ringer's solution (35–37 °C).

3.3.3. Physiological recordings

Spike recordings were made using the loose cell-attached patch-clamp technique using 5–10-MΩ electrodes filled with Ringer's solution. For current-clamp experiments, 5–8-MΩ electrodes contained 115 mM potassium gluconate, 9.7 mM KCl, 1 mM $MgCl_2$, 0.5 mM $CaCl_2$, 1.5 mM EGTA, 10 mM HEPES, 4 mM ATP-Mg_2, 0.5 mM GTP-Na_3, 0.025 mM Alexa 594 and 7.75 mM Neurobiotin. The pH was adjusted to 7.2–7.3 with KOH. Recordings were made with a MultiClamp 700B amplifier (Molecular Devices). Signals were digitized at 10 kHz (PCI-6036E acquisition board, National Instruments) and acquired using custom software written in LabVIEW. Green fluorescent protein-positive (GFP^+) directionally-selective ganglion cells (DSGCs) were targeted for recordings using two-photon laser-scanning microscopy techniques with the wavelength at 920 nm to minimize photoreceptor bleaching. GFP^- DSGCs were identified by their medium-sized elliptical somata and their ON-OFF directionally selective response properties that differed in preferred direction from GFP^+ cells.

For experiments in which spikelets were simulated with current injection, after ON-OFF DSGCs were identified, a whole-cell recording was made using a 3–6-M electrode containing 125 mM potassium aspartate, 1 mM $MgCl_2$, 10 mM KCl, 10 mM HEPES, 2 mM EGTA, 1 mM $CaCl_2$, 4 mM ATP and 0.5 mM GTP, with the pH adjusted to 7.2 using KOH. In some experiments, a small amount of hyperpolarizing current was injected through the recording electrode, to compensate for an offset introduced after making a whole-cell recording. This helped to maintain the low spontaneous spike rate

and robust light responses typical of ON-OFF DS cells seen in the loose-patch configuration.

Tetrodotoxin (TTX; 1µM; Alomone Labs), a Na^+ channel inhibitor, used in the local application experiments (**Figures 19, 20, 22, and 23**), was included in a recording electrode which had been coated in agarose (1%; Sigma-Aldrich Canada Ltd.). Positive pressure was applied manually using a mouthpiece to locally puff TTX. NBQX (20 µM), D-AP5 (50 µM) and tubocurare (50 µM), inhibitors of AMPA receptors, NMDA receptors, and nicotinic acetylcholine receptors were used to decrease sDSGC spike rates when desired (see Figure 21). Picrotoxin (50 µM), an antagonist of $GABA_A$ and $GABA_C$ receptors, was used to decrease inhibition in the DS circuit, increasing the spike rate of sDSGCs.

3.3.4. Light stimulus

Broad-spectrum white light stimuli were generated with a digital projector (Hitachi Cpx1, refresh rate 75 Hz) or with an OLED monitor (eMagin) that was controlled with custom-written software incorporating Psychtoolbox. Light stimuli were projected from below the preparation and focused on the photoreceptor layer using the sub-stage condenser. The ambient background intensity, measured with a calibrated spectrophotometer (USB2000, Ocean Optics), was set to approximately ~500 to 1000 R* per rod per s. Light stimuli, projected from below the preparation, were focused with the substage condenser onto the outer segments of the photoreceptors.

3.3.5. Cross-correlograms and correlation index

Cross-correlograms were computed from spike trains measured in neighbouring coupled DSGCs, evoked by static flashes, moving bars or moving gratings (usually 50–400 repetitions or cycles). Cross-correlograms were constructed on the basis of the relative time differences between spikes observed in neighbouring neurons C1 and C2 (that is, using the spike train from C1 as the reference and spikes from C2 to make the histogram). Relative spike times were parsed into 0.5-ms bins (unless otherwise noted) and the correlograms were averaged over multiple trials. To estimate stimulus driven correlations, we re-computed cross-correlograms after shuffling trials using conventional methods, thereby obtaining a 'shift predictor'. Cross-correlograms were not shift predicted unless otherwise stated in the text, to allow an assessment of stimulus driven activity under different experimental conditions.

To quantify correlations, we calculated a correlation index (CI). To do so, we first discretized time into 4-ms bins (to capture the peaks of the cross-correlogram) and assigned the value 1 to a bin if the neuron spiked within it and 0 otherwise. We then computed the Pearson correlation coefficient (CC) between spike trains in the two neurons (where spike covariance of the two neurons is normalized by the geometric variance of their firing rates). To remove stimulus driven correlations, we computed the CC on a shuffled set of trials (SCC) and then defined the CI as CC – SCC.

3.3.6. Simulated spikelets

Ten different spikelet patterns were generated using a 20-Hz Poisson spike generator to randomly assign spikelet times. The spikelet waveform used was the peak-aligned average of ~100 spikelet currents measured in voltage-clamp from an sDSGC.

While injecting a Poisson-generated spikelet pattern into a cell, a 300-μm bright square was flashed for 1 s over the cell's receptive field. The amplitude of the injected spikelets was controlled by scaling the entire waveform by a constant factor. The depolarization induced by each spikelet was defined as the maximum membrane potential in a 13-ms window surrounding an injected spikelet time. Depolarizations in that window that surpassed spike threshold were not considered. For each of five to six spikelet amplitudes, roughly 3,000 spikelets were injected over 60 trials for each cell. As with spike trains, cross-correlograms between binarized spike and spikelet trains were constructed. Cross-correlograms were normalized by the geometric mean of the spike and spikelet autocorrelation functions to yield a correlation value as a function of time delay.

3.3.7. Data analysis

Comparisons between groups were made with *t* tests. Comparisons made between recordings from the same cell before and after applying pharmacological agents (or before and after experimental manipulation, such as changing the contrast) were made using paired *t* tests. For comparison between multiple groups, we used a one-way ANOVA. Data are presented as mean ± s.e.m. All data used for analysis with *t* tests and paired *t* tests were tested for normality using the Shapiro-Wilk normality test and passed the test. The data for the ANOVA failed the normality test, so we used the Kruskal-Wallis one-way ANOVA on ranks.

3.4. Results

3.4.1. DSGCs exhibit fine-scale correlations

Previous studies have demonstrated that superior-coding directionally-selective ganglion cells (sDSGCs) are homologously coupled by gap junctions (Trenholm *et al.*, 2013a; Trenholm *et al.*, 2013b), allowing transmission of electrical signals between neighbouring sDGSCs with high temporal precision and fidelity (Trenholm *et al*., 2013). While correlated spiking has been shown in several ganglion cell populations (Mastronarde, 1983; Shlens *et al*., 2009), correlations have not been tested in sDSGCs. I tested for the presence of correlated spiking in coupled sDSGCs by performing paired cell-attached recordings from neighbouring neurons (**Figure 15A**) and computing cross-correlograms from light-evoked spike trains (**Figure 15B-D**; and see Methods). Stimulus correlations (on the order of several hundred milliseconds) were apparent from spike trains (**Figure 15B**) and shift predicted cross-correlograms (**Figure 15E**), consistent with neighbouring sDSGCs receiving input from overlapping populations of bipolar cells. Importantly however, sDGSC spike trains also exhibited fine-scale correlations (**Figure 15C**), with spiking in each of the respective sDSGCs the likelihood of action potential firing in the other 1-2 ms later (**Figure 15D**, and see inset). Fine-scale correlations could be specifically extracted from stimulus correlations by subtracting the shift-predicted cross-correlogram (**Figure 15E**), with the strength of correlations computed using a correlation index (CI; see Methods; n=8 pairs, CI=0.13±0.03). When ON and OFF DSGC responses were separated, fine-scale correlations were observed in both components of the response (**Figure 15G-H**) and were therefore combined (**Figure 15D/I**). Thus,

consistent with other gap junction-expressing neurons, coupled sDSGCs exhibit robust fine-scale correlations.

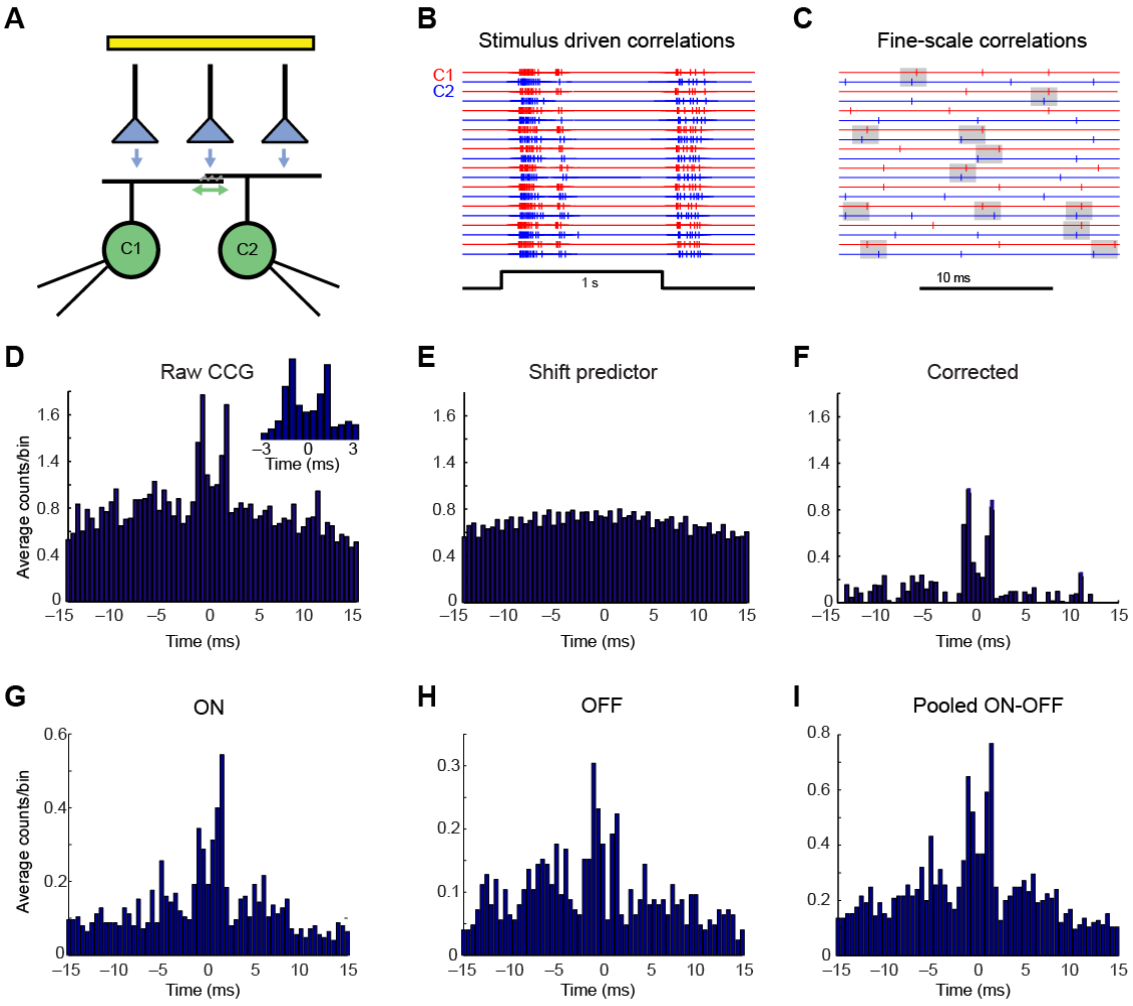

Figure 15. DSGC ON and OFF responses exhibit fine-scale correlations.
A. Schematic of a cross-section of the inner retina, depicting glutamatergic bipolar cells terminals (blue triangles) synapsing onto electrically coupled sDSGCs, labelled in the *Hb9::eGFP* retina (green cells; for simplicity only the ON dendrites are drawn). The flash used to stimulate the photoreceptors (not shown) is illustrated by the yellow bar. The vertical and horizontal arrows indicate chemical and reciprocal electrical synapses, respectively. **B.** Spike trains evoked by a high contrast spot (300 μm diameter; 10 trials), measured simultaneously from a pair of sDSGCs (C1 and C2) are synchronized on a broad time scale by the stimulus. **C.** A high temporal resolution view of a portion of the ON response shown in (b) illustrates fine-scale correlated spikes (highlighted by grey boxes; 2 ms), which are independent of the stimulus. **D.** A cross-correlogram (CCG) which indicates the distribution of spike times measured in C2 relative to each spike in C1 (0.5 ms bins), as well as the shuffled trials shift predictor (**E**) and the shift-predictor subtracted (**F**, Corrected) correlations. G-I. Cross-correlograms produced from DSGC ON (**G**) and OFF (H) responses (in response to light onset, and offset, see **B**). ON and OFF responses alike exhibit fine-scale correlations, thus all subsequent data in this chapter represents data pooled data from ON and OFF responses (**I**).

3.4.2. Fine-scale correlations are mediated by gap junctions

In order to test the role of gap junctions in establishing fine-scale correlations in sDSGCs we measured the strength of correlations before and after the bath application of the gap junction inhibitor 18β-Glycyrrhetinic acid (18βGA; 25 μM). Fine-scale correlations were absent in the presence of 18βGA (CI = 0.05±0.01; n=6 pairs; paired *t*-test: P<0.0001, t_5=6.756), despite 18βGA having a minimal effect on the spike rate (**Figure 16A;** middle) and underlying stimulus correlations (**Figure 16B**; middle). This suggests an important role for gap junctions in driving fine-scale correlations. Importantly, DSGC populations lacking gap junction input (those coding for the other three directions of motion) also lacked fine-scale correlations. Paired spike recordings were made from neighbouring uncoupled DSGCs, coding for ventral and nasal directions of motion, i.e. vDSGCs and nDSGCs (polar plots of directional responses are shown in **Figure 16D**). Despite exhibiting significant receptive field overlap (**Figure 16E**), no fine-scale correlations were present (**Figure 16F**; CI= 0.06±0.01; n=5 pairs; *t*-test: P=0.01, t_{11}=3.241). These results demonstrate a clear role for gap junctions in the generation of fine-scale correlations observed in superior-coding DSGCs.

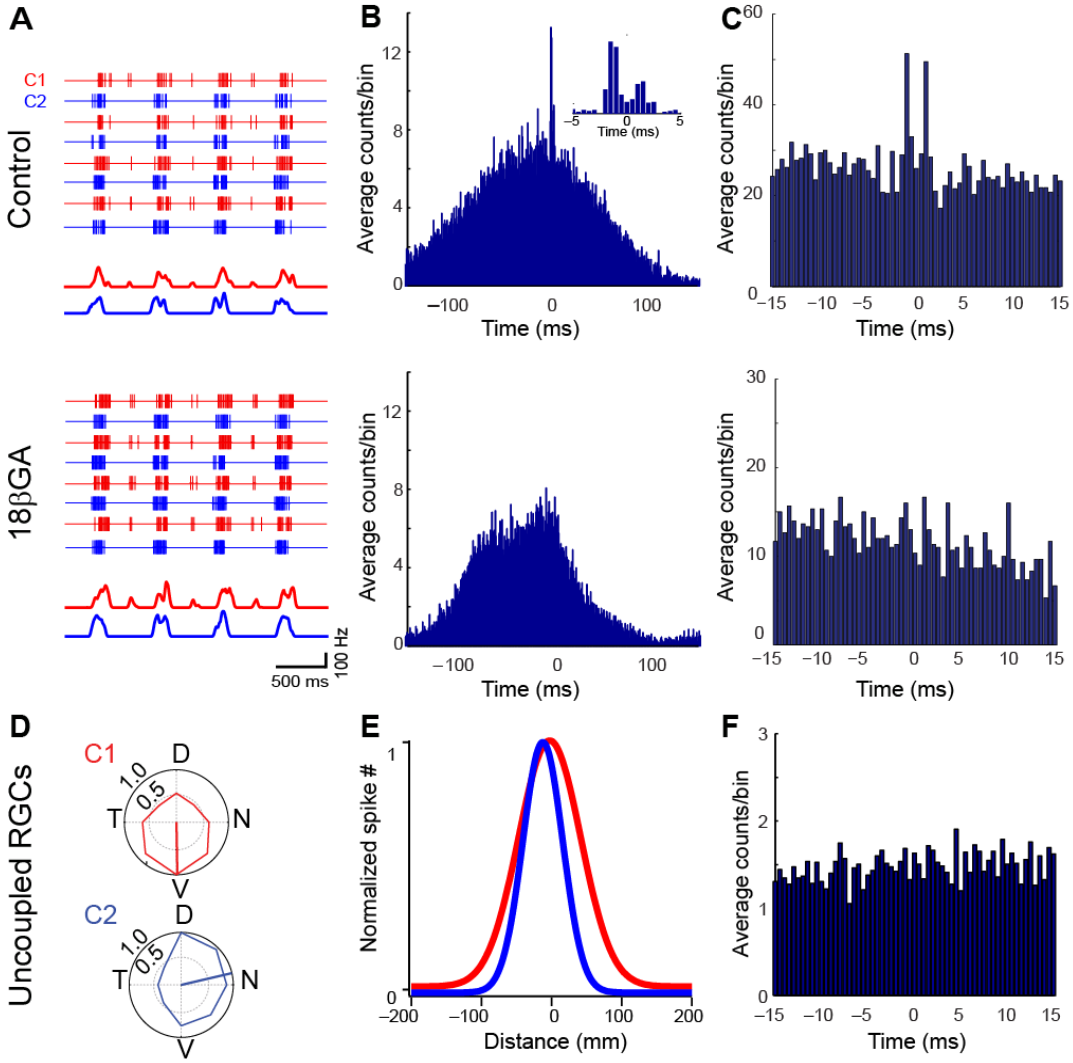

Figure 16. Fine-scale correlations are mediated by gap junctions between ganglion cells. **A**. Control (top) and 18β-glycyrrhetinic acid (18βGA, 25 μM, bottom) treated responses from a pair of sDSGCs. The traces represent extracellular spike recordings from a pair of neighbouring DSGCs (C1, red = cell 1; C2, blue = cell 2) in response to drifting gratings along the preferred direction. Gaussian fits of the spike rate are plotted below the example traces. **B**-**C**. Cross-correlograms for control (top) and 18βGA (bottom) treated responses on two different timescales, demonstrating broad, stimulus driven correlations (**B**), and fine-scale correlations (**C**) respectively. **D.** Polar plots indicating the peak spike rate (normalized to the preferred direction) evoked by stimuli moving in 8 directions, measured simultaneously in a pair of uncoupled DSGCs (C1 & C2) coding different directions. **E.** Gaussian approximations of the receptive fields of cells in (**D**), indicating the high degree of receptive field overlap between C1 and C2 (*bottom left*, see Methods). **F.** A cross-correlogram for light-evoked spike activity for this pair of uncoupled DSGCs. Legend: D = dorsal, N = nasal, V = ventral, T = temporal.

3.4.3. Gap junction inputs alone are insufficient to generate fine-scale correlations

To establish whether gap junction input alone is sufficient for generating fine-scale correlations, correlations were measured in several conditions that reduced (or abolished) specific chemical inputs. First, paired whole-cell recordings were made from coupled sDSGCs, and cross-correlations were computed from spike trains generated from depolarizing currents injected through the recording electrodes (**Figure 17A**). In this configuration no light stimulus was provided, and chemical inputs to DSGCs were likely to be minimal, however strong fine-scale correlations were observed (**Figure 17C**). Next, fine-scale correlations were computed in the presence of individual synaptic blockers. Correlations persisted following bath application of NBQX (20 µM; **Figure 17D**), D-AP5 (50µM; **Figure 17E**) and picrotoxin (Ptx; 50µM; **Figure 17F**), blocking AMPA receptors (as well as starburst amacrine cell input of acetylcholine and GABA), NMDA receptors and $GABA_A$ receptors respectively. These results suggest that gap junction input is sufficient to elicit correlations in the absence of chemical input. However, gap junction inputs are weak, giving rise to only ~1mV spikelets at the recipient cell soma, observed when the post-junctional cell fails to fire an action potential (**Figure 17B**, black arrow), or when only one cell of the pair is depolarized (Trenholm *et al*., 2013 and **Figure 19A**). Thus, how gap junction input could significantly influence spike timing at the soma is unclear.

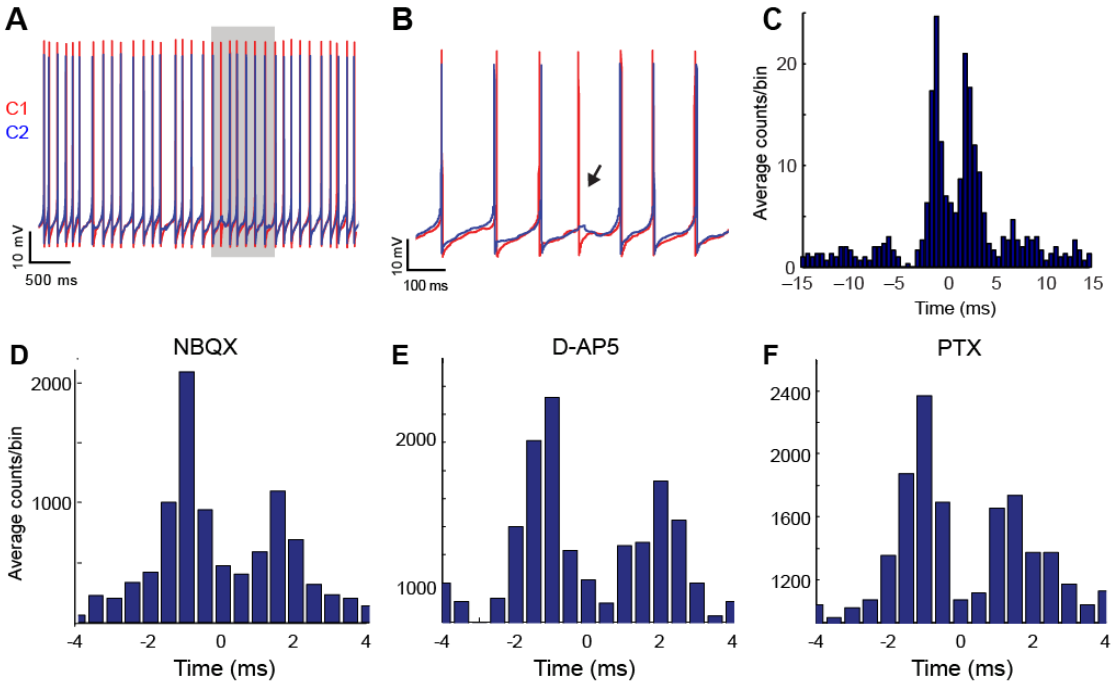

Figure 17. Correlations persist in synaptic receptor blockers and in the absence of chemical input.
A. Spiking responses in a pair of cRGCs (C1 red, C2 blue) in which both cells were injected with constant depolarizing current (~200 pA) through the patch electrode. **B.** The area shaded in grey in (**A**) is shown at higher temporal resolution. The arrow points to a coupled spikelet (driven by C1) revealed during a spike failure in C2. **C.** A cross-correlogram computed for spike trains measured in the pair of DSGCs shown in (**A**). **D-F.** Cross-correlograms for NBQX (**D**), D-AP5 (**E**) or PTX (**F**) treated responses.

To determine whether the ~1mV gap junction-mediated spikelets were sufficient to influence spike timing at the sDSGC soma on their own, we simulated gap junction input at the soma of a single sDSGC using current injections. Poisson-distributed current pulses were injected through a patch pipette to mimic gap junction-mediated somatic spikelets from a neighbouring neuron. The spike train of the hypothetical coupled neuron (which these injections are mimicking; C1) can be seen in **Figure 18A** (top). This experiment was performed several times for injected currents of different amplitudes

(20pA to 380pA), generating “coupled” spikelets ranging in amplitude from 1-4mV to 7-17mV (**Figure 18B**; and see the larger spike trains visible in the example traces of **Figure 18A**). Correlations were then calculated between the simulated spike train (C1) and the light-evoked action potentials of the sDSGC from which we recorded (C2). Injected currents that generated spikelets similar in amplitude to experimentally measured coupled spikelets (20 pA currents; ~1 mV at the soma; **Figure 18B**) had no observable effect on spike timing, generating no peaks in the cross-correlogram (**Figure 18C**, top). Much larger currents (160-320 pA), generating somatic depolarizations of 5-20 mV, were required in order to elicit significant correlations (**Figure 18B-C**, bottom; note correlations exhibit only 1 peak as a result of the single-cell recording configuration). This result suggests that the signal required for synchronization is larger than the ~1 mV coupled spikelets observed at the soma, generated exclusively by passive gap junction input. Thus, either correlations arise within distal dendrites where gap junction signals are largest, or mechanisms exist to amplify weak gap junction inputs.

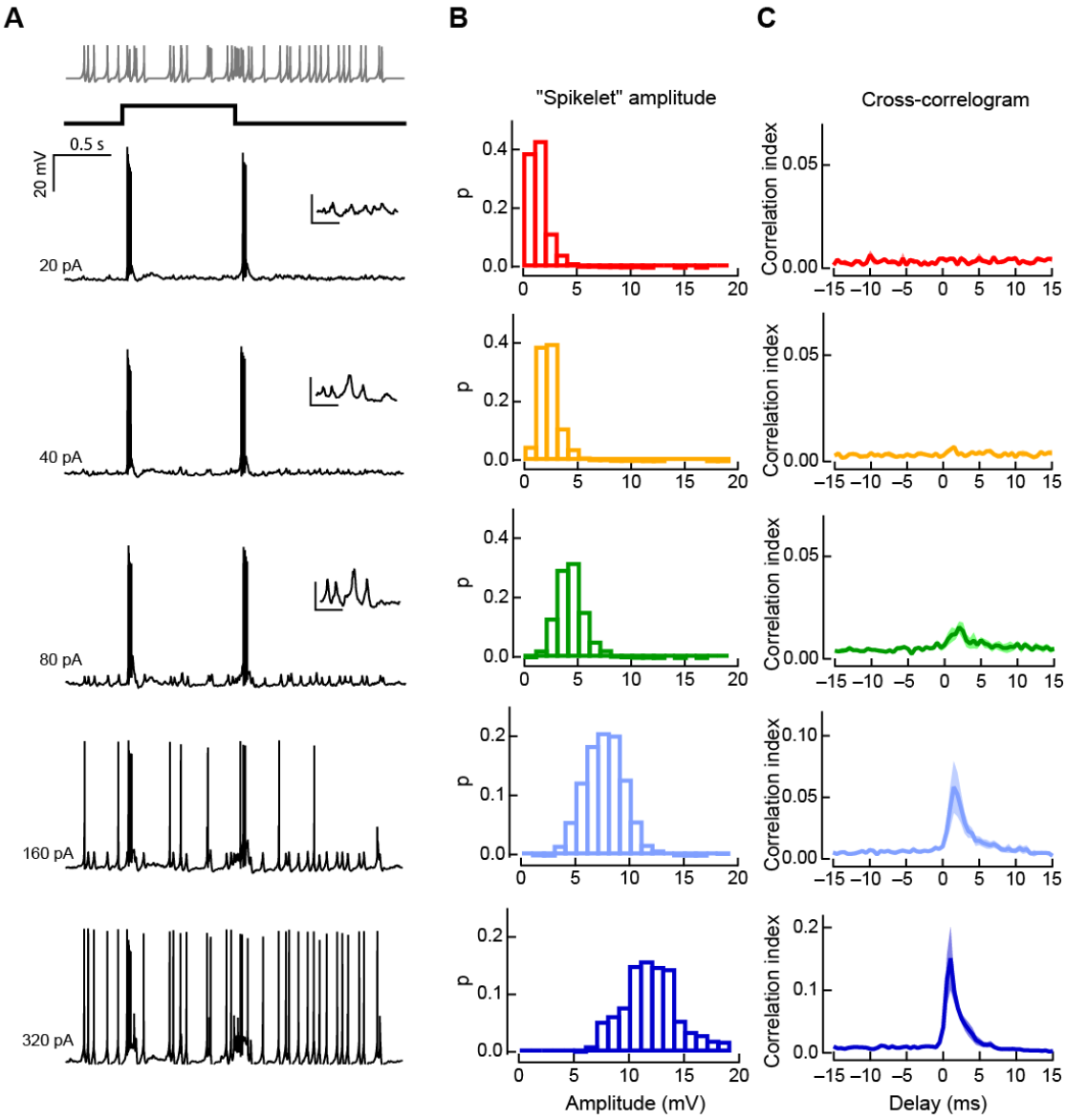

Figure 18. Simulated coupled spikelets do not act at the soma to drive correlated spiking.
A. Representative responses of a coupled DSGC to a 1 s light flash while a Poisson-distributed train of simulated spikelets (indicated on top) of varying amplitudes (indicated on the left) were injected into the soma. The insets show the voltage responses to the spikelet injections at higher magnification (Scale bar for the insets: 5 mV, 100 ms). **B.** Plots of the distribution of peak membrane depolarizations evoked by different sized current injections. **C.** Correlation index between injected spikelets (simulating input from C2) and light-evoked action potentials plotted as a function of delay in C1 (n = 6 cells).

3.4.4. DSGCs exhibit dendritic spikes

DSGCs in rabbit retina have been shown to exhibit voltage-gated channels (Oesch *et al.*, 2005), which could work to amplify weak distal inputs. We tested the hypothesis that mouse sDSGCs exhibit dendritic spiking by recording light-evoked action potentials in current-clamp configuration. Somatic action potential generation was inhibited by local application of TTX, revealing small, rapid spike-like events (**Figure 19B**). These events exhibited no refractory period (**Figure 19C**), consistent with points of origin in distinct dendrites. These events also exhibited rapid kinetics (**Figure 19D-E**). Plotting peak event amplitude as a function of the event rate of rise (amplitude of the derivative; **Figure 19F**) reveals that dendritic spikes represent a distinct population of events from both action potentials, measured prior to TTX application (**Figure 19B**, top), and gap junction-mediated coupled spikelets, measured passively in response to action potential generation in neighbouring coupled DSGCs (**Figure 19A**). These results clearly demonstrate that sDSGCs exhibit dendritic spikes. Importantly, the distinction between gap junction input and dendritic spikes (**Figure 19F**) demonstrates that gap junction inputs alone are insufficient to generate dendritic spikes. The absence of dendritic spikes in control traces suggests dendritic spikes are very effective in eliciting somatic action potentials. Interestingly, the amplitude of dendritic spikes (though likely underrepresented here as a function of TTX application) is similar to the amplitudes of events necessary to influence spike timing (**Figure 19F** and **19B**). sDSGCs therefore not only exhibit dendritic spikes, but dendritic spikes may also be ideally suited to drive correlated firing.

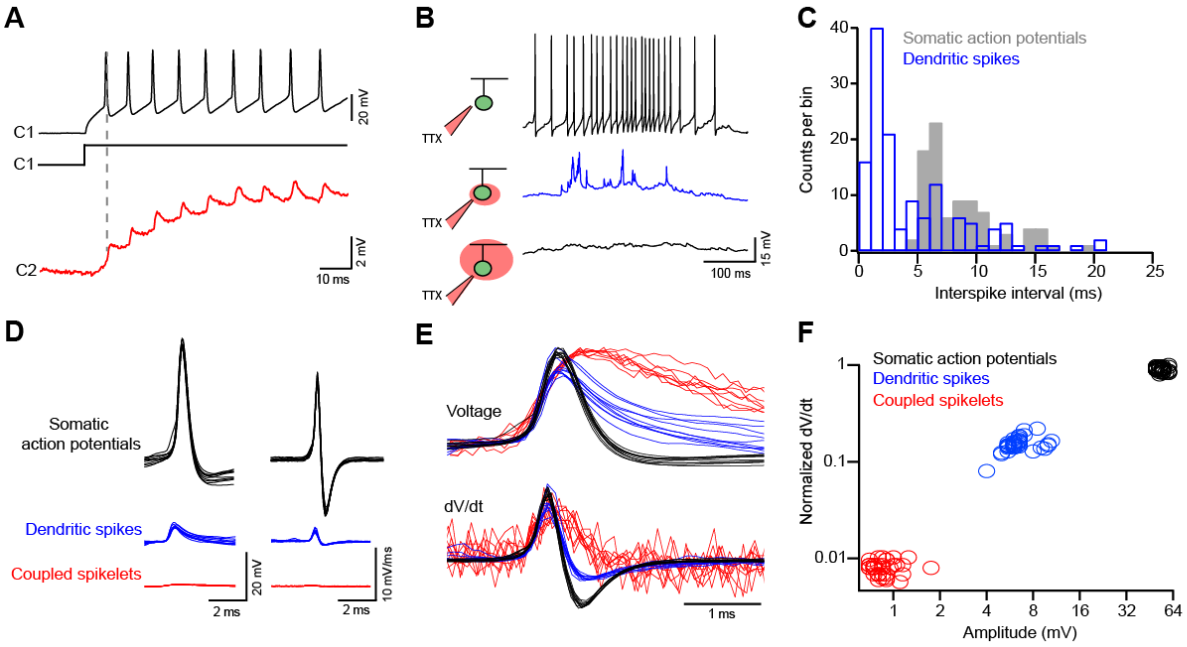

Figure 19. Gap junction inputs on their own do not trigger dendritic spikes.
A. Spike trains evoked in C1 (black; 200 pA depolarizing current step injected through the patch electrode) drive coupled spikelets in C2 (red) which are exclusively mediated by gap junctions (spikelets are shown on a magnified scale). **B.** Local application of TTX blocks somatic spikes (top, black), revealing dendritic spikes (middle, blue) which are abolished when TTX is applied over the entire cell (bottom). **C.** A plot of the interspike interval (dendritic spikes (blue) and somatic action potentials (grey); n = 89 action potentials and dendritic spikes from 4 cells) illustrates a ~5 ms refractory period for somatic action potentials but not dendritic spikes. **D.** Overlays of somatic action potentials (black), dendritic spikes (blue) and coupled spikelets (red), shown on the same scale (n = 10 events; left). The time derivative of these events is shown on the right. **E.** Normalized versions of the traces shown in (**D**), emphasizing the different kinetics of the somatically measured events. **F.** The maximum rate of change in voltage plotted against the peak voltage for the three types of events (35 events are plotted for each type). For this plot, light-evoked somatic action potentials and dendritic spikes were from the same cell, which was hyperpolarized to increase the failure of somatic action potentials, while coupled spikelets were measured using the protocol shown in (**A**).

3.4.5. Dendritic Na^+ channels are required for correlations

We next sought to assess the importance of dendritic spiking in the generation of fine-scale correlations. To test this we established a protocol for measuring correlations in the presence and absence of dendritic spiking. TTX was applied locally by diffusion of TTX through an agar-coated electrode, with the flow of TTX directed away from the

somas of sDSGCs (based on the direction of solution perfusion; **Figure 20A**). The impact of local TTX application on both somatic action potentials and gap junction currents was assessed using simultaneous extracellular and voltage-clamp recordings respectively (**Figure 20B-F**), with action potential firing elicited using a small static light stimulus. Local TTX application reduced the amplitude of the gap junction current, as measured in voltage-clamp configuration (**Figure 20F**), as well as spike rate (but see below). However, TTX had no effect on the amplitude or waveform of somatic action potentials. This drug delivery system was therefore well suited to inhibit dendritic, but not somatic action potentials. Using this methodology we assessed the impact of inhibiting dendritic spiking on the generation of fine-scale correlations. With TTX applied over regions of overlapping dendrites (**Figure 20G**), fine-scale correlations were significantly affected (**Figure 20H-I**; 58 ± 10% reduction in CI; n=5 pairs; *t*-test: P=0.017, t_4=3.959), suggesting an important role for dendritic spikes in spike synchrony.

I sought to confirm that the effect on correlations was not a result of the decreased spike rate by modulating spike rate, using either pharmacological means (NBQX, AP-5 or Ptx; **Figure 21D**), or by modulating stimulus contrast (**Figure 21A-C**). These experiments showed a relationship between spike rate and correlation strength. Interestingly however, decreasing spike rate with contrast (n=6 pairs, high contrast CI: 0.15 ± 0.03, *t*-test: P= 0.022, t_5= 3.655), or pharmacology (excitatory blockers, n=6 pairs, *t*-test: P=0.004, t_5=4.904; Ptx, n=4 pairs, *t*-test: P= 0.045, t_3= 3.311) had a positive effect on correlation strength (**Figure 21C-D**). Thus the diminished strength of correlations observed in the presence of dendritic TTX (**Figure 20I**) was not an artefact of reduced spike rate, with dendritic spikes indeed important for fine-scale correlations.

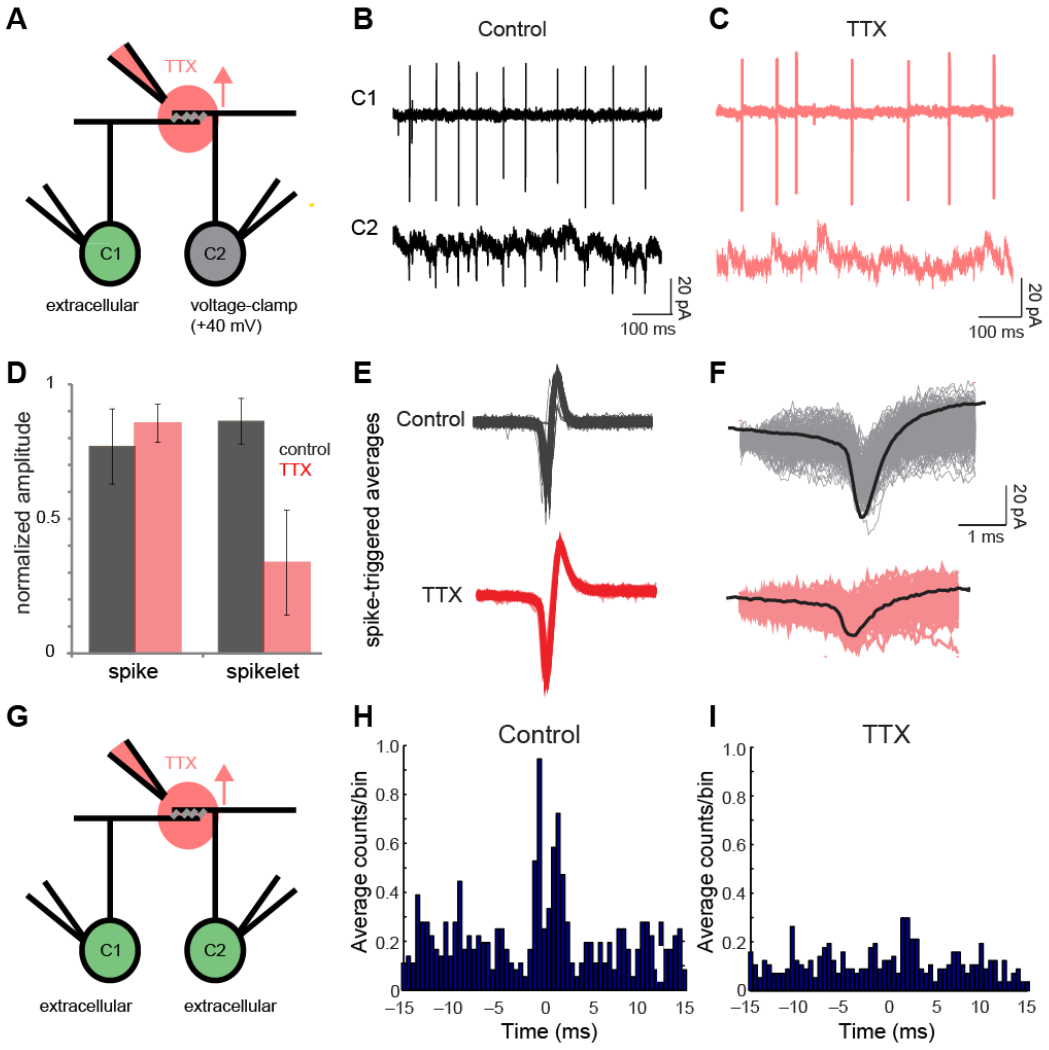

Figure 20. Dendritic Na+ channels, important for action potential backpropagation, are required for correlated activity.
A. Schematic depicting the recording configuration, in which TTX was puffed locally over the region of dendritic overlap using a recording electrode while simultaneous recordings (one in extracellular configuration, and the other in voltage-clamp configuration with V_{hold}= +40 mV) were made from neighbouring coupled DSGCs. **B-C.** Representative responses from sDSGCs in the recording configurations described in (**A**) in control conditions (**B**) and following TTX application over the region of dendritic overlap (**C**). Action potentials measured in C1 (*top*) backpropagate into the dendritic tree, and current crosses gap junctions, depolarizing the dendrites of coupled neighbours, measured as in inward current in C2 in voltage-clamp configuration (*bottom*). **D-F.** Spike-triggered averages were produced using the recordings shown in (**B-C**). Overlays of individual action potentials used for spike-triggered averaging are shown in (**E**) and the resulting spikelet produced in C2 (**F**) in control (*top*) conditions and following the TTX puff (*bottom*). **G.** Schematic depicting the recording configuration, in which TTX was puffed locally over the region of dendritic overlap using a recording electrode while simultaneous extracellular recordings were made from neighbouring sDSGCs. **H-I.** Cross-correlograms computed for light-evoked spike trains from a pair of sDSGCs in control conditions (**H**) and when TTX was locally applied over the region of dendritic overlap (**I**).

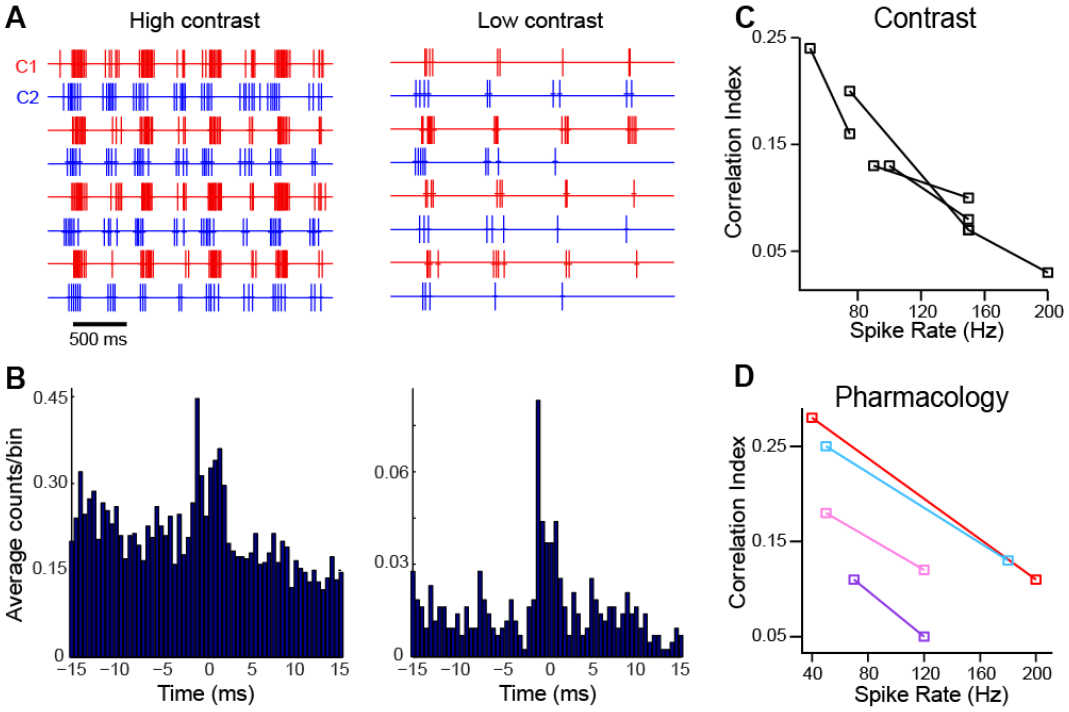

Figure 21. Correlation strength varies inversely with spike rate.
A. Representative spiking responses to moving gratings of high (left) and low contrast (right), recorded from a pair of sDGSCs (C1 and C2; 4 trials are shown). **B.** Cross-correlograms (bottom) computed from recording conditions shown in (**A**). **C.** Correlation strength, assessed using the correlation index, plotted as a function of maximal spike rate obtained by modulating stimulus contrast, as in (**A**). **D.** Spike rate was also modulated using pharmacology (see CCGs in Figure 3D-F). Correlation index was plotted as a function of speak spike rate obtained across recording conditions, with application of NBQX (red), D-AP5 (pink), and tubocurare (purple) decreasing spike rate compared to control, while application of picrotoxin (Ptx; blue) increased spike rate relative to control conditions.

3.4.6. Dendritic spikes underlie fine-scale correlations

Given the importance of dendritic spikes for correlations, I hypothesize dendritic spikes are themselves correlated with spiking from the pre-synaptic neuron of the electrical synapse. As action potentials are generated in the pre-synaptic neuron, they back-propagate, and as current crosses the gap junction it facilitates the generation of dendritic spikes (in the post-synaptic or post-junctional neuron). To assess fine-scale correlations between somatic action potentials in one cell and dendritic spikes in its

coupled neighbour, paired recordings were made from coupled sDSGCs (C1 and C2; **Figure 22A-B**), with TTX applied over the soma of one neuron (C1). TTX application revealed numerous dendritic spikes in one neuron, while not affecting somatic action potentials in its coupled neighbour, allowing for simultaneous measurement of light-evoked action potentials in one cell and dendritic spikes in the other (**Figure 22B**). Cross-correlograms were generated between pre-synaptic somatic action potentials (C1) and post-synaptic dendritic spikes (C2), with somatic action potentials and dendritic spikes from the same cell isolated based on event amplitude and kinetics (amplitude of the derivative trace; **Figure 23A-C**, and see **Figure 19E-F**). Cross-correlograms revealed a strong unilateral correlation, indicating somatic spikes in the pre-synaptic cell significantly influenced the timing of post-synaptic dendritic spikes. The reverse was not true, with dendritic spikes (in C2) unable to significantly influence the timing of somatic action potentials (in C1). This result builds on the previously defined role for dendritic spikes in establishing fine-scale correlations (**Figure 20**), suggesting that back-propagating action potentials increase the probability of correlated dendritic spikes, responsible for the generation of correlated action potentials.

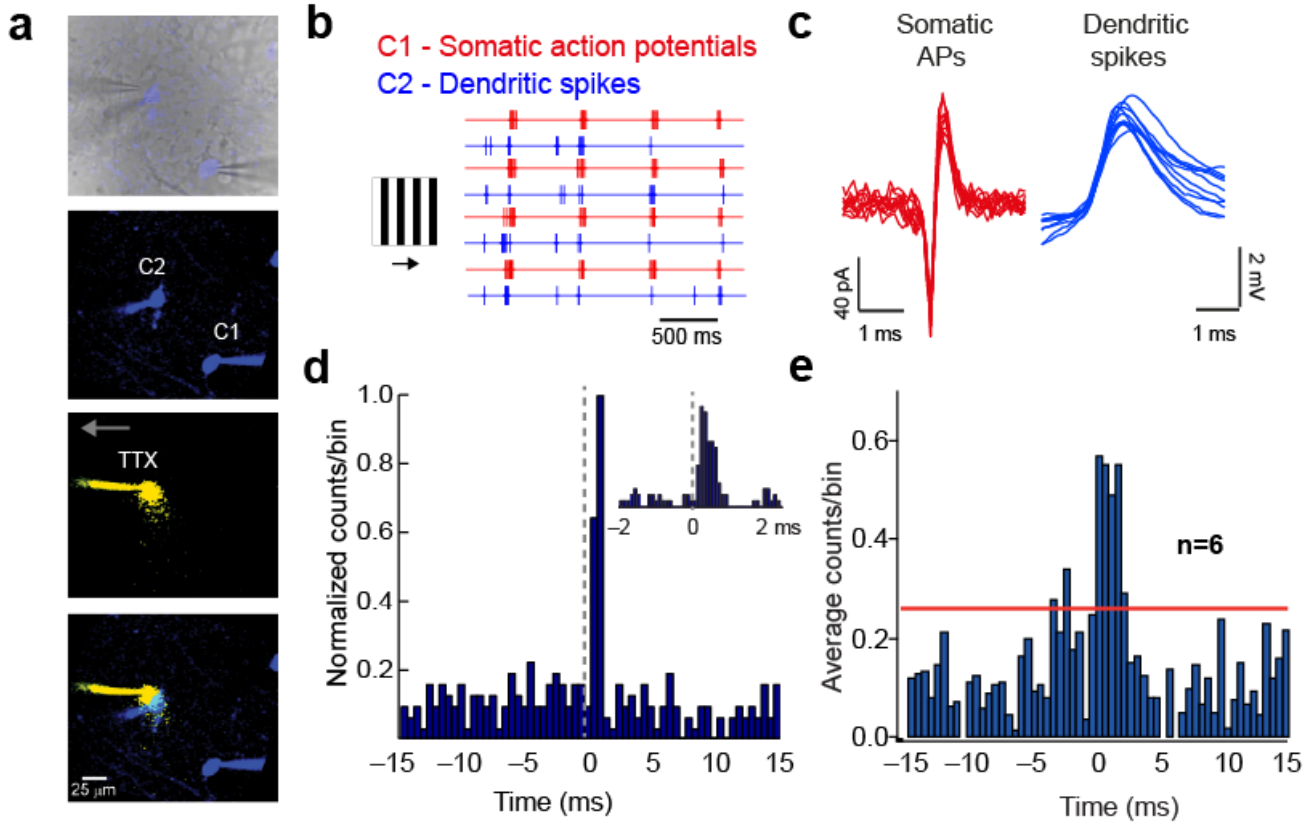

Figure 22. Somatic action potential backpropagation affects the timing of dendritic spikes in coupled neighbours.
A. *Top*, an infrared image depicting the recording configuration (a fluorescent image is overlaid to show *Hb9*$^{+}$ GFP cells in blue). The panels below show fluorescent images of the Alexa-488 filled somata of neighbouring coupled sDSGCs (green channel shown in blue), the local TTX puff imaged in a separate channel (Alexa 594 was included in the puff pipette (red channel shown in yellow)), and an overlay of these images. **B-C.** Responses to drifting gratings (4 trials) are shown for a paired recording in which TTX was locally puffed over the soma of C2. Somatic action potentials were measured extracellularly from C1 (red traces) and dendritic spikes were measured intracellularly from C2 (blue traces; see Figure 9 for experimental details). Individual extracellular spikes (C1, red) and dendritic spikes (C2, blue) are shown below at a higher resolution (10 events are shown for each; **C**). **D.** A cross-correlogram (0.5 ms bins) plotting the distribution of dendritic spike times (measured in C2) relative to action potentials in C1 (set at time 0). The inset shows a cross-correlogram of the same events but sampled at a higher time resolution (0.1 ms bins) illustrating that the dendritic spikes in C2 show an increased probability of occurring shortly after a spike in C1. **E.** An average cross-correlogram from 6 pairs of coupled DSGCs recorded in the configuration described in **D**. The red line indicates the 95% confidence interval.

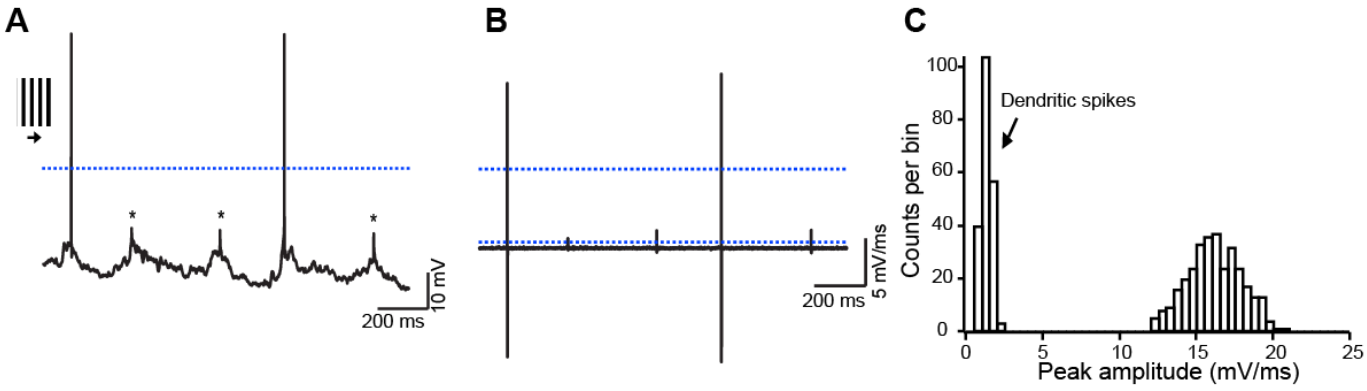

Figure 23. Detecting dendritic spikes by inhibiting somatic Na^+ channels.
A. Intracellular recording of responses of a coupled sDSGC to drifting gratings while TTX was puffed locally over the soma reveals dendritic spikes (asterisks) and larger spike like events that represent incompletely blocked somatic spikes. **B.** The time derivative of the voltage trace shown in (**A**). Events with peak amplitudes falling between the blue dotted lines were unequivocally identified as dendritic spikes and chosen for cross-correlation analysis (**Figure 8**). Larger events that potentially could have arisen from the soma (due to the incomplete block of somatic Na^+ channels by TTX) were discarded in this analysis. **C.** A histogram of the peak amplitude of spike-like events during somatic TTX application (>500 events).

3.4.7. Spatially localized coincident activity is required for correlations

Our experiments thus far have highlighted an important role for gap junction input, and subsequent generation of correlated dendritic spikes, in establishing correlated spiking between coupled sDSGCs. However, the inability of gap junction input alone to drive dendritic spikes (**Figure 19**) points to a requirement for coincident chemical activity, the extent of which has not been explicitly tested. Given our evidence that correlated spiking originates in the dendrites, we hypothesized that chemical input is required specifically within the dendrites receiving gap junction input, while depolarization elsewhere in the dendritic tree would be unlikely to result in correlated firing. In order to study the spatial component of chemical input, important for the generation of fine-scale correlations, we measured spiking from coupled sDSGCs in two conditions which differed in their spatial structure. Both however produced similar spike

rates in DGSCs. The first condition provided chemical input in close proximity to the region of electrical input (overlapping distal dendrites), while the other condition provided chemical inputs in regions distinct from those receiving electrical input (non-overlapping dendritic regions). When a single small spot was used to stimulate sDSGCs, in the region where dendrites of the two DSGCs overlap (**Figure 24A-C**; stimulus 1), robust fine-scale correlations were observed (**Figure 24D**, left). However, when two spots (of total equal area to the single spot) were presented, such that both sDSGCs were stimulated but chemical inputs were received in non-overlapping regions of the two dendritic trees (**Figure 24A-C**, stimuli 2 and 3), no fine-scale correlations were observed (**Figure 24D-E**). The lack of dendritic overlap was determined based on individual stimuli producing spiking in only one of the two cells (**Figure 24C**, stimulus 2 and 3 only). This experiment demonstrates the need for coincident chemical and electrical inputs to sDSGC dendrites for the generation of correlated spiking, a mechanism that likely operates by generating local dendritic spiking (**Figures 19, 20, 22**).

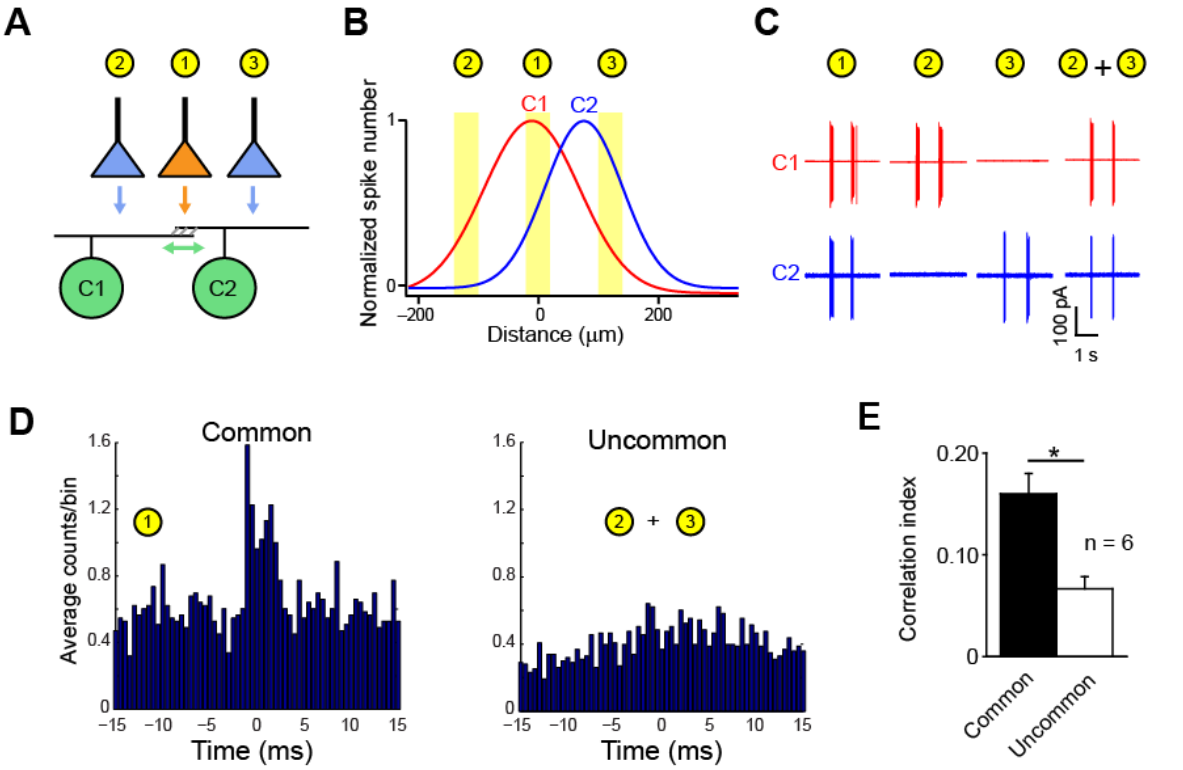

Figure 24. Gap junction-mediated correlations are spatially restricted to overlapping dendritic regions.
A. Schematic of the experimental protocol depicting a small spot stimuli positioned to stimulate common or non-overlapping regions of the receptive fields of neighbouring cRGCs. **B.** The location of the three spots are overlaid over the experimentally measured receptive fields, estimated with one-dimensional Gaussian functions (see Methods). **C.** The light-evoked spiking response of the pair of neurons shown in (**B**) upon stimulation of either common (spot 1) or uncommon regions (spot 2 + 3). **D.** Representative cross-correlograms constructed from spike trains during stimulation of common (left) or uncommon regions (right). **E.** The average CI values for activity driven by common and uncommon input as shown in (**D**).

3.5. Discussion

The work presented here (Chapter 3) support the hypothesis that electrical and chemical inputs sum, in sDSGC dendrites, to generate fine-scale correlations. Active dendritic mechanisms amplify weak dendritic inputs through the generation of correlated dendritic spikes, the action of which underlies correlated spiking at the soma.

3.5.1. Spatial and temporal coincidence detection in sDSGC dendrites

For decades, gap junctions have been known to underlie correlated firing in the retina (Mastronarde, 1983c) as well as elsewhere in the CNS (for reviews see Bennett & Zukin, 2004; Connors & Long, 2004). In some retinal cell types, gap junction inputs alone have been shown to be sufficient to drive correlated spiking. In populations of salamander retinal ganglion cells, for example, spontaneous action potentials are correlated in the absence of light stimulation (Brivanlou *et al*., 1998). In mouse OFF-alpha ganglion cells, despite an absence of such spontaneous firing, stimulation of action potentials in a single cell (by light-stimulation or stimulation through the recording electrode) alone was sufficient to drive correlated firing in correlated neighbours (Hu & Bloomfield, 2003). These results are in sharp contrast to the results observed in sDSGCs (Trenholm *et al*., 2013), where, as for many coupled neurons elsewhere in the CNS, including the cortex (Fukuda & Kosaka, 2003), the hippocampus (Fukuda & Kosaka, 2000), and the cerebellum (Dugue *et al*., 2009; Vervaeke *et al*., 2012), gap junction inputs are weak. They give rise to only small-amplitude somatic spikelets, too small to elicit action potential firing in isolation (**Figure 19A and F**).

Our results demonstrated that gap junctions in coupled sDSGCs were critical for the generation of fine-scale correlations, as correlations were lost following the pharmacological blockade of gap junctions (**Figure 16A-C**). Additionally, fine-scale correlations could be elicited in the absence of specific chemical inputs (**Figure 17D-F**), provided sDSGCs were sufficiently depolarized to elicit spiking (**Figure 17C**). Our results, therefore, suggest that chemical synaptic input is required for correlated spiking. Despite the deviation from studies (Brivanlou *et al*., 1998; Hu & Bloomfield, 2003), the

importance of chemical input as well as electrical input for the generation of fine-scale correlations has been hypothesized since the seminal work of Mastronarde (1983). Uniquely, we propose that such chemical and electrical inputs sum spatially in sDGSC dendrites, as gap junction spikelets at the soma were ineffective in influencing spike timing (**Figure 18**). This requirement for coincident chemical and electrical inputs aligns well with the previously described active mechanisms in sDSGC dendrites (Oesch *et al*., 2005), as chemical and electrical inputs would have to sum on very fine spatial scales in order to trigger activation of Na^+ channels in individual sDGSC dendrites. In line with this model, our results demonstrated a requirement for dendritic spiking in the generation of correlations (**Figure 20H-I**). In addition, using a sophisticated recording configuration we were able to specifically demonstrate fine-scale correlations between pre-synaptic action potentials and post-synaptic dendritic spikes (**Figure 22**), the latter of which underlie correlated action potentials.

3.5.2. Active dendrites in directionally-selective ganglion cells

Our results demonstrated that electrically coupled sDSGCs have dendritic Na^+ channels which endow them with the ability to generate dendritic spikes. The presence of dendritic spikes in these cells is consistent with the previously described role for dendritic spikes in rabbit DSGCs (Oesch *et al*., 2005). Similar to previously work, several lines of evidence from our study are consistent with these events being of dendritic origin, as opposed their presence being explained by artefacts of TTX application on somatic Na^+ channels. First, the events measured exhibited no refractory period (**Figure 19C**). Unlike somatic action potentials, events originating in separate dendritic branches should not be refractory to each other. Second, if TTX application blocked somatic action potentials,

we would expect a range of event amplitudes. However, when dendritic spike amplitudes were plotted, they exhibited a uniform distribution (**Figure 19F**) consistent with a discrete point of origin and firing mechanism. Importantly dendritic spike amplitude distribution did not overlap with those of action potentials, concurrent with their existence as discrete entities (**Figure 19F** and **Figure 23**). Finally, while action potential frequency decreased in the presence of dendritically applied TTX, somatic action potential waveforms were unaffected (**Figure 20D-E**), suggesting differing roles and origins for dendritic and somatic Na^+ channels.

This study provided a novel role for dendritic spiking within sDSGCs, while also demonstrating an important interaction between electrical and chemical inputs in generating dendritic spikes. Previous studies ruled out a role for electrical coupling in the generation of dendritic spikes based on the findings that all four populations of DSGCs exhibited dendritic spiking, while only a single population exhibiting electrical coupling (Oesch *et al*., 2005). Additionally, they claim electrical inputs driving dendritic spiking would extend the receptive fields of coupled DGSCs, inconsistent the sharp delineation of DSGC receptive fields with their dendritic arbours. Consistent with our previous research (Trenholm *et al*., 2013) demonstrating that electrical coupling does not extend the classical receptive field of DSGCs, I show here that gap junction input alone was insufficient to generate dendritic spikes (**Figure 19F**). I instead demonstrate that electrical inputs can affect the timing of dendritic spikes (**Figure 22D-E**), and I propose that they are able to influence the likelihood of dendritic spike generation when chemical inputs are weak. Support for this hypothesis is the increased strength of correlations for

low contrast stimuli, with few non-correlated spikes occurring in sDSGCs given only weak (low contrast) stimulus input (**Figure 21A-C**).

Interactions between chemical and electrical input has been previously shown to affect dendritic excitability in Golgi cells of the cerebellum (Vervaeke *et al*., 2012). Interactions been Na^+ channels and gap-junction mediated inputs have also been shown in many brain areas (Curti & Pereda, 2004; Dugue *et al*., 2009; Haas *et al.*, 2011), as has dendritic spiking (Oesch *et al.*, 2005; Velte & Masland, 1999; Spencer & Kandel, 1961). To my knowledge however, I have provided the first evidence of interactions between dendritic spikes and gap junction inputs. Given the abundance of both dendritic spiking and electrical coupling throughout the CNS, further studies are required to assess whether this is a concerted mechanism across electrically coupled networks for the generation of fine-scale correlations.

3.5.3. Relationship between firing rate and correlations

As demonstrated by the low contrast stimuli driving stronger correlations between neighbouring sDSGCs, the strength of correlations between spike trains from neighbouring sDSGCs exhibited an inverse relationship with the peak spike rate measured from such trains (**Figure 21**). This relationship was consistent across several conditions used to influence firing rate: decreased stimulus contrast decreased firing rate (**Figure 21A-C**); moving stimuli in the null direction decreased firing rate relative to preferred direction stimuli; inhibitors of excitatory activity (NBQX, AP5 and Tubocurare; **Figure 21D**) decreased firing rate; the inhibitory blocker Picrotoxin increased stimulus firing rate (**Figure 21D**). This inverse relationship could arise as a result of several factors. During weak stimulation, when sDSGCs receive minimal chemical synaptic

input, gap junction-mediated inputs may represent the determining factor for whether local depolarization reaches threshold for activation of Na^+ channels. Electrical input and chemical input might sum within a given spatial and temporal window, the sizes of which are dictated by the dendritic length constant and the width of the coupled spikelet (in the post-junction cell) respectively. During periods of high stimulation on the other hand, large chemical synaptic input across the dendritic arbour may dominate the membrane potential, attenuating the impact of gap junction-mediated inputs.

While rectification of electrical inputs or inactivation of dendritic Na^+ channels during periods of high activity could also explain our findings, we have previously demonstrated a lack of direct rectification of electrical inputs between sDSGCs (Trenholm *et al*., 2013). Inactivation of dendritic Na^+ channels also appears minimal, based on the effectiveness and consistency with which back-propagating spikes, measured as forward-propagating spikelets in the post-synaptic cell, are transmitted during periods of high activity (**Figure 19A**).

3.5.4. Implications of fine-scale correlations for encoding

The assumption in the study of these fine-scale correlations is that they are able to be decoded by higher order centers and thus provide these centers with relevant information about the visual world. However given our current state of knowledge, we can only speculate on the nature of information carried by such correlations. From the data collected here, we propose that fine-scale correlations could serve one of three purposes. First, given that correlations were strongest during weak stimulation protocols, such as stimulation with low contrast spots, correlations may help to improve the accuracy of weak signals. In this case, either the correlation signal itself could confirm

stimulus identity or correlated firing may be an artefact of a mechanism designed to ensure reliable spiking of neighbouring sDGSCs when chemical synaptic inputs are weak and exhibit high variability. Recordings comparing multiple DSGC populations will provide initial insights as to whether gap junctions reduce response variability to low contrast responses. Second, fine-scale correlations may endow sDSGCs with the ability to encode a correlation code entirely independent of the spike rate code, but optimized to a different feature of the visual scene. Our results demonstrated that as DSGC peak spike rate decreased with stimulus contrast, the strength of correlations significantly increased (**Figure 21**). While this effect on correlated firing was consistent across most stimuli which decreased the sDSGC peak spike rate, a significant decrease in the strength of correlations was observed when the spatial structure of the stimulus changed, from a single long bar (centered over the receptive field) to two smaller bars (centered over the non-overlapping regions of each cell's receptive field; **Figure 24**). The correlation code could therefore provide information about the stimulus structure and location within receptive fields, with high correlation strengths indicative of stimulus location within the region of dendritic overlap. Third, correlations may serve to extend the otherwise limited dynamic range of sDSGC response properties, complementing the sDSGC spike rate code in encoding contrast. Across the spectrum of stimulus contrasts, DSGC responses increase linearly over a small dynamic range relative to other ganglion cell populations (see Chapter 4; though this range is susceptible to adaptation over several time scales; Demb, 2008). This linearity is driven both by the sensitive nature of sDSGC responses to contrast (strong increases in the firing rate of over incremental increases in contrast), as well as a peak firing rate of ~250Hz, well below the physiological maximal firing rate

possible for such cells (as can be revealed by current injections, or blockade of inhibitory signalling; Chapter 3). It is possible that these small dynamic ranges allow for more effective encoding of direction, with information about stimulus contrast compromised out of necessity. However, if sDSGCs are able to encode such information by varying the strength of correlations, they may be able to extend the range of contrasts they are able to encode. However, we have only tested the midpoints of the contrast range (while full contrast was used for the high contrast stimulus, the low contrast stimulus did not approach sDSGC contrast threshold), and therefore did not get a sense of the range of correlation strengths, nor the incremental nature of correlation strength.

3.5.5. Conclusions

Given the numerous examples of correlated firing both within the retina and elsewhere in the CNS, it is likely that fine-scale correlations provide additional information to higher order centers than information contained in the spike rate alone. Here, we have demonstrated how such fine-scale correlations are generated in a population of coupled DSGCs. We demonstrated not only an interaction between electrical and chemical inputs in sDSGC dendrites, but for the first time, an interaction between these inputs and active dendritic mechanisms critical for the generation of correlated spiking.

3.6. Bibliography

Aertsen, M. H. J., Gerstein, G. L., Habib, M. K., & Palm, G. (1989). Dynamics of neuronal firing correlation: modulation of "effective connectivity." *Journal of Neurophysiology*, *61*(5), 900–917.

Bennett, M. V. L., & Zukin, R. S. (2004). Electrical coupling and neuronal synchronization in the mammalian brain. *Neuron*, *41*, 495–511.

Blankenship, A. G., Hamby, A. M., Firl, A., Vyas, S., Maxeiner, S., Willecke, K., & Feller, M. B. (2011). The role of neuronal connexins 36 and 45 in shaping spontaneous firing patterns in the developing retina. *The Journal of Neuroscience*, *31*(27), 9998–10008. http://doi.org/10.1523/JNEUROSCI.5640-10.2011

Bloomfield, S.A, & Völgyi, B. (2009). The diverse functional roles and regulation of neuronal gap junctions in the retina. *Nature Reviews Neuroscience*, *10*(7), 495–506. http://doi.org/10.1038/nrn2636

Bolte, P., Herrling, R., Dorgau, B., Schultz, K., Feigenspan, A., Weiler, R., Janssen-Bienhold, U. (2016). Expression and localization of connexins in the outer retina of the mouse. *Journal of Molecular Neuroscience*, *58*(2), 178–192. http://doi.org/10.1007/s12031-015-0654-y

Brivanlou, I. H., Warland, D. K., & Meister, M. (1998). Mechanisms of concerted firing among retinal ganglion cells. *Neuron*, *20*(3), 527–39.

Connors, B. W., & Long, M. a. (2004). Electrical synapses in the mammalian brain. *Annual Review of Neuroscience*, *27*, 393–418. http://doi.org/10.1146/annurev.neuro.26.041002.131128

Curti, S., & Pereda, A. E. (2004). Voltage-dependent enhancement of electrical coupling by a subthreshold sodium current. *The Journal of Neuroscience*, *24*(16), 3999–4010. http://doi.org/10.1523/JNEUROSCI.0077-04.2004

Degen, J., Meier, C., Van Der Giessen, R. S., Söhl, G., Petrasch-Parwez, E., Urschel, S., Willecke, K. (2004). Expression pattern of lacZ reporter gene representing connexin36 in transgenic mice. *Journal of Comparative Neurology*, *473*(4), 511–525. http://doi.org/10.1002/cne.20085

Demb, J. B. (2008). Functional circuitry of visual adaptation in the retina. *The Journal of Physiology*, *586*, 4377–4384. http://doi.org/10.1113/jphysiol.2008.156638

Dermietzel, R., Kremer, M., Paputsoglu, G., Stang, A., Skerrett, I. M., Gomes, D., … Spray, D. C. (2000). Molecular and functional diversity of neural connexins in the retina. *The Journal of Neuroscience*, *20*(22), 8331–8343. http://doi.org/20/22/8331 [pii]

Devries, S. H. (1999). Correlated firing in rabbit retinal ganglion cells. *Journal of Neurophysiology*, *81*, 908–920.

Dugue, G. P., Brunel, N., Hakim, V., Schwartz, E., Chat, M., Levesque, M., Dieudonne, S. (2009). Electrical coupling mediates tunable low-frequency oscillations and resonance in the cerebellar golgi cell network. *Neuron*, *61*(1), 126–139. http://doi.org/10.1016/j.neuron.2008.11.028

Fukuda, T., & Kosaka, T. (2000). Gap junctions linking the dendritic network of GABAergic interneurons in the hippocampus. *The Journal of Neuroscience*, *20*(4), 1519–1528.

Fukuda, T., & Kosaka, T. (2003). Ultrastructural study of gap junctions between

dendrites of parvalbumin-containing GABAergic neurons in various neocortical areas of the adult rat. *Neuroscience*, *120*(1), 5–20. http://doi.org/10.1016/S0306-4522(03)00328-2

Galarreta, M., & Hestrin, S. (1999). A network of fast-spiking cells in the neocortex connected by electrical synapses. *Nature*, *402*(6757), 72–5. http://doi.org/10.1038/47029

Gerstein, G. L., & Perkel, D. H. (1969). Simultaneously recorded trains of action potentials: analysis and functional interpretation. *Science*, *164*(3881), 828–830.

Gibson, J. R., Beierlein, M., & Connors, B. W. (1999). Two networks of electrically coupled inhibitory neurons in neocortex. *Nature*, *402*(6757), 75–79. http://doi.org/10.1038/47035

Güldenagel, M., Söhl, G., Plum, A., Traub, O., Teubner, B., Weiler, R., & Willecke, K. (2000). Expression patterns of connexin genes in mouse retina. *Journal of Comparitive Neurology*, *425*(2), 193–201.

Haas, J. S., Zavala, B., & Landisman, C. E. (2011). Activity-dependent long-term depression of electrical synapses. *Science*, *334*, 389–394.

Hu, E. H., & Bloomfield, S. a. (2003). Gap junctional coupling underlies the short-latency spike synchrony of retinal alpha ganglion cells. *The Journal of Neuroscience*, *23*(17), 6768–77.

Landisman, C. E., Long, M.A, Beierlein, M., Deans, M. R., Paul, D. L., & Connors, B. W. (2002). Electrical synapses in the thalamic reticular nucleus. *The Journal of Neuroscience*, *22*(3), 1002–9.

LeBeau, F. E. N., Traub, R. D., Monyer, H., Whittington, M. A., & Buhl, E. H. (2003). The role of electrical signaling via gap junctions in the generation of fast network oscillations. *Brain Research Bulletin*, *62*(1), 3–13. http://doi.org/10.1016/j.brainresbull.2003.07.004

Mann-Metzer, P., & Yarom, Y. (1999). Electrotonic coupling interacts with intrinsic properties to generate synchronized activity in cerebellar networks of inhibitory interneurons. *The Journal of Neuroscience*, *19*(9), 3298–306.

Mastronarde, D. N. (1983a). Correlated firing of cat retinal ganglion cells. I. spontaneously active inputs to X- and Y-Cells. *Journal of Neurophysiology*, *49*(2), 303–324.

Mastronarde, D. N. (1983b). Correlated firing of cat retinal ganglion cells. II. responses of X- and Y-Cells to singal quantal events. *Journal of Neurophysiology*, *49*(2), 326–349.

Mastronarde, D. N. (1983c). Interactions between ganglion cells in cat retina. *Journal of Neurophysiology*, *49*(2), 350–65.

Mastronarde, D. N. (1989). Correlated firing of retinal ganglion cells. *Trends in Neurosciences*, *12*(2), 75–80.

Meister, M., & Berry, B. J. (1999). The neural code of the retina. *Neuron*, *22*, 435–450.

Meister, M., Lagnado, L., & Baylor, D.A. (1995). Concerted signaling by retinal ganglion cells. *Science*, *270*(5239), 1207–10.

Migliore, M., Hines, M. L., & Shepherd, G. M. (2005). The role of distal dendritic gap junctions in synchronization of mitral cell axonal output. *Journal of Computational Neuroscience*, *18*(2), 151–161. http://doi.org/10.1007/s10827-005-6556-1

Muller, L. P., Dedek, K., Janssen-Bienhold, U., Meyer, A., Kreuzberg, M. M., Lorenz, S.,

Weiler, R. (2010). Expression and modulation of connexin 30.2, a novel gap junction protein in the mouse retina. *Visual Neuroscience*, *27*(3–4), 91–101. http://doi.org/10.1017/S0952523810000131

Nielsen, M. S., Axelsen, L. N., Sorgen, P. L., Verma, V., Delmar, M., & Holstein-Rathlou, N.-H. (2012). Gap junctions. *Comprehensive Physiology*, *2*(3), 1981–2035. http://doi.org/10.1002/cphy.c110051.

Oesch, N., Euler, T., & Taylor, W. R. (2005). Direction-selective dendritic action potentials in rabbit retina. *Neuron*, *47*(5), 739–50. http://doi.org/10.1016/j.neuron.2005.06.036

Sernagor, E., Eglen, S. J., & Wong, R. O. (2001). Development of retinal ganglion cell structure and function. *Progress in Retinal and Eye Research*, *20*(2), 139–174. Retrieved from http://www.ncbi.nlm.nih.gov/pubmed/11173250

Shlens, J., Field, G. D., Gauthier, J. L., Greschner, M., Sher, A., Litke, A. M., & Chichilnisky, E. J. (2009). The structure of large-scale synchronized firing in primate retina. *The Journal of Neuroscience*, *29*(15), 5022–31. http://doi.org/10.1523/JNEUROSCI.5187-08.2009

Syed, M. M., Lee, S., Zheng, J., & Zhou, Z. J. (2004). Stage-dependent dynamics and modulation of spontaneous waves in the developing rabbit retina. *Journal of Physiology*, *560*, 533–549. http://doi.org/10.1113/jphysiol.2004.066597

Trenholm, S., McLaughlin, A. J., Schwab, D. J., & Awatramani, G. B. (2013). Dynamic tuning of electrical and chemical synaptic transmission in a network of motion coding retinal neurons. *The Journal of Neuroscience*, *33*(37), 14927–38. http://doi.org/10.1523/JNEUROSCI.0808-13.2013

Trenholm, S., McLaughlin, A. J., Schwab, D. J., Turner, M. H., Smith, R. G., Rieke, F., & Awatramani, G. B. (2014). Nonlinear dendritic integration of electrical and chemical synaptic inputs drives fine-scale correlations. *Nature Neuroscience*, *17*, 1759-66. http://doi.org/10.1038/nn.3851

Trenholm, S., Schwab, D. J., Balasubramanian, V., & Awatramani, G. B. (2013). Lag normalization in an electrically coupled neural network. *Nature Neuroscience*, *16*, 154–56. http://doi.org/10.1038/nn.3308

Turecek, J., Yuen, G. S., Han, V. Z., Zeng, X.-H., Bayer, K. U., & Welsh, J. P. (2014). NMDA receptor activation strengthens weak electrical coupling in mammalian brain. *Neuron*, *81*(6), 1375–88. http://doi.org/10.1016/j.neuron.2014.01.024

Vaney, D. I. (2002). Retinal neurons: cell types and coupled networks. *Progress in Brain Research*, *136*, 239–254.

Velte, T. J., & Masland, R. H. (1999). Action potentials in the dendrites of retinal ganglion cells. *Journal of Neurophysiology*, *81*, 1412–1417.

Vervaeke, K., Lorincz, A., Nusser, Z., & Silver, R. A. (2012). Gap junctions compensate for sublinear dendritic integration in an inhibitory network. *Science*, *335*(6076), 1624–8. http://doi.org/10.1126/science.1215101

Völgyi, B., Kovács-öller, T., Atlasz, T., Wilhelm, M., & Gábriel, R. (2013). Gap junctional coupling in the vertebrate retina: Variations on one theme? *Progress in Retinal and Eye Research*, *34*, 1–18. http://doi.org/10.1016/j.preteyeres.2012.12.002

4. Na^+ channels enhance contrast sensitivity in a retinal circuit responsible for direction selectivity

The work found in this Chapter is unpublished, however the circuit model presented in Figure 25 is modified from Sethuramanujam et al. (2017). Alex Hoggarth contributed data to Figure 30. Dr. Malcolm Slaughter provided guidance on the manuscript.

4.1. Abstract

Contrast sensitivity appears to vary within the direction selective (DS) circuit. Just as bipolar cells differ in their responses to light (ON vs OFF), their response kinetics (transient vs sustained), they also differ in their contrast-sensitivities. These response properties are transmitted to DS ganglion cells (DSGCs) and starburst amacrine cells (SACs) downstream in the DS circuit. Recent studies have suggested that both high- and low-sensitivity bipolar cells (HSBCs; LSBCs) are present within the DS circuit, with LSBCs contacting DS ganglion cells, and HSBCs contacting both DSGCs and starburst amacrine cells, through different post-synaptic receptors (NMDA vs AMPA receptors respectively). In this chapter I test the hypothesis that differential expression of Na^+ channels in bipolar cells underlies the observed differences in contrast sensitivity.

My results demonstrate that excitatory inputs to SACs near contrast threshold are TTX-sensitive, consistent with weak bipolar cell responses being amplified by Na^+ channels. TTX also reduced low contrast responses in DSGCs. Using pharmacology to distinguish between NMDA- and AMPA-ergic inputs to DSGCs, I next investigated the TTX-sensitivity of high-sensitivity vs low-sensitivity bipolar cell inputs. My results suggest bipolar cells contacting NMDARs but not AMPARs utilize Na^+ channels, consistent with the circuit model proposed by other studies. Interestingly, similar effects

were not observed in non-DS ganglion cells, suggesting Na^+ channels might only be present in DS circuits.

Within the DS circuit, Na^+ channel-driven amplification appears to be a general feature of weak inputs rather than a low-contrast specific feature. TTX abolished DSGC responses to small high contrast spots within the excitatory receptive field center, indicating bipolar cell responses to small spots also relying on Na^+ channel amplification. This work provides further evidence for the activity of voltage-gated Na^+ channels in specific bipolar cell populations in the mouse retina and their role in enhancing weak inputs to the directionally-selective circuit.

4.2. Introduction

In the mammalian retina, bipolar cells (BCs) form the primary excitatory connection between photoreceptors (PRs), i.e., rods and cones, and ganglion cells (GCs), which send the output of the retina to the brain via the optic nerve. Across these two feed-forward synapses (PR to BC, BC to GC), simple photoreceptor output is transformed and distributed across independent parallel pathways for transmission to the brain by >20 ganglion cell populations, each of which is specialized for the coding of specific visual features. The ability of ganglion cells to encode image characteristics is in part due to the differential wiring of separate bipolar cell subtypes to specific ganglion cells. Bipolar cells therefore provide the framework for transforming the signals from a small number of PR types into the complex signals transmitted to the brain.

Anatomical studies looking at bipolar cell stratification within the inner plexiform layer (IPL) have led to the subdivision of bipolar cells into at least fifteen different cell types in mice (Ghosh *et al.*, 2004; Hartveit, 1997; Wassle *et al.*, 2009; Zeng & Sanes,

2017). Of these, eight are of ON polarity, six are of OFF polarity and the last is the rod bipolar cell (Zeng & Sanes, 2017). These parallel pathways feed excitation forward onto ~30 subtypes of amacrine cells, and ~20 types of ganglion cells. Each of these ganglion cell populations performs a functionally distinct role, by virtue of the bipolar and amacrine cells which make up their presynaptic circuits.

The bipolar cell subtype diversity is a consequence of anatomical stratification, cell morphology and variation in the expression of neurotransmitter receptors and voltage-gated ion channels (Zeng & Sanes, 2017; Baden *et al.*, 2013; Ichinose *et al.*, 2014). Studies seeking to further our understanding of channel and receptor expression in bipolar cells have demonstrated that all excitatory inputs to ON BCs are mediated by the metabotropic glutamate receptor 6 (mGluR6), which reverses the polarity of PR input (hyperpolarization of PRs leads to depolarization of BCs; Masu *et al*., 1995). The assortment of other neurotransmitter receptors and ion channels in BC dendrites and axon terminals is however highly diverse, with ON BCs varying in their expression of voltage-gated Na^+ channels (Cui & Pan, 2008; Ichinose *et al.*, 2005; Saszik & DeVries, 2012), K^+ channels (Connaughton & Maguire, 1998; Hu & Pan, 2002), and HCN channels (Ivanova & Muller, 2006; Muller *et al*., 2003). BCs are also modulated by GABAergic or glycinergic inhibitory input from circuit-specific amacrine cells (Eggers, *et al.*, 2007; Euler & Wassle, 1998; Hoggarth *et al*., 2015; Ivanova & Muller, 2006; Purgert & Lukasiewicz, 2015; Vigh *et al.*, 2011). This molecular diversity, in combination with the anatomical diversity in BC-to-GC wiring, endows BCs with differences in their temporal properties (Baden *et al.*, 2013; Ichinose *et al.*, 2014), their sensitivity to contrast (Odermatt *et al.*, 2012; Poleg-Polsky & Diamond, 2016), and their ability to generate all-

or-nothing (Na^+ or Ca^{2+}-channel mediated) spike-like events (Baden *et al.*, 2013a; and see Baden *et al.*, 2013b for review). Each retinal circuit may sample from distinct bipolar cell types, endowing GCs with unique variations in biophysical properties important for specific visual computations.

While there has been significant advancement in our understanding of bipolar cell diversity and even response properties; few studies have been able to link differences in BC molecular diversity and activity to specific ganglion cell circuits or ganglion cell responses. This is likely due to our limited understanding of how differential ion channel expression in bipolar cells map to specific retinal circuits. In this work, I demonstrate a functional importance for Na^+ channel activity in a specific population of BCs within a well-studied circuit of the mouse retina, the directionally-selective (DS) circuit. Using single and paired whole-cell patch clamp recordings from multiple cell types, in conditions which isolate excitatory input, I demonstrate that a population of ON bipolar cells, those contacting the main amacrine cell in the DS circuit (starburst amacrine cells; SACs) and DS ganglion cells (DSGCs), utilize Na^+ channels, while a second population of bipolar cells in the circuit does not. Additionally, I demonstrate a role for these Na^+ channels in encoding low contrast stimuli and in establishing spatial sensitivity.

4.3. Methods

4.3.1. Animals

Experiments were performed using 21-60 day old mice of both sexes that were maintained on a 12-hour light/dark cycle. Experiments were performed on retinal preparations from several transgenic mouse lines: Hb9eGFP (RRID: MGI_109160); ChatCre::Ai9 mice, bred from ChatCre (RRID: MGI_5475195) and floxed Ai9 reporter

mice (RRID: MGI_3809523), and; PVCre::YFP mice, bred from PVcre (RRID: IMSR_JAX:007677) and floxed YFP reporter mice (Thy1-stop-YFP; RRID: IMSR_JAX:005630). All procedures were performed in accordance with the Canadian Council on Animal Care and approved by the University of Victoria Animal Care Committee.

4.3.2. Whole mount retinal preparation

Mice were dark-adapted for approximately 60 minutes before being anesthetized by inhalation of isofluorane or injected with a lethal dose of pentobarbital, via intra-peritoneal injection, and decapitated. Eyes were removed using forceps (severing the optic nerve), with a small incision made on the nasal side of the cornea to assist with later identification of retinal orientation. Retinas from both eyes were dissected in Ringer's solution containing 110 mM NaCl, 2.5 mM KCl, 1 mM $CaCl_2$, 1.6 mM $MgCl_2$, 10 mM glucose and 22 mM $NaHCO_3$, bubbled with carbogen (95% O_2-5% CO_2) and mounted on a 0.22 mm membrane filter (Millipore) with a pre-cut window through which light could reach the retina. The preparation was viewed under IR illumination using a Spot RT3 CCD camera (Diagnostic Instruments) attached to an upright Olympus BX51WI fluorescent microscope equipped with a 40X water-immersion lens (Olympus Canada). The retina was continuously perfused with Ringer's solution maintained at 35-37°C.

4.3.3. Physiological recordings

Voltage-clamp whole cell recordings were made using 4–7MΩ electrodes containing a Cs^+-solution comprised of 112.5 mM CH_3CsO_3S, 1 mM $MgSO_4$, 10 mM EGTA, 10 mM HEPES, 4 mM ATP-Mg_2, 0.5 mM GTP-Na_3, 5 mM QX-314, 0.025 mM Alexa Fluor 594 (Invitrogen), and 7.75 mM Neurobiotin-Cl (Vector Laboratories). The

pH was adjusted to 7.2–7.3 with CsOH. Signals were digitized at 10 kHz (PCI-6036E acquisition board, National Instruments) and acquired using custom software written in LabVIEW. Green-fluorescent protein-positive (GFP^+), Td-tomato-positive, and yellow fluorescent protein-positive (YFP^+) directionally-selective ganglion cells (sDSGCs), starburst amacrine cells (SACs), and ON alpha ganglion cells (ONα GCs) were visually targeted for recordings using two-photon laser scanning microscopy techniques (λ = 950 nm).

Tetrodotoxin (TTX; 1 µM; Alomone Labs), SR-95531 (SR; 10 µM), (1,2,3,4-tetrahydropyridin-4-yl)-methylphosphonic acid (TPMPA; 100 µM), Hexamethonium (Hex; 100 µM), 2,3-dihydroxy-6-nitro-7-sulfamoyl-benzo[f]quinoxaline-2,3-dione (NBQX; 20 µM), and D-AP5 (50 µM) were applied through bath perfusion. All reagents were purchased from Sigma-Aldrich Canada, Ltd unless otherwise noted.

4.3.4. Light stimulus

Broad-spectrum, white light stimuli were generated with a digital projector (refresh rate 75 Hz; Cpx1, Hitachi) and controlled with custom software incorporating Psychtoolbox. Light stimuli were projected from below the preparation and focused on the photoreceptor layer using the sub-stage condenser. The ambient background intensity was set to approximately ~500 to 1000 R* per rod per second, based on intensity measurements using a calibrated spectrophotometer (USB2000, Ocean Optics), and a conversion according to (Lyubarsky *et al*, 1999). The null direction (and opposing preferred direction; pref) for DSGCs was determined by computing a vector sum of the peak IPSC amplitudes after presenting a 300 µm X 300µm stimulus moving at 600 µm/s in eight directions over the cell.

4.3.5. Data analysis

Single cell intracellular or extracellular responses were collected from multiple cells (as indicated within each experiment). All responses (spike number, or peak EPSC amplitude, as indicated) are expressed as a mean ± SEM. Contrast response functions (CRFs) for large stimuli (>150 µm) were generated by plotting peak excitatory post-synaptic current (EPSC) amplitudes as a function of Weber Contrast ($(I-I_b)/I_b$; where I is the luminance of the stimulus, and I_b is the luminance of the background) The responses were fitted to the Naka Rushton equation $R_{max}*(C^n/(C^n+C_{50}^n))$ (Naka & Rushton, 1966): where C indicates the contrast, R_{max} is the maximum response, C_{50} is the semi-saturation constant and n is a coefficient proportional to the slope of the contrast response function at C_{50}. CRFs for small stimuli (<50 µm) were best fit to power law functions (Mclaughlin, unpublished data): $y=y_0+Ax^k$: where y_0 represents the baseline response, *A* represents a constant, and *k* the power law exponent. Two-way ANOVAs, calculated using GraphPad Prism, were used to compare CRFs in different conditions (or across cell types) while student's *t*-tests were used to compare individual values. Differences were considered significant when $p \leq 0.05$.

4.4. Results

4.4.1. Bipolar cells within the DS circuit exhibit distinct contrast sensitivities

In recent investigations of the mechanisms underlying direction-selectivity at low contrast, two independent studies (Poleg-Polsky & Diamond, 2016; Sethuramanujam *et al.*, 2017) provided evidence to suggest that bipolar cells within the DS circuit, those contacting post-synaptic AMPA receptors (AMPARs) either on DSGCs or on SACs, differ in their sensitivity to contrast. Glutamatergic inputs to SAC AMPARs were more

sensitive to contrast than glutamatergic inputs to DSGC AMPARs, with over half a log unit separating the threshold sensitivities. Thus, Poleg-Polsky and Diamond (2016) and Sethuramanujam *et al.* (2016) hypothesized a wiring arrangement in which a high-sensitivity subtype of bipolar cells (HSBCs) contact SACs, while low-sensitivity bipolar cells (LSBCs) contact DSGCs (**Figure 25A**). DSGCs however express both NMDA- and AMPA-type glutamate receptors, and glutamate release onto DSGC NMDA receptors (NMDARs) was significantly more sensitive than glutamatergic input to AMPA receptors. Revisiting the model (**Figure 25B**), Sethuramanujam and colleagues (2017) proposed that high-sensitivity bipolar cells contact DSGCs (at NMDAR-containing synapses) in addition to SAC AMPARs, while low-sensitivity bipolar cells contact DSGCs alone (at AMPAR-containing synapses (**Figure 25B**). These studies have however failed to identify the mechanisms underlying differences in bipolar cell contrast sensitivity. In this chapter, I hypothesize that Na^+ channels serve as the mechanism underlying this difference. First, I will demonstrate that DSGC and SAC EPSCs in response to low contrast stimuli are modulated by Na^+ channels, based on the effects of the Na^+ channel inhibitor TTX on DSGC and SAC EPSCs. Next, I provide evidence that these effects are the result of Na^+ channel activity in a subset of BCs (HSBCs). Finally, I provide evidence for an additional role for BC Na^+ channels in enhancing SAC and DSGC spatial sensitivity, and discuss the possibility that Na^+ channel expression may allow for non-linear receptive fields (RFs) in BCs

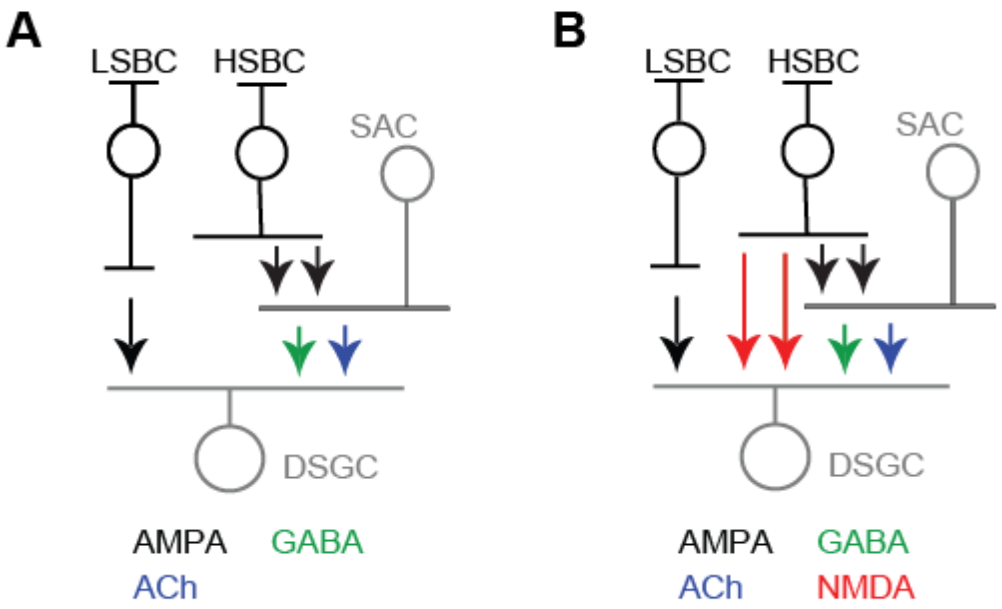

Figure 25. Wiring of high- and low-sensitivity bipolar cells within the DS circuit. Adapted with permission from Sethuramanujam *et al.,* (2017). Schematics depicting the possible wiring of bipolar cells within the DS circuit. **A.** Glutamate release (black arrows) onto AMPAR-expressing DSGCs and SACs differ in their sensitivity to contrast, consistent with SACs receiving input from high-sensitivity bipolar cells (HSBCs), and DSGCs receiving input from low-sensitivity bipolar cells (LSBCs). Glutamatergic input to SACs drives release of both ACh (blue arrow) and GABA (green arrow). This model is consistent with the findings of Poleg-Polsky & Diamond (2016) **B.** NMDAR-mediated inputs to DSGCs are as sensitive to contrast as AMPA-mediated inputs to SACs. High-sensitivity bipolar cells are therefore likely to contact DSGC NMDA-containing synapses in addition to SAC AMPA-containing synapses.

4.4.2. SAC contrast sensitivity relies on pre-synaptic Na+ channels

As differential BC contrast sensitivities could be explained by differences in voltage-gated channel expression (as discussed in Poleg-Polsky & Diamond, 2016), I first tested the effect of the Na^+ channel inhibitor TTX on contrast coding of SACs. I targeted ON SAC EPSCs for voltage-clamp recordings in whole mount ChATcre::Ai9 transgenic mouse retinas (in which tdTomato expression is limited to SACs), using 2-photon imaging. EPSCs were recorded (V_{hold} = -60 mV) in response to a series of static spots

increasing in contrast (250μm in diameter, Weber contrast 0.03-3; **Figure 26B**). SACs responded non-linearly to contrast, with EPSCs increasing in amplitude in response to initial increases in contrast, but responses reaching a plateau after which further increases in contrast produced no changes in response amplitude. Tetrodotoxin (TTX; 1 μM) was then bath-applied onto the retina (**Figure 26B**; red). Peak EPSC amplitudes, for both control and TTX conditions, were plotted as a function of stimulus Weber contrast (see Methods) to produce contrast response functions (CRFs), which were fit to the Naka-Rushton (NR) equation (Naka & Rushton, 1966). CRFs for five cells were averaged, following normalization along the Y axis to peak SAC EPSC amplitude (for control conditions) and normalizing in X to set control half-maximal contrasts (NR C_{50}; **Figure 26C** dashed line) equal to 1. TTX application significantly impacted SAC responses amplitudes across contrasts (2-way ANOVA, $F_{1/44}$=427, P<0.0001).

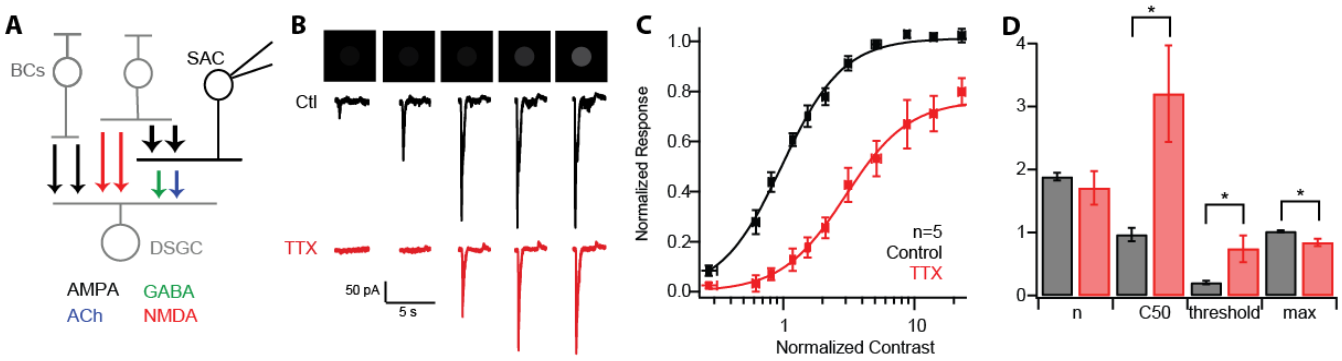

Figure 26. SAC low contrast responses are blocked by bath application of TTX.
A. Schematic of the recording configuration. Voltage-clamp recordings were made from SACs (V_{hold} = -60 mV) in order to measure AMPAR-mediated EPSCs (black arrows). **B.** EPSCs were measured in response to static spots (400 µm) increasing in contrast (top) in control conditions (middle; black traces), and in TTX (1 µM; bottom; red traces). Average traces for 3 repeated stimulus presentations are shown. **C.** Averaged normalized peak response (n=5) plotted as a function of the contrast (normalized to Control C_{50}=1). Error bars represent ±SEM. Curves are fit using the Naka Rushton equation. **D.** Naka Rushton curve fitting parameters from 5 cells (n, C_{50}, and max) for both control (black) and TTX (red) conditions. Threshold was measured as the contrast which elicited a response of 0.1 (C_{10}; asterisks represent $p<0.05$).

The effect of TTX was however not equal across contrasts, with the TTX effect greatest at low contrast (2-way ANOVA, $F_{10/44}$=2.38, P=0.023). At control C_{100} TTX reduced peak EPSCs by 17±6% (*t*-test: P=0.039; **Figure 26C-D**), while responses at C_{50} were reduced by 83±7% (*t*-test: P=0.0003; **Figure 26C**). Interestingly, in addition to TTX significantly decreasing peak response amplitudes, TTX also affected the parameters of the contrast response function. A comparison of C_{50} and threshold contrast (C_{10}) values reveals that TTX application results in a rightward shift of the contrast response function, increasing contrast threshold (0.21±0.03 for Control; to 0.74±0.21 in TTX; paired *t*-test: P=0.04) and C_{50} (0.97±0.10 for Control; to 3.20±0.76 in TTX; paired *t*-test: P=0.04); **Figure 26D**) by over 3-fold. This shift in the curve fitting parameters is interesting. If glutamate release onto SACs was simply decreased across contrasts, we

would expect to see differences in peak current, however the changes in curve fitting parameters, which are intrinsic to the properties of the receptor, may instead suggest that inputs to SACs are distinct in these conditions. I will elaborate on this idea further in the section 4.5. The results of this experiment clearly demonstrate a strong role for Na^+ channels in driving excitation to the DS circuit, particularly in enhancing SAC contrast sensitivity.

4.4.3. TTX-sensitivity of low contrast responses is passed on to DSGCs

DSGCs receive feed-forward excitation from BCs, through SAC release of ACh (**Figure 27A**; blue arrow). Given the TTX-sensitivity of SAC inputs, it follows that these would drive TTX-sensitivity of DSGC cholinergic receptor (AChR)-mediated inputs. Given the model outline in **Figure 25**, I hypothesize that DSGCs also receive input from TTX-insensitive LSBCs (via AMPA receptors; black arrows) and TTX-sensitive HSBCs (via NMDARs; red arrows). To test this hypothesis, sDSGCs were targeted for recordings using 2-photon imaging using a transgenic mouse line in which these cells express GFP (Hb9GFP; see Methods). To begin to investigate the TTX-sensitivity of sDSGC inputs, I first isolated AChR and AMPAR-mediated excitatory inputs by recording EPSCs at -60 mV (NMDA-mediated inputs are addressed in **Figure 29**. Assuming similar contrast sensitivities of sDSGC AChR- and AMPAR-mediated inputs (Poleg-Polsky & Diamond, 2016), I predicted an effect of TTX on sDSGC responses at C_{50}, though a minimal effect on contrast threshold (due to residual input from LSBCs).

sDSGCs were presented with either static (**Figure 27B-D**) or moving (**Figure 27F-H**) stimuli of increasing contrasts (moving stimuli were presented in the sDSGC's preferred direction at ~1mm/s) in the presence or absence of TTX (**Figure 27B/F**).

EPSCs (V_{hold}= -60 mV) were recorded from sDSGCs, and peak amplitudes were plotted as a function of stimulus Weber contrast for both control and TTX conditions (only ON responses were considered). Averaged curves (for 5 cells) were produced from normalization to control condition maxima (based on NR curve fitting *max*) and C_{50} values (with C_{50} set to equal normalized contrast 1). Similar to results obtained in SACs, TTX had a significant effect on CRFs (2-way ANOVAs; motion: n=6, $F=_{1/84}$=224 P<0.0001; static: n=5, $F_{1/23}$=287, P<0.0001). This effect was however different than that observed in SACs. TTX had no effect on response maxima (*t*-test: P=0.128), and the effect of contrast threshold did not increase to the same degree as in SACs (this effect however is unclear; *t*-test: P=0.258). The differences observed between SACs and DSGCs could be the result of mixed TTX-sensitive and TTX-insensitive inputs to DSGCs. Importantly however, similar to the results from SAC recordings, the effect of TTX was largest for low contrast responses (2-way ANOVAs; motion: $F_{11/84}$=7.99, P<0.0001; static: $F_{8/23}$=2.71, P=0.0291), decreasing responses at C_{50} by 88±4% (*t*-test: P=0.023), while minimally affecting max responses. These data are consistent with SAC TTX-sensitivity being passed on to sDSGC responses, with the effect of TTX on C_{50} responses larger even than observed in SACs, however the lack of effect of TTX on contrast threshold suggests some TTX-insensitive inputs remain (presumably LSBC input to AMPARs). This specific hypothesis will be explored in greater detail (**Figure 29**), but more broadly, the TTX-sensitivity of DSGC responses to low contrast stimuli provides further evidence for the involvement of Na^+ channels in establishing contrast sensitivity of BC populations.

4.4.4. TTX-sensitivity of DSGC and SAC inputs arises in bipolar cells

Experiments thus far have demonstrated an importance for Na^+ channels in encoding low contrast responses, while previous work has demonstrated differential contrast sensitivities of BCs. It is not yet clear however whether the TTX effects observed are the result of differential Na^+ channel activity across BC types, and therefore whether Na^+ channels underlie differences in BC sensitivities, or whether the effect of TTX is upstream of BCs. I therefore sought to confirm that the TTX effects described above are specific to BCs by ruling out other potential sources for Na^+ channel expression, notably AII amacrine cells (Boos *et al*., 1993) and wide-field amacrine cells (WACs; Taylor, 1999).

First, I tested the hypothesis that Na^+ channels in AII amacrine cells amplify DS circuit responses to low contrast. Differential Na^+ channel expression across BC types would limit Na^+ channel amplification of low contrast responses to distinct GC populations. Conversely, the effect predicted by Na^+ channel activity in AII amacrine cells, would, as a result of their broad connectivity, impart all BCs (and all GC circuits) with TTX-sensitivity. I therefore tested the effect of TTX on low contrast responses within a separate GC circuit, the ON alpha ganglion cell (ONα GC) circuit, whose BC inputs differ significantly from those to DSGCs (Morgan *et al.*, 2011).

ONα GCs PVcre;Th1YFP mice were targeted for voltage-clamp analysis. In these mice ONα GCs are one of eight GC populations that are fluorescently labelled (Farrow et al., 2013). ONα GCs were identified (in addition to their fluorescence) using soma size, and by their response to flashing spots of light. ONα EPSCs were recorded while exposed to static spots of light increasing in contrast (**Figure 28C**). While ONα GC receptive

fields are larger than sDSGCs' (Peichl *et al.*, 1987), larger spot sizes did not produce significant changes to CRFs (n=3, 2-way ANOVA, $F_{1/34}$=0.09, P=0/7724; **Figure 28B**), thus 250 µm stimuli were used, identical to that used for sDSGCs (**Figure 27C**). CRFs were plotted from peak EPSC amplitudes, and revealed that ONα GCs encode changes in contrast much more linearly than sDSGCs, with responses continuously increasing over nearly 2-log units (**Figure 28B/D**). Importantly, application of TTX had no effect on CRFs (n=3, 2-way ANOVA, $F_{1/34}$=2.85, P=0.1003; **Figure 28C/D**). Thus, TTX effects on low contrast responses are not ubiquitous across GC types, making it unlikely that the effects of TTX on DSGC low contrast responses are the result of Na^+ channel activity in AII amacrine cells.

In order to next test the involvement of inhibitory neurons (including WACs; **Figure 28E**) as sources of Na^+ channel activity underlying DS circuit contrast sensitivity, I tested the effect of TTX in the absence of inhibitory signalling (**Figure 28F-H**). Na^+ channels in inhibitory amacrine cells (such as wide-field amacrine cells; WACs) could enhance low contrast signalling if a dis-inhibitory circuit arrangement was present, and included an intermediate inhibitory amacrine cell (**Figure 28E**). However when GABA receptor antagonists TPMPA (100 µM) and SR-95531 (10 µM) were applied, an effect of TTX was still observed. sDSGC EPSCs (V_{hold}= -60 mV) were measured in response to spots of increasing contrast and TTX significantly reduced responses across contrasts (**Figure 28G;** n=2). Smaller spot sizes (30 µm) were used for these experiments, as the application of GABA blockers easily saturated CRF measurements. I confirmed however that across stimulus spot sizes, an effect of TTX was always observed (**Figure 28H;** C_{50} contrast used; 2-way ANOVA, n=4, $F_{1/21}$=27.83, P<0.0001). Given that the application of

TTX reduced excitatory inputs to sDSGCs even in the presence of GABA blockers, Na^+ channel activity responsible for establishing contrast sensitivity must arise in the excitatory pathway. This result, together with the previous findings (**Figure 28A-D**), is consistent with a role for Na^+ channels in BCs. Given the effect of TTX on small spots sizes Na^+ channels likely enhance excitatory responses non-specifically, this however will be investigated further (**Figure 30**).

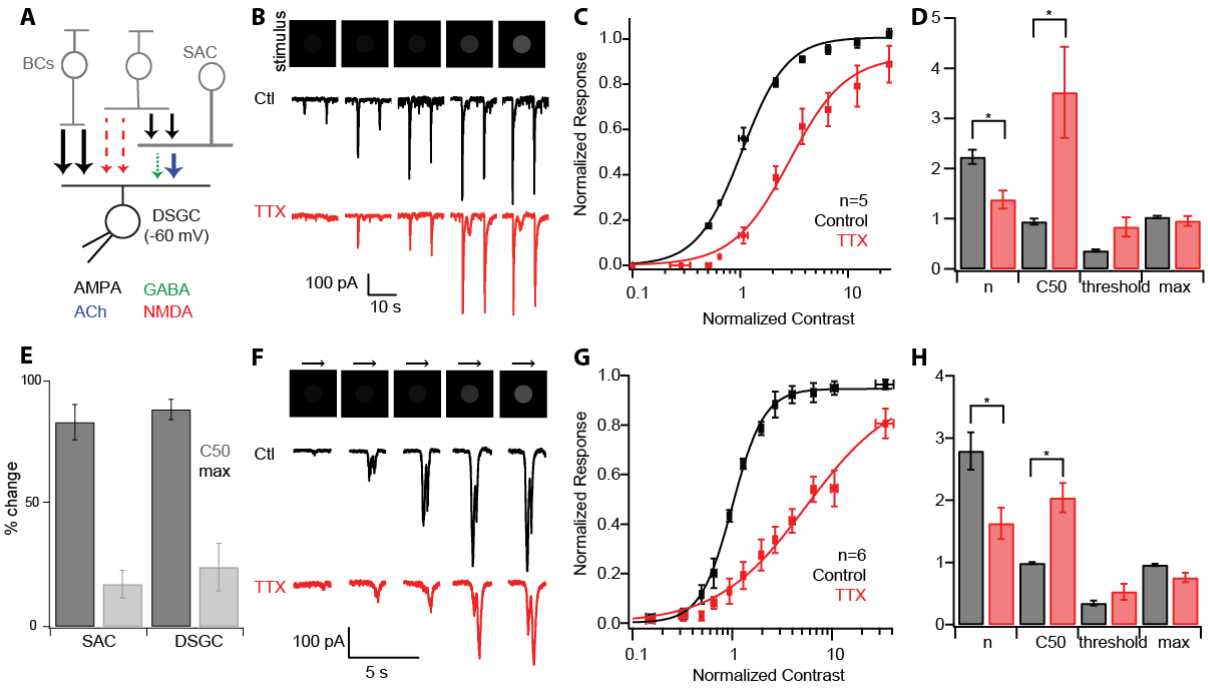

Figure 27. sDSGC low contrast responses are reduced by TTX application.
ESPCs were measured from sDSGCs, in voltage-clamp configuration, in response to static (**B-D**) and moving (**F-H**) stimuli of increasing contrasts (spot = 400µm). **A.** Schematic representing sDSGC inputs recorded at V_{hold} = -60 mV: AMPARs (black arrows), and nAChRs (blue arrows). Dashed arrows represent inputs to DSGCs which are not measured as a result of the holding potential. **B/F.** EPSCs were measured in control conditions (black), and following bath application of TTX (1 µM; red). Average traces for 3 repeated stimulus presentations are shown. **C/G.** The averaged normalize peak response (n=5 and 6 for static and moving stimuli respectively) was plotted as a function of the contrast (normalized to respective control C_{50}s). Error bars represent ±SEM. Curves were fit using the Naka-Rushton equation. **D/H** Naka Rushton curve fitting parameters (n, C_{50}, and max) and threshold (C_{10}) measurements for control (black) and TTX (red) conditions (asterisks represent $p<0.05$). **E.** Representation of the effect of TTX (in % decrease, measured as the 100%-100(TTX response/Ctl response)) on low contrast responses (C_{50}) versus high contrast responses (C_{100}), calculated from DSGC (**G**) and SAC CRFs (Figure 26C).

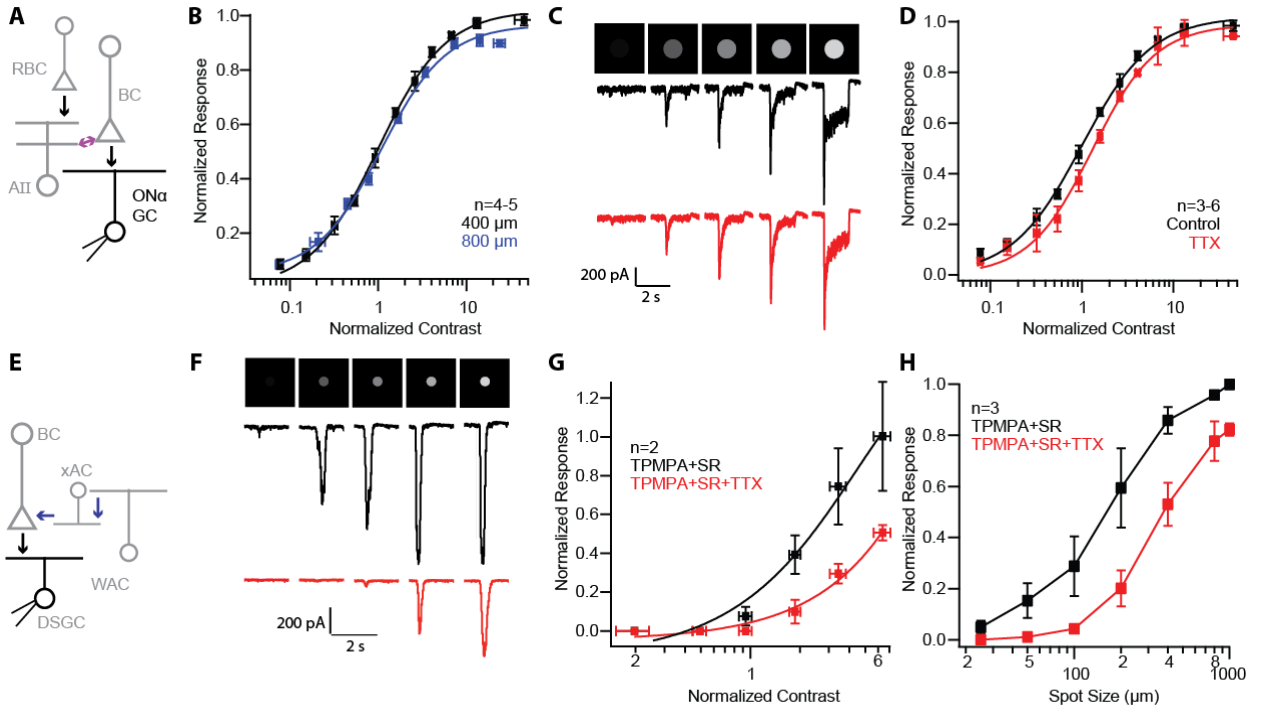

Figure 28. TTX-sensitivity is not ubiquitous across the retina, and does not rely on inhibitory signalling.
A. Schematic of the ON alpha ganglion cell (ONα GC) circuit. ONα GCs receive direct glutamatergic input onto post-synaptic AMPARs (black arrow) from cone bipolar cells (BC; different BC subpopulations than those in the DS circuit). All ON BC subpopulations (including those feeding to BCs in the DS circuit) receive input from AII amacrine cells (AII) via gap junctions (purple). This allows for coupling of the rod and cone pathways, with rod bipolar cells (RBC) providing AIIs with glutamatergic input onto post-synaptically expressed AMPARs. **B/C.** ONα GCs EPSCs measured in voltage clamp (V_{hold} = -60 mV) in response to spots of increasing contrast (**C**) for multiple spot sizes (**B**). **B.** Normalized peak amplitudes plotted as a function of stimulus contrast for stimuli 400 µm (black) and 800 µm (blue) in diameter (n=4-5). Error bars represent ±SEM. Curves are not significantly difference. **C.** EPSCs measured for 400 µm stimuli increasing in contrast, in control (black) and TTX (1 µM; red) conditions. Average traces for 3 repeated stimulus presentations are shown. **D.** Normalized peak responses plotted as a function of normalized contrast (Control C_{50}=1) for control (black) and TTX (red) conditions (n=3-6). Curves are not significantly different. **E.** Schematic depicting a hypothetical circuit arrangement permitting Na^+ channels in inhibitory neurons (here, WACs) to affect low contrast responses in sDSGCs. WACs inhibit an intermediate amacrine cell (xAC), which inhibiting cone bipolar cells, with one or both synapses relying on the GABA (blue arrow). **G-H**. The effects of TTX were assessed in the presence of inhibitors of GABAergic signalling (TPMPA, 100 µM; SR-95531, 20 µM). **F**. EPSCs were measured in TPMPA and SR (black) or in TPMPA, SR and TTX (red). Average traces for 3 repeated stimulus presentations are shown. **G**. Averaged CRFs (n=2) produced from DSGC EPSCs in the presence (black) or absence (red) of TTX for a 30 µm spot (TPMPA+SR max response =1; C_{10} in TPMPA/SR set to X=1). . **H.** Graph of normalized peak EPSC amplitude, measured from DSGCs, versus stimulus spot size for a high-contrast stimulus (C_{100}; n=3) in control (black) and TTX (red) conditions.

4.4.5. Na+ channels are differentially expressed in BCs contacting DSGC AMPARs and NMDARs

For Na^+ channels to underlie the differential contrast sensitivities of BC populations, Na^+ channel activity are predicted to be specific to high-sensitivity BCs (HSBCs; see **Figure 25**). In order to test this hypothesis, I utilized the differential wiring of high-sensitivity HSBCs and LSBCs to sDSGC synapses containing NMDARs or AMPARs respectively (Figure 1A; Sethuramanujam *et al*., 2017). I first isolated sDSGC AMPA-mediated EPSCs (V_{hold}= -60 mV) through application of Hexamethonium (Hex, 100 µM) and AP5 (50 µM; **Figure 29B**), inhibiting nAChRs and NMDARs respectively (**Figure 29A**; though NMDARs would not be significantly active at this holding potential). Averaged CRFs (n=7) were plotted from sDSGC normalized peak EPSC amplitudes as a function of normalized contrast (Control C_{50} = 1). Consistent with previous reports (Sethuramanujam *et al*., 2016), Hex and AP5 application reduced maximal responses and abolished responses at C_{50}, shifting contrast threshold to higher contrast values (**Figure 29B;** 2-way ANOVA, n=7, $F_{1/118}$=738, P<0.0001; *t*-test: C_{50} P<0.0001, max P=0.0002, threshold P=0.009). Importantly, subsequent application of TTX had no observable effect on CRFs (**Figure 29C-D**; n=2; Hex/AP5 CRF normalized to 1), suggesting LSBC inputs to sDSGCs (via AMPARs) do not require Na^+ channels.

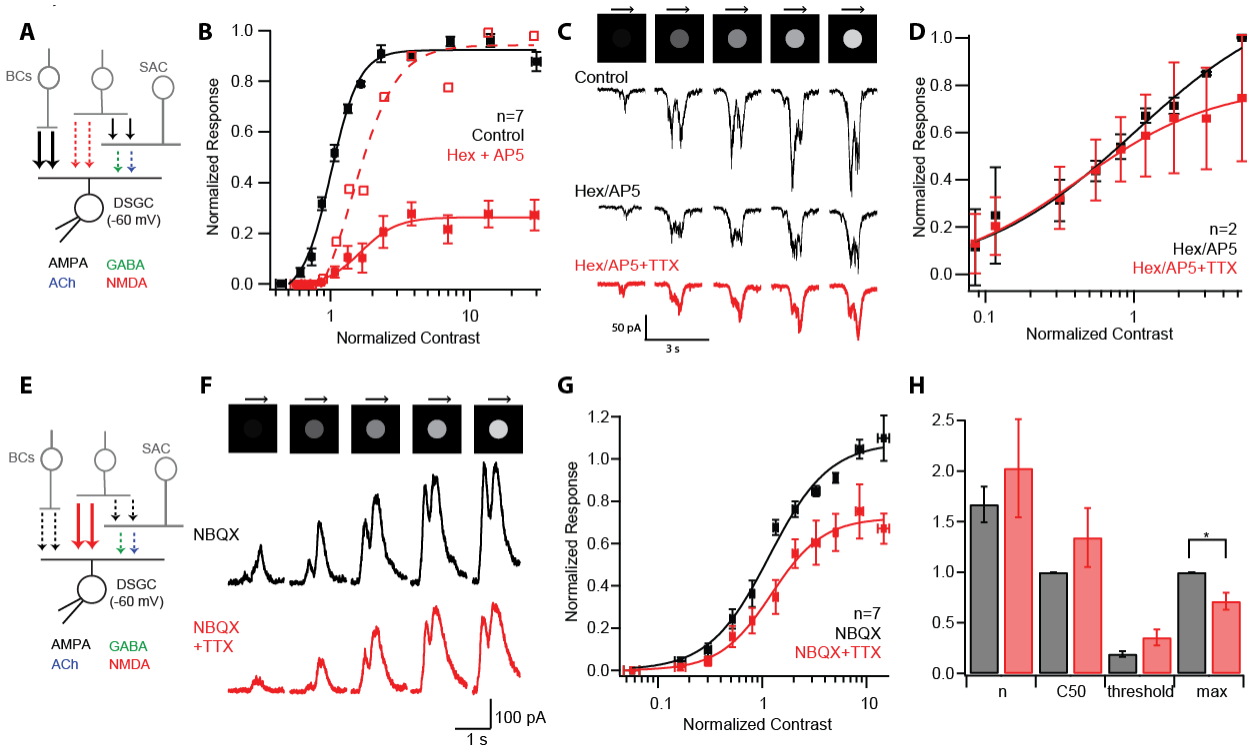

Figure 29. Na^+ channels are expressed in BCs contacting DSGCs, at NMDAR-containing synapses.

A. Schematic of the recording conditions for B-D. EPSCs (V_{hold}= -60 mV) measured in Hex and AP5 allow for isolation of AMPA inputs to DSGCs (black arrows). Dashed arrows represent inputs blocked by drug application or not measured as a result of the holding potential. **B.** CRFs produced from DSGC EPSCs (V_{hold} = -60mV), in control conditions (black), and in the presence of Hex (100 µM) and AP5 (50 µM) (red; full). CRFs were plotted by normalizing to control C_{50} and maxima (n=7). Normalized Hex+AP5 curve shown in dashed red line. Error bars represent ±SEM across cells. All curves are fit using the Naka Rushton equation. **C.** representative current traces (average of 3 traces) in control conditions (black traces; top), Hex/AP5 (black traces; middle), and after TTX application (red traces; middle). **D.** Average (n=2) CRFs (using max and C_{50} in Hex/AP5 for normalization) produced from DSGC EPSCs in Hex/AP5 and Hex/AP5/TTX. **E.** Schematic of the recording conditions for E-H in which only NMDAR-mediated currents are recorded in DSGCs (red arrows). NBQX application blocks direct AMPAR-mediated inputs (black arrows), as well as all inputs from SACs (ACh; blue arrows, GABA; green arrows) that rely on AMPARs for excitation by BCs. **F.** NMDAR-mediated currents measured from DSGCs (V_{hold}= +40 mV for de-inactivation of NMDARs), in response to 400 µm spots of increasing contrast. Representative traces (from 3 stimulus presentations) are shown for NBQX (black) and NBQX+TTX (red) conditions. **G.** Averaged (n=7) CRFs (with NBQX max and C_{50} used for normalization) for NBQX (black) and NBQX+TTX (red) conditions. **H**. Bar graph of the curve fitting parameters (n, C_{50} and max) for NBQX (black) and NBQX+TTX (red) conditions, with the asterisks representing $p<0.05$. Threshold responses represent C_{10}.

I next isolated NMDAR input to sDSGCs by blocking AMPA receptor signalling using NBQX (20 μM). In this condition, AMPA signalling to the DSGC is blocked, as are cholinergic and GABAergic inputs given the lack of excitatory input to SACs (**Figure 29E**). The application of NBQX blocked all responses at -60mV, consistent with the blockade of AMPA and ACh currents (input to SACs is also blocked by NBQX). Changing the holding potential to +40mV relieves the voltage-inactivation of NMDARs, revealing NMDAR-mediated currents. Both ON and OFF responses were visible in the presence of NBQX. ON responses were expected given the expression of mGluR6 receptors in bipolar cells. Residual OFF responses can be explained by the activity of kainate receptors in OFF bipolar cells, as AMPA receptors are blocked.

NMDA-mediated currents were measured in response to moving spots increasing in contrast. Moving stimuli were used in these experiments, in contrast to static stimuli used in previous experiments, however this should not affect the outcome of the experiment as TTX effects were observed for both static and moving stimuli (**Figure 27**). CRFs were generated for individual cells (n=7) in both conditions (NBQX and NBQX+TTX). Averaged CRFs are plotted in **Figure 29G**. TTX application minimally affected threshold contrast, however it steadily decreased all responses to contrast by ~60% (2-way ANOVA, $F_{1/39}$=74.55, P<0.0001). Unexpectedly, while TTX affected sDSGC NMDAR-mediated responses, these effects are different than those observed under control conditions, with the effect of TTX not strongest at low contrasts. I suspect that the application of NBQX, acting on the rod bipolar cell to AII synapse, affected the resting membrane potential of cone bipolar cells. If this is the case, significant depolarization of cone bipolar cell membranes may be required to recruit Na^+ channels,

consistent with the effect of TTX observed at high contrast. TTX nonetheless affected NMDA-dependent inputs to DSGCs. This suggests HSBCs within the DS circuit exhibit Na^+ channel-dependent activity.

These experiments provide preliminary evidence of a BC population-specific organization of Na^+ channels within the DS circuit, with HSBCs (selectively synapsing with post-synaptic NMDARs) exhibiting Na^+ channel-dependent activity while LSBCs (contacting AMPARs) do not. This wiring specificity, combined with the critical role for Na^+ channel activity in encoding low contrast responses in DSGCs and SACs (**Figures 26-27**), strongly supports the hypothesis that Na^+ channel variation underlies differential BC contrast sensitivities.

4.4.6. Na^+ channels in BCs endows DSGCs with increased stimulus sensitivity

Na^+ channels in a BC population may endow these BCs, not only with the ability to amplify responses to low contrast stimuli, but also with a non-linearity useful for the amplification of other weak signals. Given the well described role for voltage-gated conductances in non-linear spatial integration (Borghuis *et al.*, 2013; Takeshita & Gollisch, 2014), I investigated whether Na^+ channel activity leads to a non-linearity in the BC response that is critical for sensitivity to small stimuli. DSGC and SAC EPSCs (V_{hold}= -60 mV) were measured in control conditions and following bath application of TTX, in response to full contrast spots of varying sizes (~6 µm to ~400 µm; **Figure 30A/C**). DSGC and SAC peak EPSCs were averaged (n=5-6 and n=5) and responses plotted as a function of spot size (**Figure 30B/D**). DSGCs and SACs responded consistently to stimuli as small as 6-9µm, increasing their responses to larger stimuli up to 250 µm, before reaching a peak, and exhibiting reduced excitation thereafter

(decreased excitation to large spot sizes is the result of surround inhibition in the DS circuit, see Hoggarth *et al*., 2015). TTX application significantly decreased responses to small spot sizes, and abolished responses to the smallest stimuli for both SACs and DSGCs (**Figure 30A-D;** 2-way ANOVAs; SAC: $F_{1/35}$=21.01, P<0.0001; DSGC: $F_{1/20}$=4.76, P=0.0413; *t*-test DSGC 30µm spot: P=0.005; *t*-test SAC 30µm spot: 0.015), demonstrating a requirement of Na^+ channel activity for the encoding of small spots. The high spatial sensitivity of some BC subpopulations has been previously described (Purgert & Lukasiewicz, 2015), however the TTX sensitivity of this response provides novel insight into our understanding of BC signalling.

In summary, this work represents a significant advancement in our understanding of bipolar cell diversity, function and connectivity within the retina. I have demonstrated, for the first time in the mouse retina, BC specific Na^+ channel activity. Importantly, I have also shown this organization to be responsible for the differences in BC contrast sensitivities previously described (Poleg-Polsky & Diamond, 2016; Sethuramanujam *et al*., 2017). Additionally, I have suggested a novel role for BC Na^+ channels in establishing the impressive spatial sensitivity of the DS circuit.

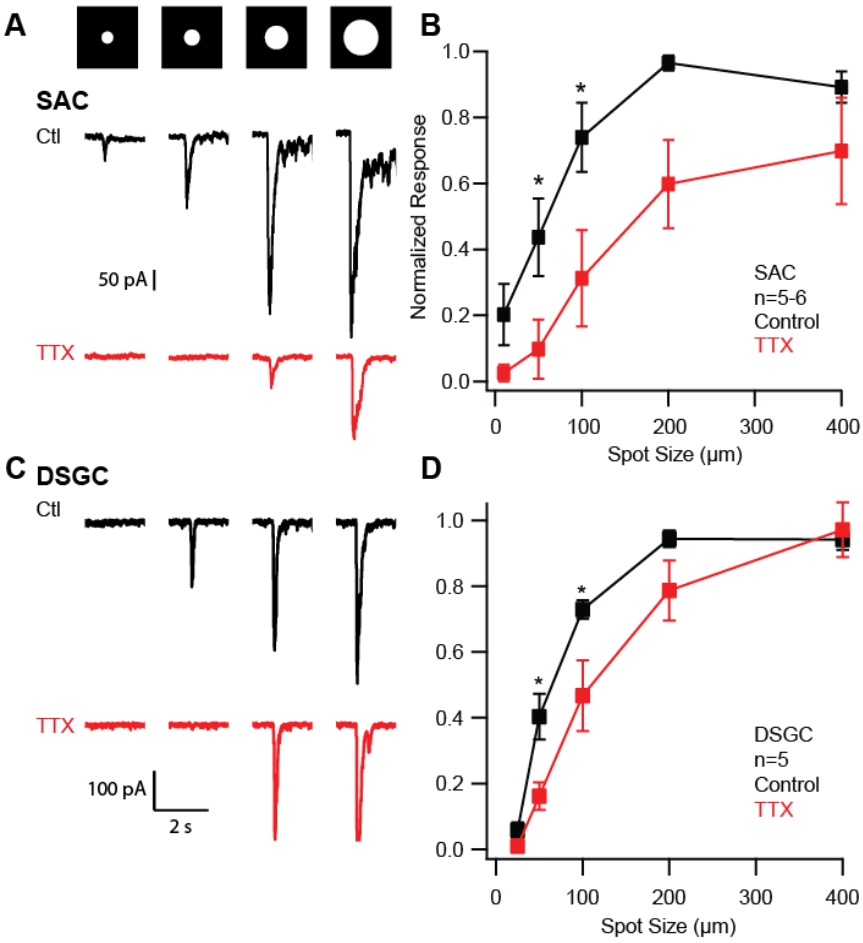

Figure 30. Na^+ channels are important for SAC and DSGC responses to small stimuli.
EPSCs were recorded from SACs (**A-B**) and DSGCs (**C-D**) in response to full contrast spots increasing in size (10-400μm), in control conditions (black) and following bath application of TTX (red; 1 μM). Traces shown are averaged across 3 stimulus presentations. **B/D**. Averaged normalized responses (to control maximum; n=5-6 for SAC and n=5 for DSGC) are plotted as a function of stimulus size. Error bars represent ±SEM. TTX significantly decreased responses to small spots in both SACs and DSGCs (asterisks represent $p<0.05$).

4.5. Discussion

DSGCs are the only cells in the retina with cholinergic, glutamatergic (via both NMDA and AMPA receptors) and gap junction-mediated excitation. Rather than redundancy, recent studies have found that each of these excitatory pathways plays a distinct role in driving the spiking activity of DSGCs (Poleg-Polsky & Diamond, 2016; Sethuramanujam *et al*., 2016, 2017; Trenholm *et al*., 2014), allowing for the encoding of stimulus direction of motion across a large range of stimulus conditions. The neurotransmitter glutamate is released onto DSGC by at least two populations of BCs (Helmstaedter *et al*., 2013). Notably, each BC conveys photoreceptor signals across different contrast sensitivity ranges (Poleg-Polsky & Diamond, 2016; Sethuramanujam *et al.*, 2017). Until now, the mechanism that underlies these differences had not been studied. In this study, I tested the hypothesis that the activity of Na^+ channels endows a subset of BCs, and subsequently their downstream targets, with a non-linearity, allowing for higher contrast sensitivity. Two major finding support this hypothesis: first, TTX decreases both sDSGC and SAC EPSC amplitudes in response to low contrast stimuli, clearly demonstrating a role for a Na^+ channels in driving excitation to sDSGCs and SACs; second, the effect of TTX is specific to high-sensitivity bipolar cell (HSBC) inputs within the DS circuit, inputs responsible for establishing contrast sensitivity of SACs and sDSGCs (Sethuramanujam et al., 2016, 2017). Together, these findings suggest that Na^+ channel activity enhances the release of glutamate from HSBCs in response to presentation of low contrast stimuli.

4.5.1. Na+ channels in mouse bipolar cells

Traditionally, BCs have been considered non-spiking neurons, driving transmitter release from axon terminals through purely graded potentials (for review see Morgans, 2000). Recent work however, suggests BC signalling is much more complex, with BCs utilizing both graded changes in membrane voltage and all-or-nothing spikes to encode light intensity (Saszik & DeVries, 2012; for review see Baden *et al.,* 2013). Na^+ channel activity has also been conclusively demonstrated in dissociated goldfish and rat bipolar cells (Pan & Hu, 2000; Zenisek *et al.*, 2001), allowing for enhanced glutamate release (Ichinose *et al.,* 2005) or the generation of spikes (Saszik & Devries, 2012). For the first time in mouse retina, I demonstrate a clear role for BC Na^+ channels, providing further evidence for their critical contribution to visual computation. Additionally, I show a specific role for integration of Na^+ channel dependent and Na^+-channel independent bipolar cells within a single retinal circuit.

The first evidence for Na^+ channel activity in DS circuit BCs was the decreased excitation of DSGCs and SACs following application of the Na^+ channel antagonist TTX (**Figure 26-27**). While bipolar cell whole-cell recordings are needed to conclusively demonstrate that the effect of TTX observed is the result of Na^+ channel activity in bipolar cells, my results have ruled out other candidates which could similarly enhance responses to the DS circuit in a Na^+ channel-dependent fashion. , As the effect of TTX was not widespread across retinal circuits (**Figure 28**), or even across BC inputs to the DS circuit (**Figure 29**), AII amacrine cells Na+ channels, which would enhance inputs to all ON cone bipolar cells, are likely not involved. Given the effect of TTX persisted in the presence of inhibitors of GABA signalling (**Figure 28E-H**), and for very small spots

(**Figure 29G, 30**), this argued against a role for wide-field amacrine cells, or any inhibitory cells. VGluT3$^+$ amacrine cells can also be discounted, as VGluT3$^+$ input is restricted to ON DSGC dendrites (Grimes *et al.*, 2011; Lee *et al.*, 2014), while ON and OFF sDSGC responses were decreased by TTX, as were inputs to ON SACs (**Figures 26-27**). Taken together, these results suggest Na^+ channels within specific populations of bipolar cells are responsible for enhancing low contrast responses to the DS.

These results add to our current understanding of voltage-gated channel distributions across BC populations, and importantly, link this activity to a specific visual function within a single ganglion cell circuit. Future studies may build on this finding by discovering new roles for spiking activity in these or other bipolar cell populations, or by drawing parallels between spiking activity in BCs and other 'spiking'-activity within the DS circuit (Hoggarth *et al*., 2015; Oesch *et al.*, 2005; Trenholm *et al*., 2014).

4.5.2. Na^+ channel activity is most important at low contrast

My results demonstrate a strong role for Na^+ channel activity at low contrast, with DSGC and SAC responses below half-maximal contrast (C_{50}) decreased by over 70% (**Figure 26-27**). I hypothesize that low contrast inputs generate a weak depolarization in BCs, triggering Na^+ channel activation leading to further membrane depolarization, increasing Ca^{2+} channel activation, and Ca^{2+}-dependent release of glutamate. This hypothesis is consistent with previous characterization of Na^+ channel physiology in BCs, as prior reports suggest BC Na^+ channels exhibit high half-activation membrane potentials, allowing for Na^+ channel activation across the entire range of BC membrane potentials (-65 to -40mV; Pan & Hu, 2000; Zenisek *et al*., 2001). These findings are also

consistent with a previously demonstrated role for Na^+ channels in amplifying low contrast responses in tiger salamander BCs (Ichinose *et al.*, 2005).

Interpreting the effect of TTX at high contrast is, however, more complicated. In DSGCs and SACs, TTX has a much weaker effect on the measured EPSCs at high contrast, decreasing SAC peak responses by 17% (**Figure 26**), and producing no significant difference in DSGCs (**Figure 27**). These results do not necessarily rule out the activity of Na^+ channels at this contrast. I hypothesize that strong depolarization of HSBCs, in response to the presentation of high contrast stimuli, continues to drive Na^+ channel activity. This hypothesis is based on the bimodal distribution of individual BC Ca^{2+} transients in response to spots of increasing contrast (Baden *et al.*, 2013), suggesting BCs that fire spikes (such as HSBCs) do so in an all-or-nothing fashion. The minimal effect of TTX on sDSGC high contrast responses, could instead be explained by the diminishing contribution of HSBCs to sDSGC encoding at high contrast, given that CRFs in this state represent inputs from both TTX-sensitive HSBCs and TTX-insensitive LSBCs (amoung others; **Figure 25**; Sethuramanujam *et al*., 2016, 2017). The effect of TTX on SAC responses is also consistent with the hypothesis that Na^+ channels at high contrast influence high contrast sensitivity, as the effects of TTX remained in SACs at high contrasts. TTX differentially affects the excitation measured in response to high contrast stimuli in DSGCs compared to SACs. Since excitation to SACs is more strongly attenuated, we would predict that the BCs governing excitation to SACs are composed of a larger fraction of TTX-sensitive BCs. The relative contributions of BC excitation and SAC excitation to DSGCs is also contrast dependent, potentially leading to an underestimation of the contribution of HSBCs to glutamatergic excitation to DSGCs at

higher contrasts (Sethuramanujam *et al*., 2016). Further work is required to determine the precise contrast dependences of excitatory inputs to SACs, as well as the precise signalling mechanisms underlying HSBC responses to high and low contrast stimuli.

4.5.3. Na^+ channels are required for responses to small spot sizes

Consistent with the role of Na^+ channels in amplifying weak inputs to from photoreceptors to bipolar cells, I demonstrated that Na^+ channel activity is also critical for sDSGC and SAC responses to small spot sizes. While a high contrast stimulus was used in these experiments, likely generating a strong depolarization in individual BC dendrites within the stimulus area, I hypothesize that this local depolarization drives only a weak depolarization at the BC soma as a result of the pooling of photoreceptor inputs from across the dendritic tree which have an averaging effect on the BC membrane potential. Na^+ channels within BCs however, may allow for such weak depolarization to nonetheless evoke significant release from BCs involved. Hence, this study showed that TTX application abolished DSGC and SAC responses to spots that were significantly smaller than individual BC receptive fields (**Figure 30**). This hypothesis would predict that differential Na^+ channel activity across BC populations endows BCs with unique spatial sensitivities. While I have not tested this hypothesis explicitly, it is in line with recent studies demonstrating differential spatial tuning of mouse ON cone bipolar cells (Purgert & Lukasiewicz, 2015). Differential Na^+ channel activity in BCs may therefore allow for the amplification of multiple independent stimuli representing weak inputs to the DS circuit: here demonstrated via small spot sizes and low contrast responses. Further investigation in the sub-optimal stimulation range of other visual stimuli properties (such as low temporal frequencies; Hoggarth *et al*., 2015) should provide evidence for similar

roles for spiking BCs. This study nonetheless provides further insights into these BC signalling differences, previously poorly understood.

4.5.4. Conclusions

This work provides the first evidence for Na^+ channel activity in mouse bipolar cells, while also demonstrating key roles for such Na^+ channels in establishing contrast sensitivity and spatial sensitivity of ganglion and amacrine cells within the directionally-selective circuit. While interesting questions remain, pertaining to the precise functional organization of bipolar cell receptive fields and bipolar cell wiring to starburst amacrine cells or across other ganglion cell circuits, this work further unravels the functional role of different sources of excitation to the directionally-selective circuit. Additionally, the data presented supports a model in which excitation changes in composition across varying stimulus properties (such as size and contrast), with directionally-selective ganglion cells recruiting different proportions of separate neurotransmitters (or the same neurotransmitter acting at different receptors), to best suit the needs of visually driven behaviours.

4.6. Bibliography

Baden, T., Berens, P., Bethge, M., & Euler, T. (2013). Spikes in mammalian bipolar cells support temporal layering of the inner retina. *Current Biology*, *23*(1), 48–52. http://doi.org/10.1016/j.cub.2012.11.006

Baden, T., Euler, T., Weckström, M., & Lagnado, L. (2013). Spikes and ribbon synapses in early vision. *Trends in Neurosciences*, *36*(8), 480–488. http://doi.org/10.1016/j.tins.2013.04.006

Boos, R., Schneider, H., & Wassle, H. (1993). Voltage- and transmitter-gated currents of AII-amacrine cells in a slice preparation of the rat retina. *The Journal of Neuroscience*, *13*(7), 2874–2888.

Borghuis, B. G., Marvin, J. S., Looger, L. L., & Demb, J. B. (2013). Two-photon imaging of nonlinear glutamate release dynamics at bipolar cell synapses in the mouse retina. *The Journal of Neuroscience*, *33*(27), 10972–85. http://doi.org/10.1523/JNEUROSCI.1241-13.2013

Connaughton, V. P., & Maguire, G. (1998). Differential expression of voltage-gated K+ and Ca 2+ currents in bipolar cells in the zebrafish retinal slice. *European Journal of Neuroscience*, *10*, 1350–1362.

Cui, J., & Pan, Z.-H. (2008). Two types of cone bipolar cells express voltage-gated Na+ channels in the rat retina. *Visual Neuroscience*, *25*(5–6), 635. http://doi.org/10.1017/S0952523808080851

Eggers, E. D., McCall, M. A., & Lukasiewicz, P. D. (2007). Presynaptic inhibition differentially shapes transmission in distinct circuits in the mouse retina. *The Journal of Physiology*, *582*, 569–582. http://doi.org/10.1113/jphysiol.2007.131763

Euler, T., & Wassle, H. (1998). Different contributions of GABAa and GABAc receptors to rod and cone bipolar cells in a rat retinal slice preparation. *Journal of Neurophysiology*, *79*, 1384–1395.

Farrow, K., Teixeira, M., Szikra, T., Viney, T. J., Balint, K., Yonehara, K., & Roska, B. (2013). Ambient illumination toggles a neuronal circuit switch in the retina and visual perception at cone threshold. *Neuron*, *78*(2), 325–38. http://doi.org/10.1016/j.neuron.2013.02.014

Ghosh, K. K., Bujan, S., Haverkamp, S., Feigenspan, A., & Wässle, H. (2004). Types of bipolar cells in the mouse retina. *Journal of Comparative Neurology*, *469*(1), 70–82. http://doi.org/10.1002/cne.10985

Hartveit, E. (1997). Functional organization of cone bipolar cells in the rat retina. *Journal of Neurophysiology*, *77*, 1716–1730.

Helmstaedter, M., Briggman, K. L., Turaga, S. C., Jain, V., Seung, H. S., & Denk, W. (2013). Connectomic reconstruction of the inner plexiform layer in the mouse retina. *Nature*, *500*(7461), 168–74. http://doi.org/10.1038/nature12346

Hoggarth, A., McLaughlin, A. J., Ronellenfitch, K., Trenholm, S., Vasandani, R., Sethuramanujam, S., Awatramani, G. B. (2015). Specific wiring of distinct amacrine cells in the directionally selective retinal circuit permits independent coding of direction and size. *Neuron*, *86*(1), 276–291. http://doi.org/10.1016/j.neuron.2015.02.035

Hu, H.-J., & Pan, Z.-H. (2002). Differential expression of K+ currents in mammalian

retinal bipolar cells. *Visual Neuroscience*, *19*(2), 163–173. http://doi.org/017.S0952523802191140

Ichinose, T., Fyk-Kolodziej, B., & Cohn, J. (2014). Roles of ON cone bipolar cell subtypes in temporal coding in the mouse retina. *The Journal of Neuroscience*, *34*(26), 8761–71. http://doi.org/10.1523/JNEUROSCI.3965-13.2014

Ichinose, T., Shields, C. R., & Lukasiewicz, P. D. (2005). Sodium channels in transient retinal bipolar cells enhance visual responses in ganglion cells. *The Journal of Neuroscience*, *25*(7), 1856–65. http://doi.org/10.1523/JNEUROSCI.5208-04.2005

Ivanova, E., & Muller, F. (2006). Retinal bipolar cell types differ in their inventory of ion channels. *Visual Neuroscience*, *23*, 143–154.

Lyubarsky,A.L., Falsini, B., Pennesi, M. E., Valentini, P., & Pugh, E. N. (1999). UV- and midwave-sensitive cone-driven retinal responses of the mouse: a possible phenotype for coexpression of cone photopigments. *The Journal of Neuroscience, 19*(1), 442–455.

Masu, M., Iwakabe, H., Tagawa, Y., Miyoshi, T., Yamashita, M., Fukuda, Y., … Nakanishi, S. (1995). Specific deficit of the ON response in visual transmission by targeted disruption of the mGIuR6 gene. *Cell*, *80*(5), 757–765. http://doi.org/10.1016/0092-8674(95)90354-2

Morgan, J. L., Soto, F., Wong, R. O. L., & Kerschensteiner, D. (2011). Development of cell type-specific connectivity patterns of converging excitatory axons in the retina. *Neuron*, *71*(6), 1014–1021. http://doi.org/10.1016/j.neuron.2011.08.025.

Morgans, C. W. (2000). Neurotransmitter release at ribbon synapses in the retina. *Immunology and Cell Biology*, *78*, 442–446.

Muller, F., Scholten, A., Ivanova, E., Haverkamp, S., Kremmer, E., & Kaupp, U. B. (2003). HCN channels are expressed differentially in retinal bipolar cells and concentrated at synaptic terminals. *European Journal of Neuroscience*, *17*, 2084–2096. http://doi.org/10.1046/j.1460-9568.2003.02634.x

Naka, K. I., & Rushton, W. A. H. (1966). S-Potentials from luminosity units in the retina of fish. *Journal of Physiology*, *185*, 587–599.

Odermatt, B., Nikolaev, A., & Lagnado, L. (2012). Encoding of luminance and contrast by linear and nonlinear synapses in the retina. *Neuron, 73*(4), 758–773. http://doi.org/10.1016/j.neuron.2011.12.023

Oesch, N., Euler, T., & Taylor, W. R. (2005). Direction-selective dendritic action potentials in rabbit retina. *Neuron*, *47*(5), 739–50. http://doi.org/10.1016/j.neuron.2005.06.036

Pan, Z., & Hu, H. (2000). Voltage-dependent Na+ currents in mammalian retinal cone bipolar cells. *Journal of Neurophysiology*, *84*, 2564–2571.

Peichl, L., Ott, H., & Boycott, B. (1987). Alpha ganglion cells in mammalian retinae. *Procedings of the Royal Society of London*, *231*, 169–197.

Poleg-Polsky, A., & Diamond, J. S. (2016). Retinal circuitry balances contrast tuning of excitation and inhibition to enable reliable computation of direction selectivity. *Journal of Neuroscience*, *36*(21), 5861–5876. http://doi.org/10.1523/JNEUROSCI.4013-15.2016

Purgert, R. J., & Lukasiewicz, P. D. (2015). Differential encoding of spatial information among retinal on cone bipolar cells. *Journal of Neurophysiology*, *114*(3), 1757–1772. http://doi.org/10.1152/jn.00287.2015

Saszik, S., & DeVries, S. H. (2012). A mammalian retinal bipolar cell uses both graded changes in membrane voltage and all-or-nothing Na+ spikes to encode light. *The Journal of Neuroscience*, *32*(1), 297–307. http://doi.org/10.1523/JNEUROSCI.2739-08.2012

Sethuramanujam, S., McLaughlin, A. J., deRosenroll, G., Hoggarth, A., Schwab, D. J., & Awatramani, G. B. (2016). A central role for mixed acetylcholine/GABA transmission in direction coding in the retina. *Neuron*, *90*(6), 1243–1256. http://doi.org/10.1016/j.neuron.2016.04.041

Sethuramanujam, S., Yao, X., Rosenroll, G., Briggman, K. L., Field, G., & Awatramani, G. B. (2017). "Silent" NMDA synapses enhance motion sensitivitiy in a mature retinal circuit, *Neuron, 96*(5), 1099-1011

Takeshita, D., & Gollisch, T. (2014). Nonlinear spatial integration in the receptive field surround of retinal ganglion cells. *Journal of Neuroscience*, *34*(22), 7548–61. http://doi.org/10.1523/JNEUROSCI.0413-14.2014

Taylor, W. R. (1999). TTX attenuates surround inhibition in rabbit retinal ganglion cells. *Visual Neuroscience*, *16*(2), 285–90. http://doi.org/10.1017/S0952523899162096

Trenholm, S., McLaughlin, A. J., Schwab, D. J., Turner, M. H., Smith, R. G., Rieke, F., & Awatramani, G. B. (2014). Nonlinear dendritic integration of electrical and chemical synaptic inputs drives fine-scale correlations. *Nature Neuroscience, 17*, 1759-66. http://doi.org/10.1038/nn.3851

Vigh, J., Vickers, E., & von Gersdorff, H. (2011). Light-evoked lateral GABAergic inhibition at single bipolar cell synaptic terminals is driven by distinct retinal microcircuits. *The Journal of Neuroscience*, *31*(44), 15884–15893. http://doi.org/10.1523/JNEUROSCI.2959-11.2011

Wassle, H., Puller, C., Muller, F., & Haverkamp, S. (2009). Cone contacts, mosaics, and territories of bipolar cells in the mouse retina. *The Journal of Neuroscience*, *29*(1), 106–117. http://doi.org/10.1523/JNEUROSCI.4442-08.2009

Zeng, H., & Sanes, J. R. (2017). Neuronal cell-type classification: challenges, opportunities and the path forward. *Nature Reviews Neuroscience*, *18*(9), 530-46 http://doi.org/10.1038/nrn.2017.85

Zenisek, D., Henry, D., Studholme, K., Yazulla, S., & Matthews, G. (2001). Voltage-dependent sodium channels are expressed in nonspiking retinal bipolar neurons. *The Journal of Neuroscience*, *21*(13), 4543–4550.

5. Discussion

Photoreceptors respond via graded potentials to local changes in luminance. These changes drive glutamate release onto bipolar cells where, again, the strength of the stimulus is reflected in the graded release of glutamate. Ganglion cells, which fire all-or-nothing action potentials instead of graded signals, integrate graded chemical synaptic inputs from cone bipolar cells and amacrine cells. Ganglion cells also receive information from other ganglion cells via gap junction-mediated electrical synapses. It is unclear however why ganglion cells in the retina would transmit signals laterally, at the possible expense of signal acuity. I postulate that gap junction-mediated lateral signalling leads to ganglion cell spiking when bipolar cell- and/or amacrine cell-mediated post-synaptic responses are insufficient to drive spiking (for example when visual stimuli have low contrast).

In this dissertation I have investigated the hypothesis that sub-threshold currents elicited through chemical synapses sum with gap junction-mediated currents to drive spiking. Further, I hypothesize that these two forms of input (chemical and electrical) are actively amplified by Na^+ channels in ganglion cell dendrites. Thus, in conditions where both electrical and chemical signalling occurs, ganglion cell spiking is enhanced.

Within a ganglion cell circuit that encodes stimulus motion in the superior direction (superior coding directionally-selective ganglion cells; sDSGCs), I have characterized both chemical and electrical pre-synaptic signalling. In doing so I have described several mechanisms by which responses to weak stimulus conditions are enhanced. In this Chapter, I will discuss how the observations reported in Chapters 2-4 may work in concert within the superior-coding directionally-selective (DS) circuit.

Then, I discuss how my findings translate to other visual circuits, both within the retina, and in other areas of the brain.

5.1. Summary

Directionally-selective ganglion cells (DSGCs) are responsible for the encoding of stimulus direction, with each of the four subpopulations tuned to one of the four cardinal directions (superior, anterior, posterior and inferior). Superior-coding DSGCs (sDSGCs) are unique in their expression of gap junctions. I characterized the biophysical properties of gap junction coupling in sDSGCs (Chapter 2). Current flow across DSGC gap junctions exhibited a weak conductance, no rectification and no voltage-dependence. These observations suggested that the gap junctions are comprised of connexin 36 (CX36) subunits. Experiments in transgenic animals deficient in CX36 confirmed this hypothesis by demonstrating that CX36 is necessary for the functional electrical coupling of superior-coding DSGCs.

The weak conductance of these gap junctions however appeared at odds with the previously described role for electrical coupling in driving neural synchronization. In Chapter 3, I confirmed that spike trains between coupled sDGSCs exhibited fine-scale correlations. Then I investigated the possible mechanisms underlying the synchronization of spike trains. This work confirmed the critical role for gap junctions in driving correlations but showed that correlations also require the activation of voltage-gated Na^+ channels in DSGC dendrites. My observations suggest that coincident chemical and electrical synaptic inputs sum in sDSGC dendrites, activating dendritic Na^+ channels responsible to for correlated spiking.

In Chapter 4, I focussed on the glutamatergic synapses within sDSGCs circuits. Consistent with previous findings, I observed that glutamatergic synapses across the DS circuit exhibited distinct contrast sensitivities: AMPA-mediated currents to SACs were more sensitive to contrast than AMPA-mediated currents in DSGCs. Physiological experiments using specific ion channel antagonists revealed an important role for voltage-gated Na^+ channels in establishing the high-contrast sensitivity. I provided evidence for the presence of these Na^+ channels in select bipolar cell populations within the DS circuit. Thus the work in Chapter 4 provided insight into the mechanisms underlying an important coincidence detection mechanism, in addition to providing insight into the various ways in which retinal circuits encode weak visual stimuli.

5.2. Weak electrical coupling and fine-scale correlations

5.2.1. Electrical coupling and correlations in other ganglion cell circuits

Dendritic spiking might be used to amplify low-conductance (such as CX36-containing) gap junction currents in other retinal ganglion cells, not just the superior-coding DSGCs studied in Chapters 2 and 3. Variation in the abundance and/or distribution of gap junctions and/or an impedance mismatch between the pre- and post-synaptic neurons could influence (i.e. enhance) gap junction-mediated current amplitudes. Indeed, a large enough gap junction current could bypass the need for dendritic spiking in establishing fine-scale correlations, as is the case in salamander retina (Brivanlou *et al.*, 1998). Thus, the mechanism I have described, where coincident electrical and chemical synaptic inputs, in addition to dendritic spiking, are required for eliciting fine-scale correlations, might be most important in neurons with low baseline firing.

5.2.2. What information are correlations providing?

Understanding the mechanisms underlying correlations does not provide us with any insights regarding the information these correlations are encoding. Further work in superior-coding DGSCs (see Trenholm *et al.*, 2014) has however provided us with some insight. The strength of correlations between coupled sDSGCs was examined in experiments that varied the stimulus contrast and spatial structure (stimulus size and location; Trenholm *et al.*, 2014). Correlations increased as stimulus contrast decreased, while correlations decreased as stimulus structure changed (one large centered spot compared to two smaller spots separated in space; Trenholm *et al.*, 2014). This suggests that correlations might allow mice to discriminate between changes in stimulus contrast and stimulus spatial structure, in conditions that similarly change the spike rate. That correlations provide additional information than that contained in the spike rate, relies on the assumption that higher order visual centers are able to decode fine-scale correlations. In Chapter 4, I therefore suggested that correlated firing serves an alternate function in the retina. It might be that correlated firing simply enhances spiking in coupled neurons. In conditions where input to superior-coding DGSCs is sub-threshold, correlated firing may facilitate the generation of spikes (Trenholm *et al.*, 2013). This might decrease the variability of spike timing, thus increasing signal reliability in conditions where sDSGCs are weakly stimulated. I observed that correlated firing was strongest when stimulus contrast was low, suggesting that dendritic spikes are reliably generated in these conditions (Chapter 3). I predict that gap junction coupling, and generation of correlated dendritic spikes decreases sDSGC response variability near contrast threshold. These predictions however remain to be tested experimentally.

Independent of the roles played by correlations, it is unclear why only a single population of DS ganglion cells exhibits gap junction coupling and correlated firing. It is possible that the encoding of superior motion is particularly important for mouse prey survival mechanisms, such as predator detection, especially when contrast is reduced. In this case, the encoding of additional information or the enhanced sensitivity of these neurons may be crucial to survival.

5.3. Na^+ channels enhance weak inputs

5.3.1. Dendritic spiking across DS circuits

In Chapter 3, I described a role for dendritic Na^+ channels in establishing fine-scale correlations. These correlations were shown to require both chemical synaptic input and gap junction-mediated currents (Chapter 4). Given the lack of gap junction coupling between other DSGC populations, fine-scale correlations are unlikely between DSGCs coding for the other three directions of stimulus motion. Similarly, it is possible that dendritic Na^+ channels are not a conserved feature of all DS populations. Superior-coding DSGCs differ from other DS ganglion cells in that they exhibit an asymmetric morphology (Trenholm *et al.,* 2011) and express gap junctions (Trenholm *et al.,* 2013a; Trenholm *et al.,* 2013b). This asymmetric morphology confers superior-coding DSGCs with the ability to remain direction selective in the absence of directional GABAergic signalling from starburst amacrine cells (Trenholm *et al*., 2011). While it remains unclear why this population is unique in these respects, Na^+ channels may be an additional specialization of these neurons, required specifically for establishing fine-scale correlations. Alternatively, dendritic Na^+ channels may serve to improve the centrifugal

direction selectivity of DSGCs created by their asymmetric arbors (Trenholm *et al.*, 2011).

Experiments in rabbit however, suggest dendritic spiking is conserved across all four DSGC populations (Oesch *et al.*, 2005). In these neurons, dendritic spikes may play an important role in enhancing directional responses, based on evidence that DS ganglion cells exhibit weaker direction selectivity when Na^+ channels are inhibited (Oesch *et al.*, 2005). In mouse DSGCs, the amplification of weak DS signalling has been previously attributed to non-linear dendritic NMDA receptors (Poleg-Polsky & Diamond, 2016). I hypothesize that NMDA receptor activation and Na^+ channel recruitment work in concert, with NMDA receptor-mediated depolarization activating voltage-gated Na^+ channels. In DSGC populations without electrical coupling (and the associated depolarization of DSGC dendrites), the activation of NMDA receptors could be particularly important for ensuring the generation of dendritic spikes. Further experiments however will be required to determine whether the weak input, enhanced in DSGC dendrites by post-synaptic NMDA receptors, is similarly non-linearly amplified by dendritic Na^+ channels.

5.3.2. Dendritic spiking in other retinal ganglion cells

A large body of work, dating back to the 1950's, described dendritic spiking in the central nervous system (Andersen, 1960; Cragg & Hamlyn, 1955; Fujita & Sakata, 1962; Llinas *et al.*, 1968; Spencer & Kandel, 1961). Landmark studies by Spruston *et al.* (1995) and Stuart and Sakmann (1994) demonstrated that neuronal dendrites in CA1 neurons of the hippocampus can be excitable, with voltage-gated channels allowing for the generation of dendritic spikes, preceding the generation of somatic action potentials.

Dendritic spiking has since been demonstrated in neurons in many regions of the brain (Gulledge *et al.*, 2005; Stuart *et al.,* 1997), including pyramidal neurons of the visual cortex (Hirsch *et al.*, 1995; Shai *et al.*, 2015; Smith *et al.*, 2013). Only recently however has dendritic spiking been observed in retinal neurons, and this work has largely been confined to the DS circuit (see 5.3.1). This begs the question of whether dendritic spiking takes place in other ganglion cells.

Active dendrites in the retina likely serve a number of roles in addition to facilitating correlated spiking in gap junction coupled neurons (see 5.2.1.). This hypothesis is based on the observation that dendritic spiking has been observed in ON alpha ganglion cells in the mouse retina (Velte & Masland, 1999) and all four populations of DSGCs in the rabbit retina (Oesch *et al.*, 2005), despite these neurons exhibiting no fine-scale correlations (Hu & Bloomfield, 2003; and see Chapter 5.3.1).

First, Dendritic spiking might serve to enhance stimulus tuning. In DSGCs of the rabbit retina, dendritic spiking improves directional tuning (Schachter *et al.,* 2010), while dendritic spikes in the visual cortex improve orientation tuning (Smith *et al.,* 2013).

Second, dendritic Na^+ channels might play a role in extending the dynamic range of neurons (the range of stimulus characteristics which can be differentially encoded by the neuron in its synaptic output). This was proposed by Publio *et al.,* (2012) and Stuart *et al.,* (1997), who provided evidence that dendritic Na^+ channels allow for the active propagation of action potentials through the dendritic tree following action potential generation at the soma (action potential back-propagation). The large and simulataneous depolarization of neuronal dendrites following Na^+ channel activation could effectively

reset the charge on neuronal dendrites. This in turn might allow for greater sensitivity to input near the detection threshold, which may otherwise be lost in the synaptic noise.

Further roles for dendritic spiking may be gleaned from the conditions that most strongly drive dendritic spiking. In Chapter 3, I demonstrated that strong local stimulation, from electrical and chemical synaptic inputs effectively drives dendritic spiking. Similar local depolarization may be produced by small, high contrast visual stimuli. In this case, dendritic spiking may ensure that spatially localized depolarizing currents are more effectively translated into action potentials. This role is worth investigating in ON alpha ganglion cells, as the large dendritic arbors of these neurons may make the amplification of spatially localized depolarizing currents particularly important.

5.3.3. Bipolar cell spiking across retinal circuits

In Chapter 4, I showed an important role for Na^+ channel activity within a specific bipolar cell population in the direction-selective circuit. I also showed that inputs to the ON alpha ganglion cell circuit, and possibly AMPA receptor-mediated currents to sDSGCs, are not TTX-sensitive. It is unclear however whether Na^+ channels are limited to bipolar cell populations which contact SACs and DSGCSs (at postsynaptic NMDA receptors), or whether Na^+ channels are shared by many bipolar cell populations in the retina.

In experiments which utilize slice preparations, enabling direct recordings of bipolar cell voltage and bipolar cell subtype-identification, Na^+ channel activity was consistently limited to bipolar cells which stratified in the mid-inner plexiform layer (Cui & Pan, 2008; Ichinose *et al*., 2005; Puthussery *et al*., 2013; Saszik & DeVries, 2012),

near the border of the ON and OFF sublamina. Anatomical analysis of rat retinal bipolar cells, filled during electrophysiological recordings, suggested as few as two populations of bipolar cells express Na^+ channels. As the presence of Na^+ channels has been demonstrated in both ON and OFF cone bipolar cells (Baden *et al.*, 2011; Cui & Pan, 2008; Zenisek *et al*., 2001), these populations may be ON and OFF counterparts of each other. ON cone bipolar cells that express Na^+ channels might contact ON SACs and DSGC ON dendrites, while OFF Na^+-channel expressing CBCs might contact OFF SACs and DSGC OFF dendrites. Consistent with this hypothesis the two populations thought to exhibit TTX-sensitive currents co-localize at least in part with ON and OFF cholinergic bands of the inner plexiform layer (Cui & Pan, 2008). Thus, Na^+ channel expression may be limited to bipolar cell populations found in the DS circuit (Cui & Pan, 2008; Ichinose *et al*., 2005; Puthussery *et al*., 2013; Saszik & DeVries, 2012). Should this be the case, the superior-coding DS circuit (and presumably other DS circuits) may possess greater contrast sensitivity than all other ganglion cell circuits, given the role for Na^+ channels in enhancing contrast sensitivity of DSGCs and SACs (Chapter 4). This may provide the retina with the ability to detect moving objects below detection threshold for static objects.

Within DS circuits, bipolar cell Na^+ channels may do more than lower contrast sensitivity (Ichinose et al., 2005; and see Chapter 4). Na^+ channels may improve signal fidelity by increasing bipolar cell response amplitudes and the rate at which bipolar cell terminals are depolarized (Baden *et al*., 2011; Zenisek *et al*., 2001). Bipolar cell Na^+ channels may also improve the encoding of sharp transitions in light stimuli, or sudden motion (Baden *et al*., 2011; Saszik & DeVries, 2012). This hypothesis is based on

evidence that bipolar cells containing Na^+ channels can fire spikes, but often generate only single spikes when presented with light stimuli. These single spikes occur consistently in response to strong stimulation if the stimulus is repeated (Baden et al., 2011; Saszik & DeVries, 2012), suggesting a role in marking sharp transitions.

Direct recordings from bipolar cells within the DS circuit will be needed to assess the response properties of Na^+ channels in these neurons. Alternatively, a further understanding of the molecular identity of these neurons, and the other circuits contacted by Na^+-channel expressing bipolar cells may indirectly shed some light on the benefits provided by this specialization.

5.4. Future directions for the study of signal integration

Work on this dissertation began shortly following the identification of gap junctions between superior-coding DSGCs (Trenholm *et al.*,2013) . I first characterized the molecular and biophysical characterization of these gap junctions, and investigated the role of gap junctions in establishing fine-scale correlations. Studying the mechanisms underlying fine-scale correlations lead to the identification of voltage-gated channels in DSGC dendrites, which now require further study.

While my results have demonstrated Na^+ channel activity in sDSGC dendrites and bipolar cells, it will be important to understand the molecular composition and distribution of Na^+ channels within these neurons. In bipolar cells the location of Na^+ channels will impact the roles played by Na^+ channels in these neurons (Puthussery *et al*., 2013). The subcellular localization of Na^+ channels in sDSGC dendrites may allow for some pre-synaptic inputs to be amplified more effectively than others (Brombas *et al.*, 2017). Similarly, this may provide insights into the interactions between excitation and

inhibition in the generation of dendritic spikes. Studies thus far have disagreed on whether inhibition is able to shunt dendritic spiking once dendritic spikes are initiated, or whether inhibition is important in shunting excitatory currents prior to Na^+ channel activation.

The molecular characterization of Na^+ channels in both sDSGCs and bipolar cells can provide insights into the activation and inactivation ranges of these channels. Na^+ channels previously described in bipolar cells exhibit a small range of voltages over which they are able to be activated (Baden *et al*., 2011). This may explain the ability of cone bipolar cells to switch between two encoding states, one in which Na^+ channels are active and signals are encoded in an all-or-nothing fashion, or a state in which signals are encoded gradually and Na^+ channels are inactive (Saszik & DeVries, 2012). AII amacrine cells have been shown to control the membrane potential of cone bipolar cells (CBCs; Grimes *et al.*, 2014) as ambient light levels change. Ambient light may therefore toggle the resting membrane potential of the cone bipolar cells, altering the ability of CBCs to recruit Na^+ channels and their release of glutamate onto downstream amacrine and ganglion cells. Analysis of the TTX-sensitivity of DGSC and SAC excitatory responses across light levels will help test this hypothesis, as will an in depth analysis of direction-selectivity across ambient light levels. If bipolar cell spikes are modulated by light level, this may help explain other light-dependent switched that have been described in the retina, such as the activation of surround inhibition (Hoggarth *et al*., 2015).

5.5. Conclusions

This work has provided novel insights into the electrical and chemical synaptic inputs to DS ganglion cells. I have described two novel circuit features in the mouse

retina: bipolar cell Na^+ channels and sDSGC dendritic Na^+ channels, both of which are likely a conserved feature of directionally-selective circuits. I have described the subunit composition of gap junctions between coupled sDSGCs (Chapter 2), and described an interaction between gap junctions and sDSGC dendritic Na^+ channels in establishing fine-scale correlations between coupled sDSGCs (Chapter 4). I have also described a role for bipolar cell Na^+ channels in amplifying low contrast responses to sDSGCs. These results (Chapters 2-4) advance our current understanding of the complex and unique superior-coding directionally-selective circuit.

5.6. Bibliography

Andersen, P. (1960). Interhippocampal impulses: II. Apical dendritic activation of CAI neurons. *Acta Physiologica Scandinavica*, *48*(2), 178–208. http://doi.org/10.1111/j.1748-1716.1960.tb01856.x

Baden, T., Esposti, F., Nikolaev, A., & Lagnado, L. (2011). Spikes in retinal bipolar cells phase-lock to visual stimuli with millisecond precision. *Current Biology*, *21*(22), 1859–69. http://doi.org/10.1016/j.cub.2011.09.042

Bloomfield, S.A, & Völgyi, B. (2009). The diverse functional roles and regulation of neuronal gap junctions in the retina. *Nature Reviews Neuroscience*, *10*(7), 495–506. http://doi.org/10.1038/nrn2636

Brivanlou, I. H., Warland, D. K., & Meister, M. (1998). Mechanisms of concerted firing among retinal ganglion cells. *Neuron*, *20*(3), 527–39.

Brombas, A., Croft, S. K., & Williams, S. R. (2017). Dendro-dendritic cholinergic excitation controls dendritic spike initiation in retinal ganglion cells. *Nature Communications*, *8*(15683), 1–14. http://doi.org/10.1038/ncomms15683

Cragg, B., & Hamlyn, L. H. (1955). Action potentials of the pyramidal neurones in the hippocampus of the rabbit. *Journal of Physiology*, 129, 608–627.

Cui, J., & Pan, Z.-H. (2008). Two types of cone bipolar cells express voltage-gated Na+ channels in the rat retina. *Visual Neuroscience*, *25*(5–6), 635. http://doi.org/10.1017/S0952523808080851

Fujita, Y., & Sakata, H. (1962). Electrophysiological properties of CA1 and CA2 apical dendrites of rabbit hippocampus. *Journal of Neurophysiology*, *25*(2), 209 LP-222.

Grimes, W. N., Schwartz, G. W., & Rieke, F. (2014). The synaptic and circuit mechanisms underlying a change in spatial encoding in the retina. *Neuron*, *82*(2), 460–73. http://doi.org/10.1016/j.neuron.2014.02.037

Gulledge, A. T., Kampa, B. M., & Stuart, G. J. (2005). Synaptic integration in dendritic trees. *Journal of Neurobiology*, *64*(1), 75–90. http://doi.org/10.1002/neu.20144

Helmstaedter, M., Briggman, K. L., Turaga, S. C., Jain, V., Seung, H. S., & Denk, W. (2013). Connectomic reconstruction of the inner plexiform layer in the mouse retina. *Nature*, *500*(7461), 168–74. http://doi.org/10.1038/nature12346

Hirsch, J. A., Alonso, J.-M., & Reid, R. C. (1995). Visually evoked calcium action potentials in cat striate cortex. *Nature*, *378*, 612.

Hoggarth, A., McLaughlin, A. J., Ronellenfitch, K., Trenholm, S., Vasandani, R., Sethuramanujam, S., Awatramani, G. B. (2015). Specific wiring of distinct amacrine cells in the directionally selective retinal circuit permits independent coding of direction and size. *Neuron*, *86*(1), 276–291. http://doi.org/10.1016/j.neuron.2015.02.035

Hu, E. H., & Bloomfield, S. a. (2003). Gap junctional coupling underlies the short-latency spike synchrony of retinal alpha ganglion cells. *The Journal of Neuroscience*, *23*(17), 6768–77.

Ichinose, T., Shields, C. R., & Lukasiewicz, P. D. (2005). Sodium channels in transient retinal bipolar cells enhance visual responses in ganglion cells. *The Journal of Neuroscience*, *25*(7), 1856–65. http://doi.org/10.1523/JNEUROSCI.5208-04.2005

Llinas, R., Nicholson, C., Freeman, J. A., & Hillman, D. E. (1968). Dendritic spikes and their inhibition in alligator pukinje cells. *Science*, *160*(3832), 1132–1135.

Oesch, N., Euler, T., & Taylor, W. R. (2005). Direction-selective dendritic action potentials in rabbit retina. *Neuron*, *47*(5), 739–50. http://doi.org/10.1016/j.neuron.2005.06.036

Poleg-Polsky, A., & Diamond, J. S. (2016). NMDA receptors multiplicatively scale visual signals and enhance directional motion discrimination in retinal ganglion cells. *Neuron*, 1–14. http://doi.org/10.1016/j.neuron.2016.02.013

Poleg-Polsky, A., & Diamond, J. S. (2016). Retinal circuitry balances contrast tuning of excitation and inhibition to enable reliable computation of direction selectivity. *The Journal of Neuroscience*, *36*(21), 5861–5876. http://doi.org/10.1523/JNEUROSCI.4013-15.2016

Publio, R., Ceballos, C. C., & Roque, A. C. (2012). Dynamic range of vertebrate retina ganglion cells: importance of active dendrites and coupling by electrical synapses. *PLoS ONE*, *7*(10). http://doi.org/10.1371/journal.pone.0048517

Puthussery, T., Venkataramani, S., Gayet-Primo, J., Smith, R. G., & Taylor, W. R. (2013). Nav1.1 channels in axon initial segments of bipolar cells augment input to magnocellular visual pathways in the primate retina. *The Journal of Neuroscience*, *33*(41), 16045–16059. http://doi.org/10.1523/JNEUROSCI.1249-13.2013

Saszik, S., & DeVries, S. H. (2012). A mammalian retinal bipolar cell uses both graded changes in membrane voltage and all-or-nothing Na+ spikes to encode light. *The Journal of Neuroscience*, *32*(1), 297–307. http://doi.org/10.1523/JNEUROSCI.2739-08.2012

Schachter, M. J., Oesch, N., Smith, R. G., & Rowland Taylor, W. (2010). Dendritic spikes amplify the synaptic signal to enhance detection of motion in a simulation of the direction-selective ganglion cell. *PLoS Computational Biology*, *6*(8). http://doi.org/10.1371/journal.pcbi.1000899

Sethuramanujam, S., McLaughlin, A. J., deRosenroll, G., Hoggarth, A., Schwab, D. J., & Awatramani, G. B. (2016). A central role for mixed acetylcholine/GABA transmission in direction coding in the retina. *Neuron*, *90*(6), 1243–1256. http://doi.org/10.1016/j.neuron.2016.04.041

Sethuramanujam, S., Yao, X., Rosenroll, G., Briggman, K. L., Field, G., & Awatramani, G. B. (2017). "Silent" NMDA synapses enhance motion sensitivitiy in a mature retinal circuit. *Neuron. 96*(5), 1099-1111

Shai, A. S., Anastassiou, C. A., Larkum, M. E., & Koch, C. (2015). Physiology of layer 5 pyramidal neurons in mouse primary visual cortex: coincidence detection through bursting. *PLoS Computational Biology*, *11*(3), 1–18. http://doi.org/10.1371/journal.pcbi.1004090

Smith, S. L., Smith, I. T., Branco, T., & Häusser, M. (2013). Dendritic spikes enhance stimulus selectivity in cortical neurons in vivo. *Nature*, *503*(7474), 115–20. http://doi.org/10.1038/nature12600

Söhl, G., Güldenagel, M., Traub, O., & Willecke, K. (2000). Connexin expression in the retina. *Brain Research Reviews*, *32*(1), 138–145. http://doi.org/10.1016/S0165-0173(99)00074-0

Spencer, W. A., & Kandel, E. R. (1961). Electrophysiology of hippocampal neurons: IV. Fast prepotentials. *Journal of Neurophysiology*, *24*(3), 272 LP-285.

Spruston, N., Jonas, P., Sakmann, B., Forschung, M., & Zellphysiologie, A. (1995). Dendritic glutamate receptor channels in rat hippocampal CA3 and CAl pyramidal

neurons. *Journal of Physiology*, 325–352.

Stuart, G. J., & Sakmann, B. (1994). Active propagation of somatic action potentials into neocortical pyramidal cell dendrites. *Nature*, *367*(6458), 69–72. http://doi.org/10.1038/367069a0

Stuart, G., Spruston, N., Sakmann, B., & Hausser, M. (1997). Action potential initiation and back propagation in neurons of the mammalian central nervous system. *Trends in Neurosciences*, *20*(3), 125–131. http://doi.org/10.1016/S0166-2236(96)10075-8

Trenholm, S., Johnson, K., Li, X., Smith, R. G., & Awatramani, G. B. (2011). Parallel mechanisms encode direction in the retina. *Neuron*, *71*(4), 683–694. http://doi.org/10.1016/j.neuron.2011.06.020

Trenholm, S., McLaughlin, A. J., Schwab, D. J., & Awatramani, G. B. (2013). Dynamic tuning of electrical and chemical synaptic transmission in a network of motion coding retinal neurons. *The Journal of Neuroscience*, *33*(37), 14927–38. http://doi.org/10.1523/JNEUROSCI.0808-13.2013

Trenholm, S., McLaughlin, A. J., Schwab, D. J., Turner, M. H., Smith, R. G., Rieke, F., & Awatramani, G. B. (2014). Nonlinear dendritic integration of electrical and chemical synaptic inputs drives fine-scale correlations. *Nature Neuroscience*, (October). http://doi.org/10.1038/nn.3851

Trenholm, S., Schwab, D. J., Balasubramanian, V., & Awatramani, G. B. (2013). Lag normalization in an electrically coupled neural network. *Nature Neuroscience*, *17*, 1759–66. http://doi.org/10.1038/nn.3308

Velte, T. J., & Masland, R. H. (1999). Action potentials in the dendrites of retinal ganglion cells. *Journal of Neurophysiology*, *81*, 1412–1417.

Völgyi, B., Chheda, S., & Bloomfield, S. a. (2009). Tracer coupling patterns of the ganglion cell subtypes in the mouse retina. *The Journal of Comparative Neurology*, *512*(5), 664–87. http://doi.org/10.1002/cne.21912

Völgyi, B., Kovács-öller, T., Atlasz, T., Wilhelm, M., & Gábriel, R. (2013). Gap junctional coupling in the vertebrate retina: Variations on one theme? *Progress in Retinal and Eye Research*, *34*, 1–18. http://doi.org/10.1016/j.preteyeres.2012.12.002

Zenisek, D., Henry, D., Studholme, K., Yazulla, S., & Matthews, G. (2001). Voltage-dependent sodium channels are expressed in nonspiking retinal bipolar neurons. *The Journal of Neuroscience*, *21*(13), 4543–4550.